Palacký University in Olomouc

Faculty of Science

Department of Experimental Physics

Ph.D. Thesis

Mgr. Radek Melich

Optical Systems Compound of Thin and Thick Anisotropic Layers

Supervisor: Ing. Jaromír Křepelka, CSc.

Department: Department of Experimental Physics, Joint Laboratory of Optics of Palacký University and Institute of Physics of the Academy of Sciences of the Czech Republic

Olomouc 2012

Acknowledgement

I hereby confirm that this Ph.D. thesis has been worked out independently under supervision of Ing. Jaromír Křepelka, CSc. and exclusively with the use of quoted sources, literature and other professional sources.

In Olomouci, date ....   Author signature

Title: Optical Systems Compound of Thin and Thick Anisotropic Layers

Author: Mgr. Radek Melich

Department: Department of Experimental Physics, Joint Laboratory of Optics of Palacký University and Institute of Physics of the Academy of Sciences of the Czech Republic

Supervisor: Ing. Jaromír Křepelka, CSc.

Abstract:

Ph.D. thesis concerns a detailed study and an application of uniaxial crystals in astronomical optics, mainly design techniques, production process, tolerances of individual optical parts and different ways of operation of polarization-interference filters. Such filters are in these days used especially for solar observation in many different astronomically interesting spectral lines. Spectrally various observations of the solar atmosphere allow astronomers to study solar behavior and its physics. To deal with aims of the thesis it was created dedicated MATLAB toolbox enabling detailed analysis of current birefringent filter issues and enabling later synthesis of novel type of birefringent filter tuning. The theoretical results and own measurement of relevant material constants were applied in a research and later development of an universal birefringent filter prototype that is spectrally tunable.

Keywords:

anisotropic materials, crystal optics, birefringent filters, Solar research

Název práce: Optické systémy složené z tenkých a tlustých anizotropních vrstev

Autor: Mgr. Radek Melich

Pracoviště: Společná laboratoř optiky Univerzity Palackého a Fyzikálního ústavu Akademie věd České republiky

Vedoucí disertační práce: Ing. Jaromír Křepelka, CSc.

Abstrakt:

Disertační práce se zabývá aplikací jednoosých krystalů v astronomické optice, zvláště metodami návrhu, technikou výroby, tolerancemi jednotlivých optických prvků a způsobem provozu polarizačně-interferenčních filtru. Ty se v dnešní době využívají zvláště pro pozorování Slunce, a to v celé řadě spektrálních čar. Spektrálně odlišná pozorování umožňují astronomům sledovat sluneční atmosféru v různých hladinách a studovat tak zákonitosti sluneční fyziky. Pro řešení disertační práce byl vytvořen specializovaný toolbox v programovém prostředí MATLAB, který umožnil detailní analýzu současného stavu problematiky dvojlomných filtrů a následnou syntézu nového typu jejich ladění. Výsledky provedených výpočtů a vlastní měření potřebných materiálových konstant byly využity pro výzkum a následný vývoj spektrálně laditelného univerzálního dvojlomného filtru.

Klíčová slova:

anizotropní materiály, krystalová optika, dvojlomné filtry, sluneční výzkum

Contents

List of Figures

List of Tables

Glossary

B	thickness of Beilby layer
C	material temperature dependency coefficient
D	birefringence
D_ψ	birefringence of a crystal for rays traveling under angle ψ
$D_{\max}$	maximum birefringence of a crystal
$E_{x,y}$	complex envelope of a monochromatic wave
FT_0	ideal filter transmission
FT_{err}	error loaded filter transmission
I	output intensity or one of four Stokes parameters where relevant
I_0	input intensity
K	plate order
K_T	order of certain transmission peak with respect to temperature T
M	unit thickness
M_T	unit thickness characteristics with respect to temperature T
M_Y	unit thickness M of Y-cut crystalline plate
M_ϕ	unit thickness M of oblique cut crystalline plate
N	number of plates within a filter
Q	one of four Stokes parameters
R	reflectance of FP filter surface
T	temperature or transmission function of FP filter where relevant
$T_{11}, T_{12}, T_{21}, T_{22}$	elements of Jones matrix $\mathbf{T}$
U	one of four Stokes parameters

V	one of four Stokes parameters
Δ	path retardance
ΔT	temperature increment
$\Delta \lambda$	wavelength temperature increment
$\Delta \lambda_T$	difference between wavelengths measured at 35°C and temperature T
Γ	phase retardance
$\varnothing$	optical diameter
α	angle between the polarizer and optical axis of birefringent plate
α_i	angle used for azimuth variation
β	angle of BF inclination
β'	angle of ray traveling through BF when inclined about β
χ	electrical susceptibility
δ	angle of a polarization plane rotation through the optical activity
δS	geometrical distance corresponding with $\delta \lambda$
$\delta \lambda$	considered wavelength region
ϵ	permitivity
ϵ_ϕ	tolerance of crystal lattice orientation angle
ϵ_ρ	tolerance of azimuth angle
ϵ_d	tolerance of plate thickness
ϵ_0	permittivity of vacuum
$\epsilon_{1,2,3}$	permittivity of anisotropic material with respect to the main axis of a crystal
γ	grating diffraction angle
λ	wavelength
λ_0	designed wavelength of the filter

λ_K	spectral position of transmitted peak K
λ_T	wavelength measured at temperature T
λ_S	spectral position of known solar line
$\mathbf{B}$	Berreman matrix
$\mathbf{J}$	Jones (column) vector
$\mathbf{J}^\dagger$	hermitian conjugate vector to $\mathbf{J}$
$\mathbf{L}$	wavelength matrix
$\mathbf{S}$	Stokes vector
$\mathbf{T}$	Jones matrix
$\boldsymbol{\Psi}$	Berreman vector
$\mathbf{d}$	vector of plate thicknesses
$\mathbf{k}$	wave vector
$\mathbf{r}$	space vector
$\mathcal{B}$	vector of magnetic induction
$\mathcal{D}$	vector of electric induction
$\mathcal{E}$	electric field vector
$\mathcal{F}$	finesse of a filter
$\mathcal{H}$	magnetic field vector
$\mathcal{M}$	magnetization
$\mathcal{P}$	polarization density
$\mathrm{inv}(\mathbf{D})$	inverse birefringence matrix
μ_0	permeability of vacuum
ν	frequency of a monochromatic wave
ω	angular frequency
ϕ	angle of crystal lattice orientation
ϕ_0	crystal lattice orientation angle of plate with zero tolerance
ϕ_err	estimated value of a production error of crystal lattice orientation angle

ψ	angle of ray traveling through a crystal plate
$\psi_{\max}$	maximal deviation of extraordinary ray
ψ_φ	deviation of extraordinary ray for oblique cut φ
ρ	azimuth angle
ρ'	azimuth angle basis
ρ_0	azimuth angle with zero tolerance
ρ_{err}	estimated value of a production error of azimuth angle
σ	angle of convergency of optical system beam
θ	angle of refraction in FP filter
θ_0	spherical coordinate of an incident wave direction
φ	incident angle of ray on a crystal plate
φ_0	spherical coordinate of an incident wave direction
$\varphi_{x,y}$	phase of complex envelope $E_{x,y}$ of a monochromatic wave
a	grating constant
c	speed of light in a vacuum
c_{S}	solar line position on CCD in pixel units
$c_{x,y}$	coefficients of Maxwell-Berreman calculus
d	thickness of a crystal
d_0	thickness of a plate with zero tolerance
d_{M}	thickness of $\mathrm{MgF_2}$ plate
d_{Q}	thickness of quartz plate
d_{err}	estimated value of a production error of plate thickness
ds'	value of spherochromatic aberration

$e_{x,y}$	amplitude of complex envelope $E_{x,y}$ of a monochromatic wave
f	focal length of an imaging objective
f'	focal length
g	dispersion coefficient
k	wave number
l	geometrical length
m	grating order
n	refractive index of a matter
n_0	refractive index of surrounding matter
$n_{1,2,3}$	components of refractive index of an anisotropic material with respect to the main axis of the crystal
n_{e}	extraordinary refractive index
$n_{\mathrm{e}}(\psi)$	extraordinary refractive index of a ray traveling through a crystal under an angle ψ
n_{o}	ordinary refractive index
o_K	filter transmission peak position on CCD in pixel units
p	coefficient used for side maxima decrease; ratio of path retardance first derivatives with respect to wavelengths; spectral size of one pixel
p_1 to p_6	coefficient of unit thickness characteristics
q	integer number
t	time variable
v	speed of light in a matter
$D_{1,2,3}$	vector components of electric induction of anisotropic material with respect to the main axis of a crystal

$E_{1,2,3}$	electric field vector components of anisotropic material with respect to the main axis of a crystal
i	imaginary unit
BaII	solar spectral line at 4554.03 Å
BF	birefringent filter
C1	birefringent plate of Lyot element
C2	birefringent plate of Lyot element
CaIIK	solar spectral line at 3933.682 Å
D1	solar spectral line at 5895.940 Å
D2	solar spectral line at 5889.973 Å
D3	solar spectral line at 5875.625 Å
DF1	first set of dielectric sub-filters
DF2	second set of dielectric sub-filters
DOT	Dutch Open Telescope
F/♯	optical system F-number
FP	Fabry-Peròt filter
FSR	free spectral range
FWHM	full width in a half maximum
Hα	solar spectral line at 6562.808 Å
Hβ	solar spectral line at 4861.342 Å
Hγ	solar spectral line at 4340.475 Å
IRF	infrared filter

M	diffraction grating
obj1	imaging objective
obj2	collimating objective
obj3	imaging objective
P	polarizer
p1	polarizer
P1 ... P4	polarizers
p2	polarizer
S	slit
SF1	first barrier element of Šolc type
SF2	second barrier element of Šolc type
SF3	third barrier element of Šolc type
SST	Swedish Solar Telescope
Z1	heliostat mirror
Z2	heliostat mirror

1   Introduction

Optical systems compound of thin and thick anisotropic layers can be found in many fields of current optical science. Among them belong thin film optics where interference phenomenon is used to enhance system performance, non-linear optics where stacks of different anisotropic materials can express unusual performance, optical fiber optics where specially designed fibers are produced, up to crystal optics where layered systems are used to change the light properties [1]. And there could be surely named many other applications.

A scope of this work, however, is focused on layered anisotropic systems that utilizes interference-polarization phenomenon. The phenomenon is employed for construction of narrow band birefringence filters. Its demanding production technique is balanced with achieved extreme performance of spectral filtering. Filters with full width in a half maximum (FWHM) of an order of tens of pikometers can be easily achieved.

A pioneer in this field of optics was in 1920s and 1930s French astronomer Bernard Lyot who designed a filter concept that is compounded of birefringent plates where each next plate has a double thickness of previous one and individual plates are separated by polarizers [2]. Independently on Lyot work, Swedish astronomer Yngve Öhman designed the same filter conception in 1938 [3]. In 1950s the completely new conception was developed in Czechoslovakia by Ivan Šolc that apart from Lyot-Öhman filter employs birefringent plates of same thickness and does not separate them by polarizers [4, 5]. In the field of birefringent filters worked in that time also American astronomer John W. Evans [6]. Usage of birefringent filter into the close UV spectral region was applied by Swedish astronomer Kerstin Fredga [7]. Recently, theory and production of birefringent filter is realized on several places. In Russia at Institute of Solar Physics there is a group of V.I. Skomorovski [8], [9]. Utrecht University in Netherland is running a solar telescope DOT (Dutch Open Telescope) which employs birefringent filter for observation [10]. Big Bear Solar Observatory in USA also employs birefringent filters for their research [11],

[12]. Birefringent filters are used also for space solar missions as for instance in Hinode project[13].

In the Czech Republic the problem of birefringent filters is studied since an invention of the new concept by Šolc. It is group of TOPTEC research center where also Ivan Šolc has up to 1990's worked in and where he is even recently giving lecture talks concerning crystal optics.

1.1   Formulation of an issue

The scope of this work is focused on birefringent filters of Šolc type because they express advantage of higher throughput and simpler production comparing to other birefringent filters. During my Ph.D. studies I took a great advantage of training position in TOPTEC research centre, where crystal optics is both studied and produced already from its foundation in 1960s. I was enabled to participate on design, production and troubleshooting of several birefringent filters in cooperation with TOPTEC team and also with its inventor Ivan Šolc.

Another great advantage was a six months trainee position at Solar Group of Utrecht University who runs a solar telescope DOT (Dutch Open Telescope; see figure 6.9) at Gran Canaria Islands and another six months trainee position at Solar Institute of Royal Swedish Academy in Stockholm who runs solar telescope SST (Swedish Solar Telescope) also at Gran Canaria Islands. During both trainees I have been contributing to work of professional solar astronomers. I involved in solar data processing, telescopes operation and most important discussed astronomical needs as regards solar filters.

Nowadays, birefringent filters are mostly used in astronomy for solar observation in many spectral lines of different chemical elements. Among most important lines we can find for instance hydrogen spectral line Hα (656.28 nm or 6562.8 Å as solar physicists exclusively use). A spectral width of these lines determines the performance of the filter that is used for an observation. Hα line width is approx. 1 Å , therefore filters with FWHM

of at least 1 Å need to be used. Such filters belong to the class of high performance filters and they are challenging both to design and to manufacture. A designer needs to have precise material characteristics and a knowledge of manufacture processes to be able to construct a desired filter. A manufacturer needs to employ very precise and time-consuming techniques to keep produced filter parts under required tolerances; also a high grade material is necessary which is usually hard or expensive to obtain. It is very important especially for the designer to get a feedback both from the manufacturer who produces the filter and from astronomers who employ the filter for their observations. Objectives of the thesis deal with design and manufacturing procedures.

1.2   Objective of the thesis

To be able to provide a proper analysis and an advanced synthesis that could provide novel possibilities of birefringent filters (BF) usage the thesis consists of the following objectives:

1. Programming of MATLAB BF toolbox

2. BF manufacturing tolerance simulations

3. Crystalline SiO_2 dispersion characterization including temperature dependency

4. Novel design of oblique cut BF and its testing

5. Prototype of BF

The first objective of the thesis is to employ one of possible mathematical description of birefringent filters and to create a programmed environment that would be suitable enough to illustrate spectral characteristics of the filter with respect to the way the filters are designed. For the program codes I have chosen MATLAB environment. Series of individual functions, procedures and routine files I have summarized into so called "MATLAB BF toolbox".

The second objective of the thesis is to employ MATLAB BF toolbox and to analyze an influence of design tolerances on a performance of Šolc birefringent filters. Tolerances of individual filter characteristics and as well as their mutual interactions are analyzed. I also discuss a possible re-distribution of filter individual parts in order to minimize the influence of production tolerances on the filter performance.

The third objective concerns a determination of crystalline quartz material characteristics which precise knowledge is essential for high performance filters. Those are dispersion characteristics and their dependency on temperature.

The fourth objective employs the preprogrammed BF toolbox and using of its analytic capabilities to design a novel and fast ways of Šolc BF tuning.

The fifth objective of the thesis is to employ so far familiar and in this thesis newly proposed theoretical and practical knowledge to design and manufacture a prototype of tunable high performance BF of Šolc type that would be useful for astronomical observations in interesting spectral lines. As a part of the system, an optical design of solar chromospheric telescope is provided.

1.3   Structure of the thesis

A structure of the work satisfies a recommended structure of Ph.D. thesis and can be divided as follows:

- objectives of the Ph.D. thesis

- characterization of an issue current state with references on scientific literature

- methods of thesis solution

- solving of thesis objectives

- results of the thesis and new knowledge

- specific conclusions for a usage of thesis results in a practice

2 Characterization of the current state of an issue

2.1 Description of electromagnetic field

Behavior of electromagnetic field in a space without current and charge sources can be described using Maxwell equations [1] as

$$\text{rot}\mathcal{E} + \frac{\partial \mathcal{B}}{\partial t} = 0, \tag{2.1}$$

$$\text{div}\mathcal{B} = 0, \tag{2.2}$$

$$\text{rot}\mathcal{H} - \frac{\partial \mathcal{D}}{\partial t} = 0, \tag{2.3}$$

$$\text{div}\mathcal{D} = 0. \tag{2.4}$$

In this set of equations vector $\mathcal{E}(\mathbf{r}, t)$ is called an electric field vector and is a function of space coordinates $\mathbf{r} = (x, y, z)$ and time t. Vector $\mathcal{H}(\mathbf{r}, t)$ (also a function of space and time coordinates) describes a magnetic part of the field and therefore it is called the magnetic field vector.

Taking into account an influence of a matter on a propagation of an electromagnetic field it is necessary to establish another two field vectors - vector of electric induction $\mathcal{D}(\mathbf{r}, t)$ and vector of magnetic induction $\mathcal{B}(\mathbf{r}, t)$. Relation between fields $\mathcal{E}$ and $\mathcal{D}$ is dependent on the electrical nature of the matter whereas relation between fields $\mathcal{H}$ and $\mathcal{B}$ depends on the magnetic nature of the matter. These kinds of relations are described by following equations

$$\mathcal{D} = \epsilon_0 \mathcal{E} + \mathcal{P}, \tag{2.5}$$

$$\mathcal{B} = \mu_0 \mathcal{H} + \mathcal{M}, \tag{2.6}$$

where ϵ_0 is a permittivity of vacuum, μ_0 is a permeability of vacuum, $\mathcal{P}$ is a polarization density and $\mathcal{M}$ is a magnetization.

In the following we concentrate on a dielectric matter where the polarization density is a sum of electrical dipole moments inducted by an electric field. In the classical optics we usually introduce several assumptions about the dielectric matter:

- Linearity of the matter - the polarization density is linearly proportional to the intensity of the electrical field.

- Non-dispersive matter - a response of the matter to the change of the field is immediate.

- Homogeneity of the matter - a relation between the polarization density and the intensity of electric field does not rely on a position of the space vector $\mathbf{r}$.

- Non-magnetic matter - the magnetization $\mathcal{M} = 0$.

As a consequence of the non-magnetic matter restriction the equation 2.6 turns into

$$\mathcal{B} = \mu_0 \mathcal{H}. \tag{2.7}$$

The polarization density and the electric field vector can be expressed as

$$\mathcal{P} = \epsilon_0 \chi \mathcal{E}, \tag{2.8}$$

where χ is an electrical susceptibility. Putting the equation 2.8 into 2.5 results in

$$\mathcal{D} = \epsilon \mathcal{E}, \tag{2.9}$$

where ϵ is a permittivity defined as

$$\epsilon = \epsilon_0 (1 + \chi). \tag{2.10}$$

If we consider an isotropic matter, ϵ is a scalar and vectors $\mathcal{P}$ and $\mathcal{E}$ are in any time at any place directly proportional to each other. However, in this work we will deal with an anisotropic matter where the permittivity is no more a scalar value. It is generally characterized by a 3×3 matrix, it means by tenzor with 9 (generally complex) components. However, a character of a matter growing into a crystalline lattice signs a certain symmetry, meaning that some of the permittivity matrix elements have to be equal. In addition to that we can always choose such a coordinate system with respect to the crystalline matter that the permittivity tenzor can be diagonalized. Such the

diagonalization enable us to rewrite relation between $\mathcal{D}$ and $\mathcal{E}$ for anisotropic materials as

$$D_1 = \epsilon_1 E_1, \quad D_2 = \epsilon_2 E_2, \quad D_3 = \epsilon_3 E_3. \tag{2.11}$$

Axes $1, 2$ and 3 of selected coordinate system are called main axes of a crystal and quantities

$$n_1 = \sqrt{\frac{\epsilon_1}{\epsilon_0}}, \quad n_2 = \sqrt{\frac{\epsilon_2}{\epsilon_0}}, \quad n_3 = \sqrt{\frac{\epsilon_3}{\epsilon_0}} \tag{2.12}$$

are called main refractive indexes of a crystal.

Using this notation we recognize two kinds of anisotropic crystals: uniaxial and biaxial. Biaxial crystals have all three values of main refractive indexes different, whereas uniaxial crystals have two main refractive indexes the same (we called them an ordinary refractive index n_o) and only the third one differs (it is an extraordinary refractive index n_e). A direction of this axis is identical with the optical axis of the crystal. When $n_\mathrm{e} > n_\mathrm{o}$ uniaxial crystals are called positive, whereas negative crystals experience $n_\mathrm{e} < n_\mathrm{o}$.

In the following text we will focus on uniaxial crystals because they are most widely used in crystal optics.

2.2   Definition of used quantities

Here we define several quantities that will be later used for calculations.

2.2.1   Path and phase retardance

A path retardance is defined as

$$\Delta = d|n_\mathrm{e} - n_\mathrm{o}|, \tag{2.13}$$

where d is a crystal thickness. As there can be seen from the definition a ray entering a uniaxial birefringent material can be split into two modes usually called ordinary and extraordinary ray. Each experiences corresponding refractive index n_e, resp. n_o. A

product of path retardance and wave number $k = \frac{2\pi}{\lambda}$ gives a phase retardance

$$\Gamma = \frac{2\pi}{\lambda} d |n_e - n_o| \tag{2.14}$$

which describes a difference between two mode's phases.

2.2.2   Birefringence and the crystal orientation

A difference between extraordinary and ordinary refractive indexes defines a birefringence of a crystal

$$D = n_e - n_o. \tag{2.15}$$

A magnitude of the birefringence D depends on directions the extraordinary and ordinary rays traveling through a crystal. The maximal birefringence occurs when rays travel through the crystal in the direction that is perpendicular to an optical axis ($\psi = 0°$). Minimal when traveling parallel with the optical axis ($\psi = 90°$). The reason for this fact is that the extraordinary refractive index depends on the angle ψ of a ray traveling through the crystal. The dependency is as follows:

$$\left(\frac{1}{n_e(\psi)} \right)^2 = \left(\frac{\sin \psi}{n_o} \right)^2 + \left(\frac{\cos \psi}{n_e} \right)^2. \tag{2.16}$$

Birefringence of the oblique cut crystal can be then expressed as

$$D_\psi = n_e(\psi) - n_o \doteq D_{\max} \cos^2 \psi. \tag{2.17}$$

2.2.3   Azimuth of a birefringent plate

On every birefringent plate we can determine two basic orthogonal directions that correspond with ordinary and extraordinary refractive indexes. These are called principal directions. The direction of higher refractive index is called the slow axis, whereas the direction of lower refractive index is called the fast axis. A reason for that is derived from an equation for the speed of light in the matter, $v = c/n$, where c is the speed of light in

vacuum and n is a refractive index of the matter.

If a linearly polarized light beam perpendicularly incidents these principal directions, it is split in two vectors and travels through the crystal as two independent rays linearly polarized in the directions of principal directions. Passing the plate both vectors are superimposed together with different phases. Depending on the phase retardance a linearly, circularly or elliptically polarized beam is created.

Consider a birefringent plate placed between two crossed linear polarizers in such a way that one of the principal direction holds an angle $\rho = 45°$ with the direction of linearly polarized light coming from the first polarizer. This angle ρ is called an azimuthal angle (see figure 2.1). The second polarizer enables the interference of both fast and slow beams so that the output intensity I varies with the phase retardance as

$$I = I_0 \sin^2 \frac{\Gamma}{2}, \tag{2.18}$$

where I_0 is the input intensity.
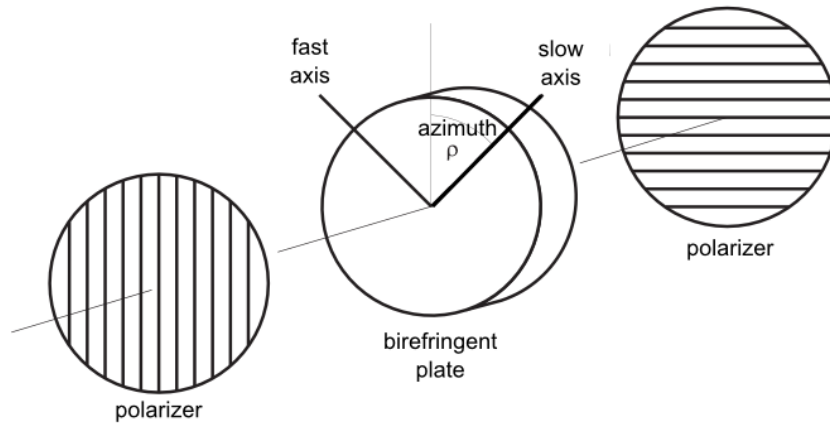
Figure 2.1: Two crossed polarizers with a birefringent plate at 45° azimuth angle.

It can be seen from this equation that a maximum transmission occurs for

$$\Gamma = (2q - 1)\pi, \tag{2.19}$$

where $q = 1, 2, 3, \ldots$. Combining equations 2.19 and 2.14 we get an expression

$$d \cdot D = K \cdot \lambda, \tag{2.20}$$

where $K = 0.5, 1.5, 2.5, \ldots$. This equation expresses the plate thickness d of a material with the birefringence D and the plate order K be in order to transmit the wavelength λ. This equation is the basic one for a design of birefringent filters.

A similar equation can be achieved for a situation when polarizers are in a parallel order. Then for the phase retardance there is a condition $\Gamma = 2q\pi$ and the plate order $K = 1, 2, 3, \ldots$. The situation is complementary to the previous one.

2.2.4   Unit thickness

A unit thickness M is defined as

$$M = \frac{\lambda}{D}. \tag{2.21}$$

From a physical point of view it expresses the thickness of a birefringent plate (a cut of a maximal birefringence - an optical axis is parallel with the cut) when the path retardance of ordinary and extraordinary waves is just λ or the phase retardance is just 2π.

2.3   Birefringent narrow band filters of Šolc type

This type of a birefringent filter (BF) was invented in 1950's by Dr. Ivan Šolc in Czechoslovakia and was first described in publications [4] and [5]. Detailed description was done in [14] and in [15].

2.3.1   Principle of birefringent filters of Šolc type

A basic principle of birefringent narrow-band filters comes from an interference of a polarized light that is described by one of four Fresnel-Arago law [16]: "Two rays, linearly polarized with a perpendicular polarization, if derived from the same linearly polarized ray and subsequently brought into the same plane, can interfere."

This law determines a structure of the filter itself. The filter consists of entrance and exit polarizers and birefringent retardance plates that are placed between these polarizers (see figure 2.2). An unpolarized beam of light travels through the entrance polarizer that makes the beam polarized. After that the beam travels through birefringent plates where it is phase shifted with respect to the azimuth orientation of the plate and with respect to the proper refractive index. It can be imagined as that one plate divides the beam into two beams - fast and slow - where both beams experience its own refractive index of the uniaxial crystal (n_e and n_o). Because the next plate is azimuthally shifted with respect to the previous plate each beam is again divided into two new beams. We have now four beams that are phase shifted with respect to each other. After traveling through N birefringent plates there is 2^N phase shifted beams. To enable an interference of all these beams they need to be, according to Fresnel-Arago law, brought into the same plane. That is assured by the exit polarizer which all beams travel through.
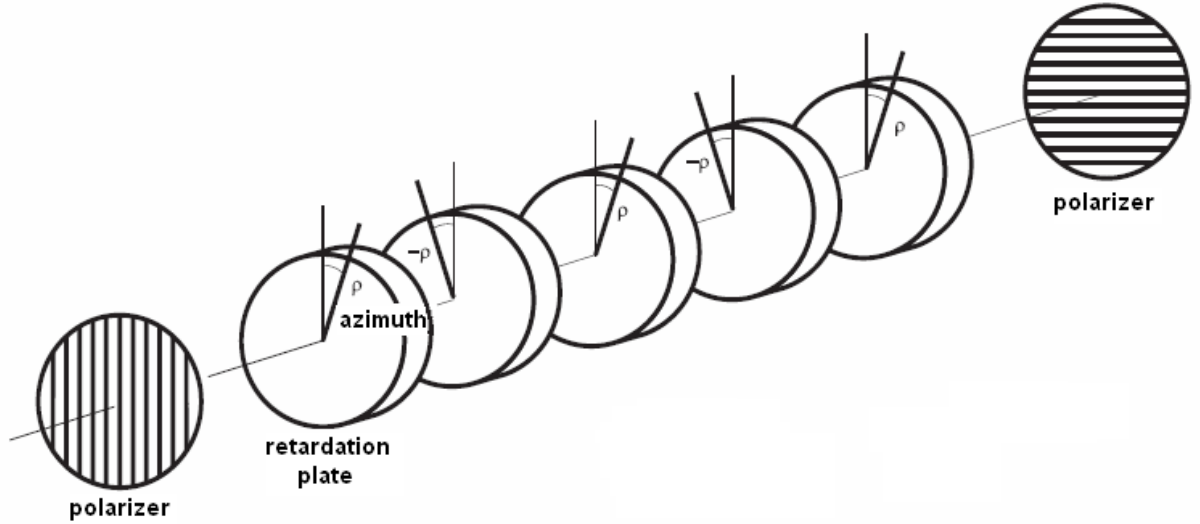
Figure 2.2: Typical structure of a birefringent narrow band filter of Šolc type.

To achieve a maximal transmission Šolc [17, 18] proposed a requirement for plate azimuths

$$|\rho| = \frac{45°}{N} \tag{2.22}$$

where N is a number of plates within a filter. A typical spectral profile of such a filter

can be seen on figure 2.3.
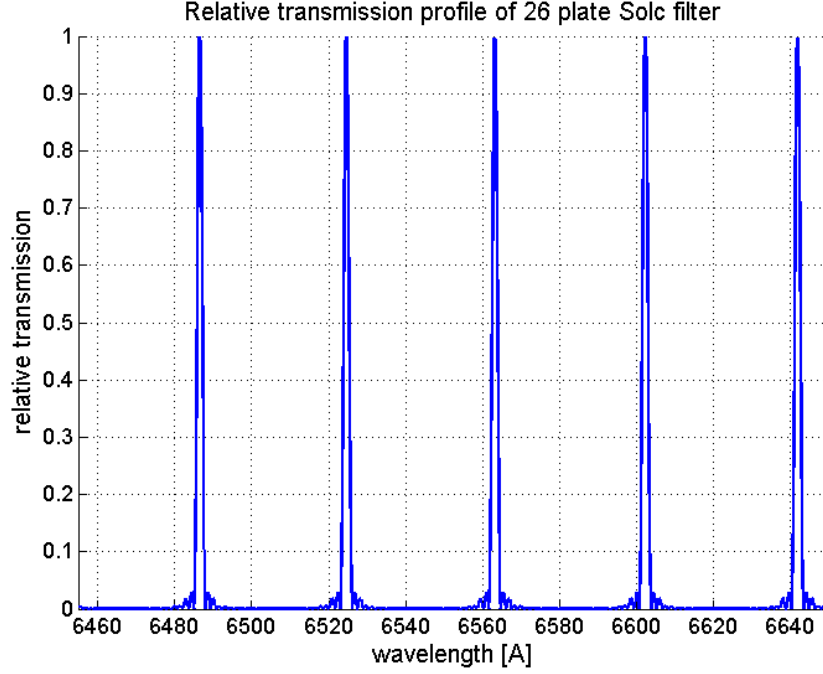
Figure 2.3: Typical relative transmission profile of a 26 plates birefringent narrow band filter of Šolc type. The thickness of one plate is 11.4000 mm.

2.3.2   Filter transmission

Spectral transmission characteristics of Šolc filter depend on four basic properties:

- thickness of plates in a filter

- number of plates within a filter

- birefringence of used material for filter plates

- azimuth distribution of plates

Varying these four properties we can control a full width in a half of a maximum (FWHM) of transmitted peaks, a free spectral range (FSR) of the filter, the magnitude of side transmission peaks and of course a spectral position of transmitted peaks.

Spectral position of transmitted peak

To design a filter for a desired wavelength λ it is convenient to use a combination of equations 2.20 and 2.21 in a form

$$d = K \cdot M(\lambda, T), \qquad (2.23)$$

where d stands for the plate thickness, order of the plate $K = 0.5, 1.5, 2.5, \ldots$ and $M(\lambda, T)$ is a unit thickness for considered material. It is necessary to have in a mind that the unit thickness M is a function of the wavelength λ but also of the temperature T. A filter is usually designed for a higher working temperature (usually about $35\,^\circ\mathrm{C}$ - $40\,^\circ\mathrm{C}$) to prevent its heating from the Sun. Therefore it is necessary to know the function $M(\lambda, T)$ to manufacture the right thickness of the plate. Šolc published a dispersion formula for a crystalline quartz for $22\,^\circ\mathrm{C}$ valid in a spectral region between $0.18\ \mu\mathrm{m} - 4\ \mu\mathrm{m}$ [19]

$$M_{\lambda+\Delta\lambda, 22^\circ\mathrm{C}} = 119.27\lambda + 5\log(\lambda - 0.15) + 0.5\lambda^{4.5} + \frac{5.85}{1 + 1.6\lambda^2} - 7.59 \quad [\mu\mathrm{m}], \qquad (2.24)$$

where

$$\Delta\lambda_{\mathrm{SiO_2}} = -\lambda \cdot 10^{-5}[5.5\log(\lambda - 0.12) + 12.3] \cdot (T - 22) \qquad (2.25)$$

is a wavelength increment we need to consider when the filter is produced for different temperatures then $22\,^\circ\mathrm{C}$.

Šolc birefringent filter can be also designed to transmit more than one desired wavelength at once time (for instance Hα - 6563 Å and HeI line - 10830 Å) [8, 20]. To do this we use the equation 2.23. Šolc birefringent filter is based on plates having the same thickness. The plate of the thickness d has to transmit both wavelengths λ_1 and λ_2, so that

$$d = K_1 \cdot M(\lambda_1, T) = K_2 \cdot M(\lambda_2, T). \qquad (2.26)$$

Choosing the order K_1 we can calculate the value of K_2 as

$$K_2 = K_1 \frac{M(\lambda_1, T)}{M(\lambda_2, T)}. \qquad (2.27)$$

From the equation 2.20 we see that the plate order K_2 needs to be a half of integer number. Therefore we are looking for such a number K_1 that fulfills this condition or is very close to it. Then the condition 2.26 is satisfied and the plate of thickness d transmits both wavelengths λ_1 and λ_2.

Figures 2.4 shows the transmission spectrum for Šolc BF compound of 26 plates of 11.2644 mm thickness designed for $40\,°C$ working temperature at solar spectral lines CaII and HeI.
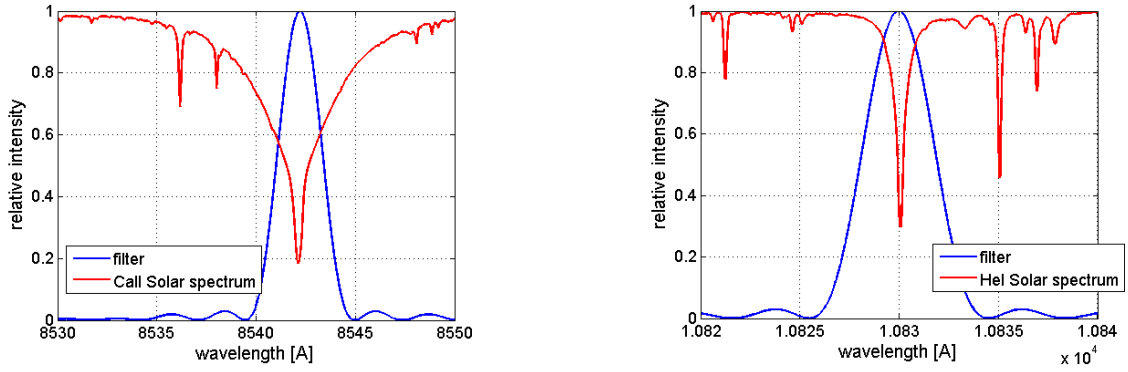
Figure 2.4: Transmission spectrum for Šolc BF compounded of 26 plates of 11.2644 mm thickness designed for $40\,°C$ working temperature at solar spectral lines CaII and HeI.

When deciding on the final plate thickness d it is necessary to be aware also of other things as the possibility to produce the plate (must not be too thin or too thick) or free spectral range of the final filter.

Free Spectral Range

Free spectral range (FSR) is directly determined by a thickness of plates d (if a certain material with a birefringence D is considered) used within a filter through the equation

$$\text{FSR} = \frac{\lambda^2}{d \cdot D} \cdot g, \tag{2.28}$$

where g is defined as

$$g = \left(1 - \frac{\lambda}{D}\frac{\partial D}{\partial \lambda}\right)^{-1}. \tag{2.29}$$

The dependency for a crystalline quartz is shown at figure 2.5.

Full width at half maximum

A full width at a half maximum (FWHM) of a filter is determined by a filter optical thickness. If changed (change of a number of plates N, a plate thickness d or a material birefringence D) one can control FWHM of the filter. This is described as

$$FWHM = 0.90 \cdot \frac{\lambda^2}{N \cdot d \cdot D} \cdot g, \tag{2.30}$$

and expressed at figure 2.6.
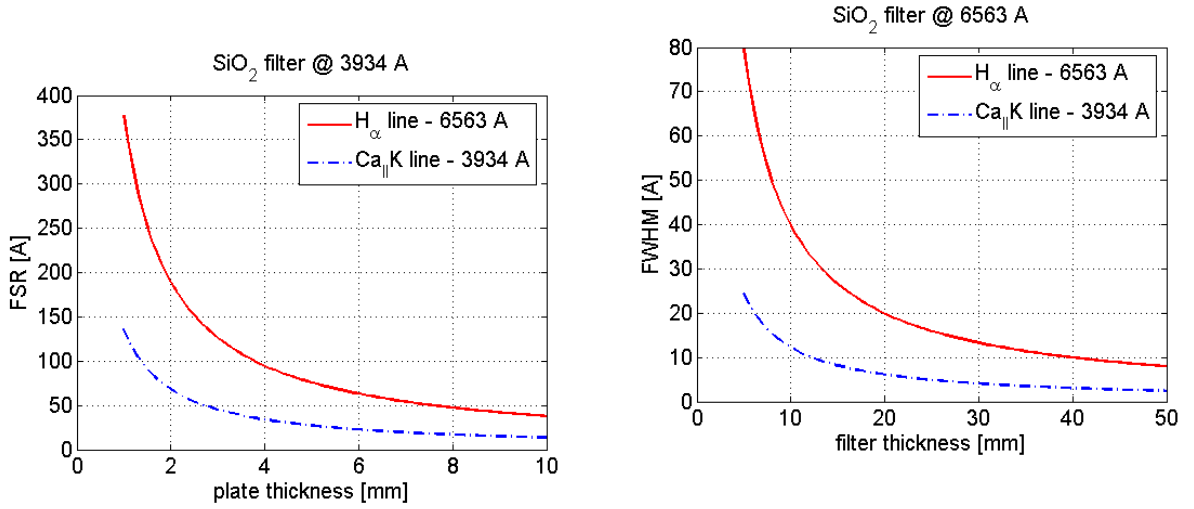
Figure 2.5: Free spectral range of a filter can be controlled by a thickness of plates within a filter.

Figure 2.6: Full width in a half maximum of transmitted peak can be controlled by overall thickness of a filter. One can alter both a thickness of filter plates or a number of plates within a filter.

Magnitude of side peaks

An important characteristic of birefringent narrow band filters is a magnitude of side peaks. A structure of Šolc BF allows controlling this characteristic by changing of a plate azimuth distribution within the filter.

Šolc recognizes two basic modifications of filters with respect to the azimuth distribution. A folded filter and a fan filter [17] (see figure 2.7). The folded filter has crossed

polarizers and the azimuth distribution is

$$\rho_1 = \rho_3 = \rho_5 = \ \ldots \ = \rho_{N-1} = \rho,$$

$$\rho_2 = \rho_4 = \rho_6 = \ \ldots \ = \rho_N = -\rho, \tag{2.31}$$

where N is a number of plates and ρ_i is a plate azimuth. The folded filter has parallel polarizers and the azimuth distribution as follows

$$\rho_1 = \rho, \quad \rho_2 = 3\rho, \quad \rho_3 = 5\rho, \quad \ldots, \rho_q = (2q-1)\rho. \tag{2.32}$$

An intensity of the first side peaks rise over 10 % of the main peak by both basic fan and basic folded BF which is unsatisfactory for many applications. Šolc has shown in [17] and [21] that by using a certain type of the azimuth re-distribution it is possible to achieve a complete attenuation of side peaks in an expense of a main peak widening. In a practise, however, this is not always necessary and a balance between certain values of side peaks amplitutes and the main peak widening is used.
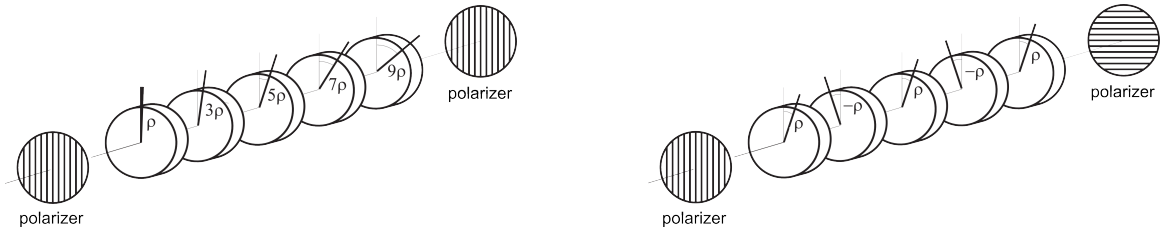
Figure 2.7: Fan and folded type of Šolc birefringent filter.

For further analysis we focus on the folded filter because of its wide usage caused by an easier production technique. However, all concluded results are valid also for the fan filter. In the folded filter the each following azimuth will still change its sign as expressed in equations 2.31 but the absolute values of azimuths ρ_i will no more be a constant as in the basic design but will follow a chosen function. For the maximal transmission of the filter a generalized version of equation 2.22 comes in true

$$\sum_{i=1}^{N} |\rho_i| = 45, \tag{2.33}$$
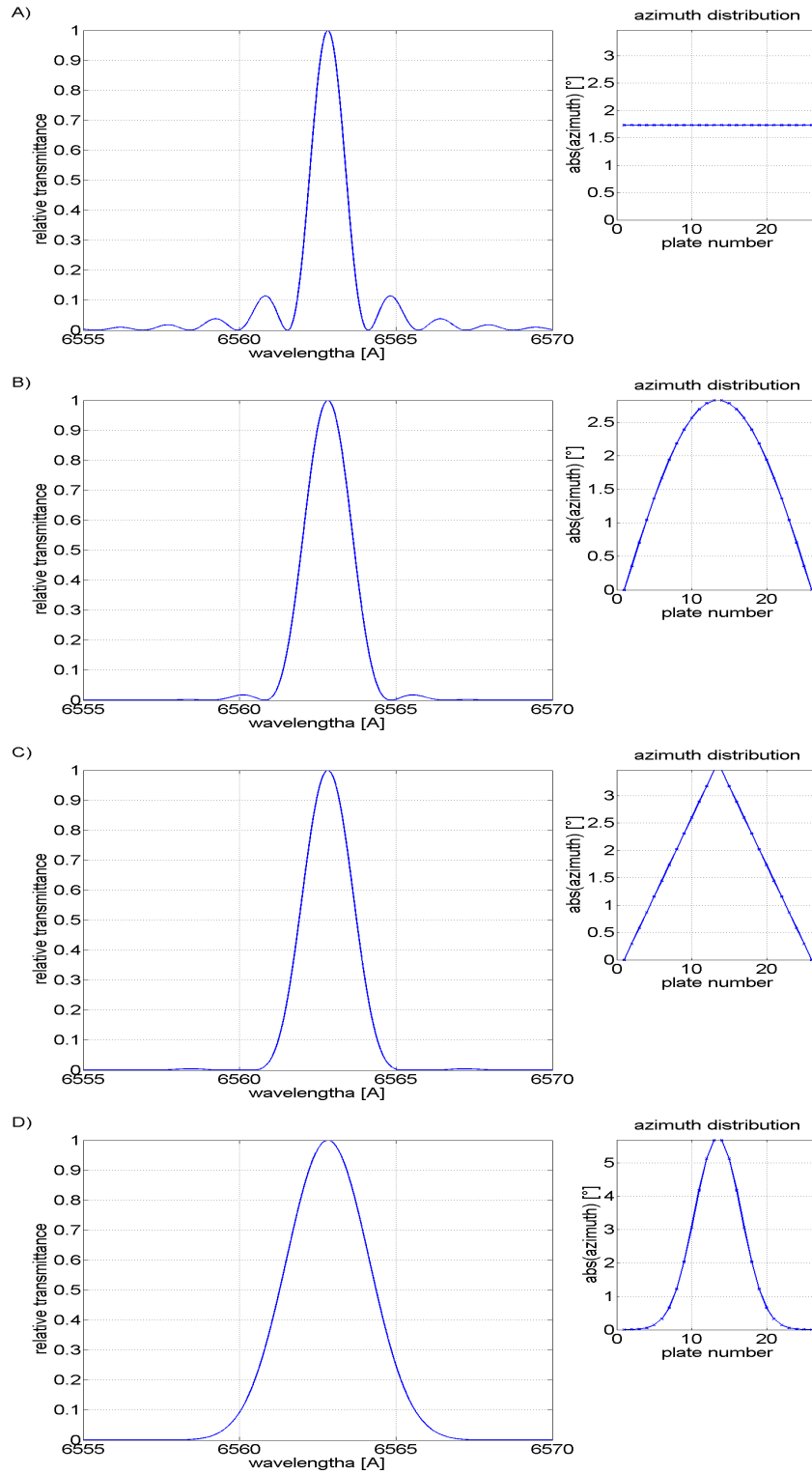
Figure 2.8: Relative filter transmission for different azimuth distributions. A) basic distribution, B) sinus distribution C) triangular distribution and D) Gauss distribution.

Table 2: Characteristics of Šolc BF when applying different azimuth distributions. The calculated filter is compound of 26 crystalline quartz plates of 11.4000 mm thickness each, tuned for Hα line at 6562.8 Å. The main peak FWHM of the filter with basic azimuth distribution is taken as 100 % (1.19 Å) - with respect to that the rest of comparisons are made. Intensities of side peaks are expressed in % of the main peak.

azimuth distribution	FWHM of main maximum [%]	intensity of first side maximum [% of main maximum]
basic distr.	100	11.4
sinus distr.	143	1.8
triangular distr.	155	0.5
Gauss distr.	260	0.0

together with a requirement to be a symmetrical distribution so that

$$\rho_1 = \rho_N, \ \rho_2 = \rho_{N-1}, \ \rho_3 = \rho_{N-2}, \ \ldots . \tag{2.34}$$

The figure 2.8 shows the filter transmission for different azimuth distribution functions. Case A) represents the basic distribution described by equation 2.31; B) describes a sinus azimuth distribution; C) shows a triangular azimuth distribution and D) stands for Gauss azimuth distribution. Numerical values of transmission profiles showed at figure 2.8 are expressed in table 2.

Results from these figures and the table 2 show that suppressing side peaks by the gauss azimuth distribution leads approximately to 2.5× widening of the main peak. Because in a practise it is not necessary to beat the side maxima completely, we can look for a compromise solution when these side maxima are suppressed to tolerable values and simultaneously the width of a main peak is kept minimal.

That can be achieved when the azimuth distribution function slope is less steep in a sense of the figure 2.9. Firstly, a basic azimuth is set as

$$|\rho'| = \frac{45}{N} \, p, \tag{2.35}$$

where a factor p is set from 0.6 to 0.8 [14]. The smaller factor p the smaller values of the side peaks but the FWHM of the main peak stays wide. The higher factor p makes FWHM of the main peak thinner whereas side peaks stays almost unsuppressed. For $p = 1$ we get back to the basic azimuth distribution. The plate azimuth consists of the base azimuth angle ρ' and an angle α_i that is used for the azimuth variation. It can be expressed as

$$\sum_{i=1}^{N} |\rho_i| = |\rho'|N + \sum_{i=1}^{N} |\alpha_i|, \tag{2.36}$$

where $\sum_{i=1}^{N} |\alpha_i|$ is dedicated for the variation of azimuths. However, it is still necessary to keep the sum of absolute azimuth values equal to 45° and the sign of each next azimuth keep swapping a positive and negative value.
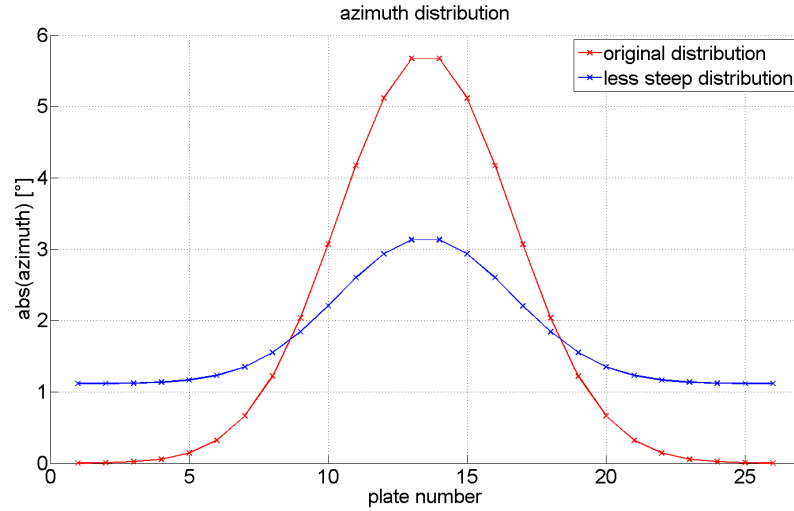
Figure 2.9: Gauss azimuth distribution - original and less steep one.

Figure 2.10 shows an influence of the azimuth distribution slope on transmission peak profiles. Blue lines represent normal azimuth distribution whereas red lines express azimuths variation with factor $p = 0.64$. The numerical values are summarized in table 3. The factor p allowed us to achieve such a BF transmission when side peaks are sufficiently suppressed and main peaks FWHM change within a 126 % range at the same time. Šolc very often used the triangular azimuth distribution with the factor $p \approx 0.65$ when FWHM of the main peak is only 1.1× wider than by the basic distribution without any factor

Table 3: Characteristics of Šolc BF for the modified azimuth distribution ($p = 0.644$). The calculated filter is compound of 26 crystalline quartz plates of 11.4000 mm thickness each, tuned for Hα line at 6562.8 Å. The main peak FWHM of the filter with the basic azimuth distribution is taken as 100 % (1.19 Å) - with respect to that the rest of comparisons are made. Intensities of side peaks are expressed in % of the main peak.

azimuth distribution	FWHM of main maximum [%]	intensity of first side maximum [% of main maximum]
basic distr.	100	11.4
sinus distr.	112	4.7
triangular distr.	114	2.9
Gauss distr.	126	4.7

p and the value of side maxima reaches 2.9 % what is satisfactory for most applications [14].

2.3.3 Tuning of Šolc birefringent filter

Fast and precise tuning of filters is becoming very important these days. Solar physicists use it to get information on dynamics of solar flares mass that travel in different directions with certain velocities for instance. This information is projected into observed spectral characteristics as wavelength shifts.

There are several possibilities how to control spectral position of transmitted peaks. Some of them are used also for final correction when the filter is calibrated because of their stability (temperature tuning) whereas others are used for fast re-tuning of BF (inclination of BF or oblique cut filters).

A chosen way of tuning affects a filter design and the way it is produced. Some of tuning strategies make the filter very complex and easy to tune whereas others enable an easy production of the filter but low tuning capabilities.
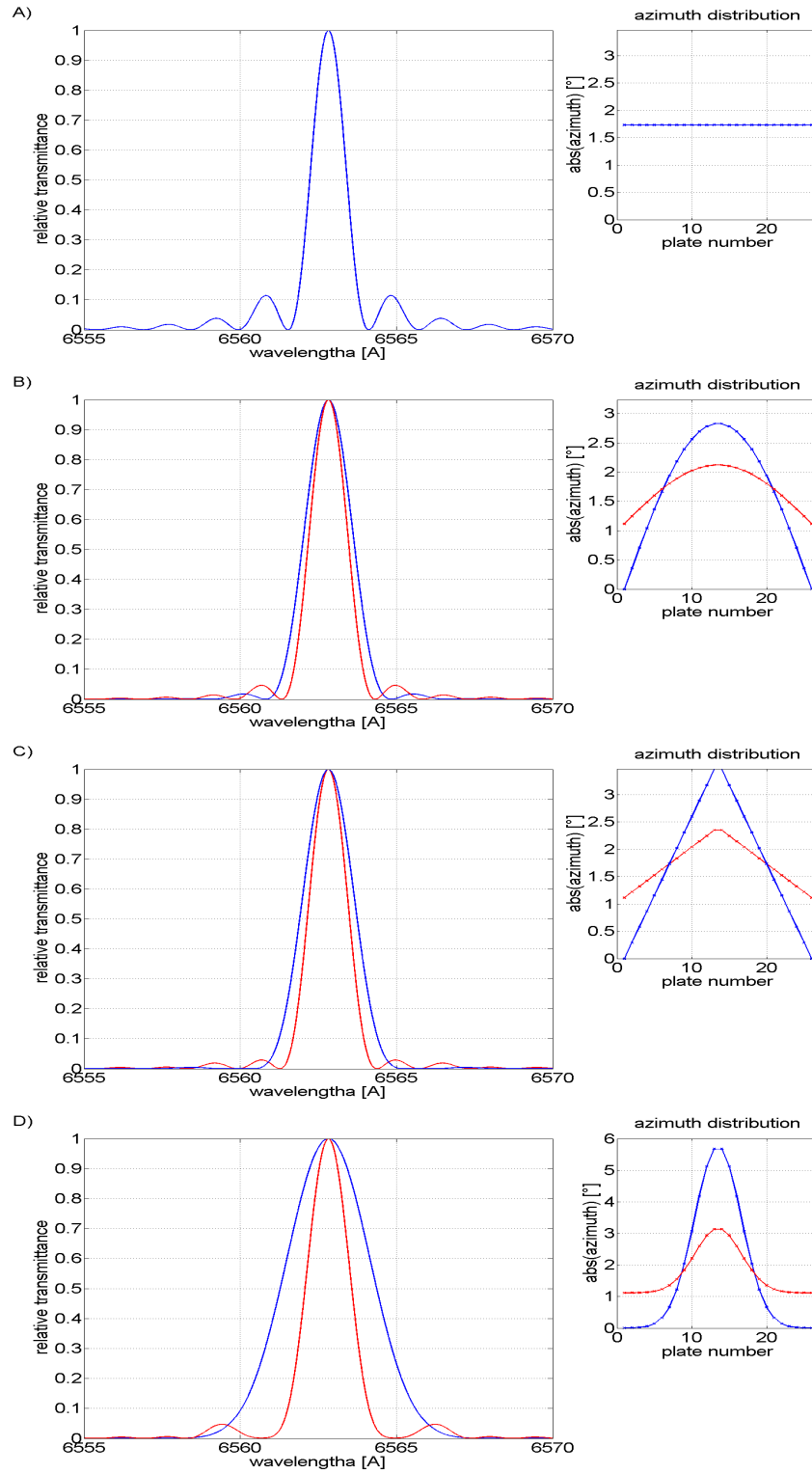
Figure 2.10: Relative filter transmission for different azimuth distributions. Blue lines represent original azimuth distributions whereas red lines show modified ones.

crystal	C [1/°C]
quartz	$-1.05 \cdot 10^{-4}$
calcite	$-0.06 \cdot 10^{-4}$

crystal	thermal conductivity [$\frac{\mathrm{W}}{\mathrm{mK}}$]
quartz	$a\| = 9.5, a\perp = 6.10$ @ 300 K
calcite	$a\| = 5.526, a\perp = 4.646$ @ 273 K

Table 4: Coefficients of birefringent temperature dependency characteristics.

Table 5: Thermal conductivity for selected birefringent materials.

Temperature tuning

The ability of the filter temperature tuning is driven by a dependency of a birefringence on a temperature. The characteristics of the filter spectral tuning can be approximately expressed as

$$\Delta\lambda = C \cdot \lambda \cdot \Delta T, \tag{2.37}$$

where $\Delta\lambda$ stands for a shift of filter transmitted wavelength λ caused by a temperature change ΔT. Table 4 shows coefficients C for two most often used materials BF are made of.

The change of 1 °C of quartz filter at Hα line (6562.8 Å) leads to approx. 0.7 Å spectral shift. Having a fine performance filter it is necessary to have it placed in a thermostated cavity in order to keep the filter spectrally stabilized.

A thermal conductivity of used materials (see table 5) determines a speed of the spectral tuning. Usual re-tuning times for a typical BF from one spectral line to another is in a range of tenths of minutes. Such times are not suitable for observation of fast events. However, this type of tuning can be used for long time observations when fast tuning is not necessary.

Inclination tuning

Another type of BF tuning employs an ellipsoidal shape of optical indicatrix of uniaxial crystals. Filter plates are usually cut from a crystal in a way that an optical axis lies in a plane of the plate. This cut of plates assures a maximal birefringence D.

For simplicity we consider one plate. When a beam of light incidents the inclined plate a path retardance is changed depending on a direction of the inclination. There are two main directions of the inclination. In the first one the light beam incidents the plate under an angle φ in a plane determined by a plate normal and a main direction that is perpendicular to the crystal optical axis z (see figure 2.11). The birefringence does not vary with a change of the incident angle φ. The path retardance is changed via the plate thickness and can be expressed as

$$\Delta_{(\varphi,\perp)} = D \; d_{(\varphi)} = D \, d \, \frac{1}{\cos(\psi)} = D \, d \, \frac{n}{\sqrt{n^2 - \sin^2 \varphi}}. \tag{2.38}$$

where n stands for $\frac{n_e + n_o}{2}$ for small angles of inclinations.

In the second direction of the inclination the light beam is inclined from the plate's normal in a plane that is determined by the plate's normal and the crystal optical axis z (see figure 2.12). This time both the birefringence D and the plate thickness d vary with φ as

$$D_{(\varphi)} = D \; \cos^2 \psi, \tag{2.39}$$

$$d_{(\varphi)} = \frac{d}{\cos(\psi)}. \tag{2.40}$$

The path retardance can be expressed as

$$\Delta_{(\varphi,\parallel)} = D_{(\varphi)} \; d_{(\varphi)} = D \, d \; \cos(\psi) = D \, d \, \frac{\sqrt{n^2 - \sin^2 \varphi}}{n}. \tag{2.41}$$

The dependency of tuning λ/λ_0 on the inclination angle φ defined by equations 2.38 and 2.41 is expressed by figure 2.13.

Special way of tuning

There are also another way of tuning birefringent filters. One of them is electro-optical tuning that employs electro-optical activity of several crystals to change its birefringence. Or there can be used liquid crystals that change orientation of their optical axis by applying electrical field. Change of birefringence can be achieved also by magneto-optics. Even thought all these type of tuning are possible they are out of this thesis scope. Detailed description of the physical tuning principles can be found for example in [22].
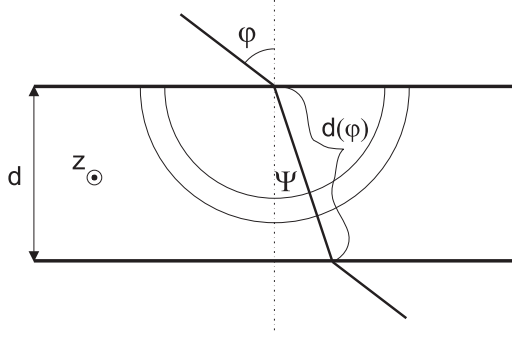
Figure 2.11: Direction of an incident ray is deviated by an angle φ in a plane determined by a plate normal and crystal main direction lying perpendicular to the crystal optical axis. The birefringence D is not dependent on the incident angle φ.
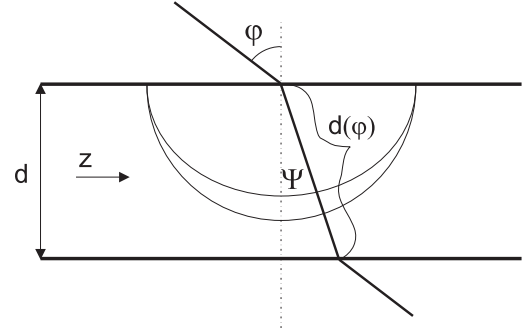
Figure 2.12: Direction of an incident ray is deviated by an angle φ in a plane determined by a plate normal and the crystal optical axis. The birefringence D is in this case dependent on the incident angle φ.
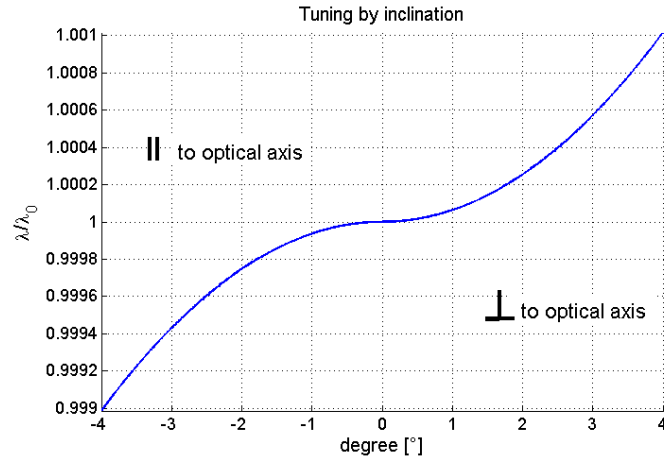
Figure 2.13: Inclination tuning dependency of a filter.

2.3.4   Field of view of Šolc birefringent filter

Another important characteristic of BF is a field of view or an acceptance angle at which it collects light of a tolerable wavelength region. BF exhibits a very broad field of view (in contrast to e.g. Fabry-Perot filters) what makes them perfect for spectrally discrete observation of angularly wide object as for an instance the Sun is. Moreover the field of view can be even more expanded by a certain combination of crystalline plates.

A shape of the spectrally discrete field of view of the BF is driven by an ellipsoidal shape of optical indicatrix of used material. We have already mentioned that in the section 2.3.3 describing the inclination way of BF tuning. In a BF plate there are two main directions with respect to the maximal change of the plate retardance. They are expressed by equations 2.38 and 2.41. From these equations we can express the change of the wavelength with the angle of the beam with respect to the optical axis as

$$\lambda_\perp = \lambda_0 \; \frac{n}{\sqrt{n^2 - \sin^2 \varphi}}, \tag{2.42}$$

$$\lambda_\parallel = \lambda_0 \; \frac{\sqrt{n^2 - \sin^2 \varphi}}{n}. \tag{2.43}$$

Graphically it can be presented with the same figure as 2.13. Figure 2.14 shows a 2D transmission profile of a BF designed for Hα line (6562.8 Å) with 1 Å FWHM that observes 1° object of interest - e.g. Sun with its corona. We can see that directions parallel with an optical axis transmits shorter wavelength whereas directions perpendicular to the optical axis transmits longer wavelengths.
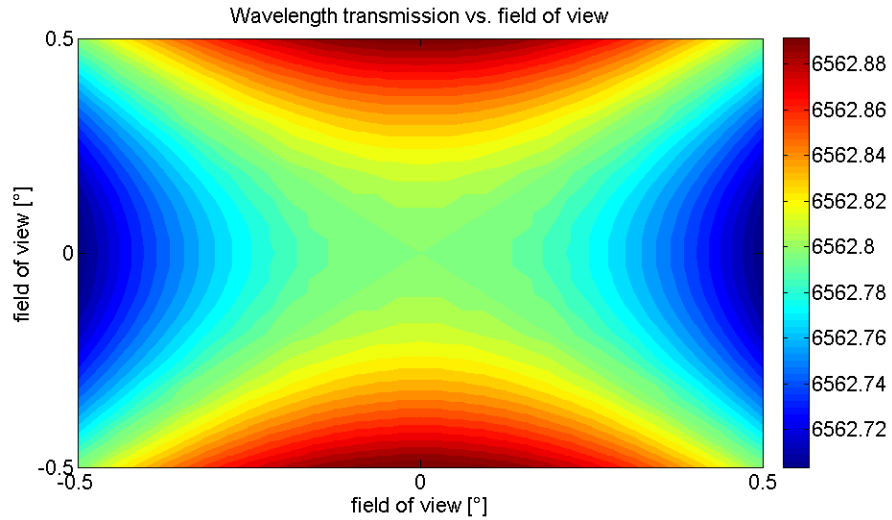
Figure 2.14: Field of view vs. wavelength transmission of BF designed for Hα line (6562.8 Å) with 1 Å FWHM that observes 1° object of interest.

If there is a need of a wider field of view there are possibilities how to achieve that with a combination of birefringent plates. The first way is to combine positive and negative

crystal plates (e.g. ADP and quartz). When combining such two plates we need to set them in a way that their path retardance is added. That occurs when their optical axes lie perpendicularly to each other (see figure 2.15). From this figure we can also see that by an inclination of this set of plates the multiple $d \cdot D$ is increasing in one plate while in the other one it is decreasing. To beat the dependency on the incident angle φ the sum of plates path retardance need to be equal to the sum of path retardance for perpendicular incident

$$d_1 \; D_1 \; \frac{n_1}{\sqrt{n_1^2 - \sin^2 \varphi}} + d_2 \; D_2 \; \frac{\sqrt{n_2^2 - \sin^2 \varphi}}{n_2} = d_1 \; D_1 + d_2 \; D_2, \qquad (2.44)$$

where index numbering 1 and 2 express positive and negative birefringent material. It is convenient to define a ratio $P = \frac{d_1 D_1}{d_2 D_2}$ that will define the ratio of negative and positive crystal plate thickness. From the previous equation we got

$$P \; \frac{n_1}{\sqrt{n_1^2 - \sin^2 \varphi}} + \frac{\sqrt{n_2^2 - \sin^2 \varphi}}{n_2} = P + 1. \qquad (2.45)$$

where the P can be extracted from as

$$P = \frac{(n_2 - \sqrt{n_2^2 - \sin^2 \varphi}) \cdot \sqrt{n_1^2 - \sin^2 \varphi}}{n_2(n_1 - \sqrt{n_1^2 - \sin^2 \varphi})}. \qquad (2.46)$$

Making an assumption of small angle φ we can write

$$P = \frac{2n_1^2 - \sin^2 \varphi}{2n_2^2}. \qquad (2.47)$$

When we neglect $\sin^2 \varphi$ against $2n_1^2$ we got

$$P = \frac{n_1^2}{n_2^2}, \qquad (2.48)$$

or

$$\frac{d_1}{d_2} = \frac{n_1^2}{n_2^2} \cdot \frac{D_2}{D_1}, \qquad (2.49)$$

what actually is the seeking ratio. By applying of this technique we can achieve about $20\times$ wider field of view [23]. The basic formula for a calculation of the filter plate thickness 2.20 reaches a form

$$d_1 \cdot D_1 + d_2 \cdot D_2 = K \cdot \lambda. \qquad (2.50)$$

Another possibility how to wider a field of view is to combine the same crystal plates. Each crystal plate is divided into two halves. Their optical axes are perpendicular to each
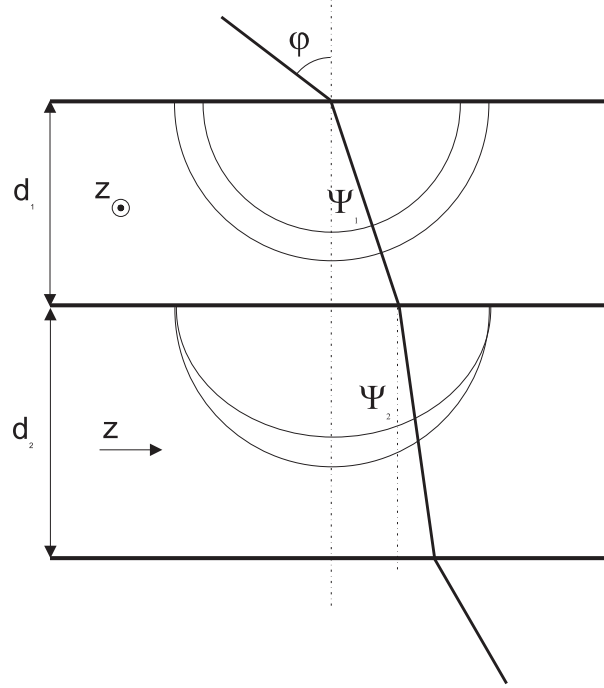
Figure 2.15: Additive set of positive and negative birefringent crystal plates.

other and there is placed another additional $\lambda/2$ waveplate with $45°$. This setting of plates is the same from the optical point of view as the positive-negative crystal combination. The $\lambda/2$ waveplate takes care about the additive setting of both half plates (see figure 2.16).

The basic formula for a calculation of the filter plate thickness 2.20 then reaches a form

$$2 \cdot d \cdot D = K \cdot \lambda. \tag{2.51}$$

By applying this method where we realized the independency of BF on the incident beam angle φ we eliminate the inclination tuning possibility so that the tuning needs to be achieved by another techniques described in the section 2.3.3.

There is also possibility to use another types of materials those allow wider "monochromatic" field of view. The fractional wavelength shift as a function of an angle away from
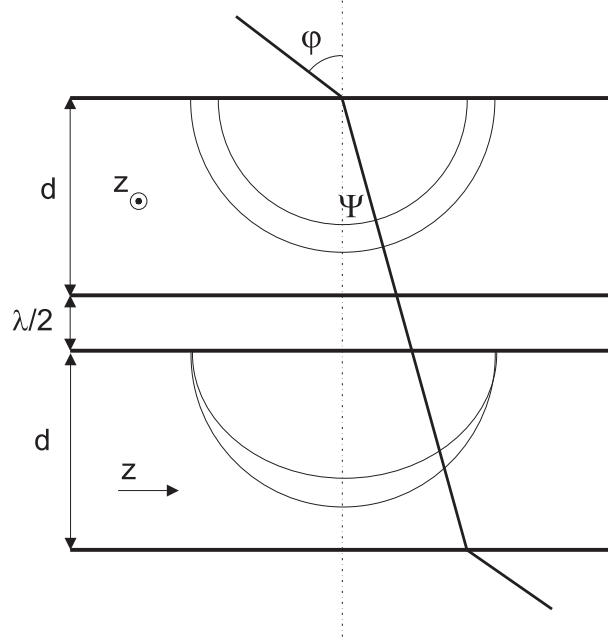
Figure 2.16: Set of two halves of a birefringent plate with $\lambda/2$ waveplate that provides an additive setting.

the filter normal φ can be expressed to the second order [24] as

$$\frac{\Delta\lambda}{\lambda} = -\frac{1}{4n_{\mathrm{o}}^2}\left(\frac{D}{n_{\mathrm{e}}}\right)\sin^2(\varphi) = F\cdot\sin^2(\varphi). \tag{2.52}$$

Taking a detailed look at the given formula we can see that materials with a high refractive index and a low birefringence (F value) give a better angular performance. Table 6 summarize currently available birefringent materials and its F values.

There are also another ways how to enlarge the field of view of BFs but their are rare in use. One of them applies a change of a surface shape of a birefringent plate. To determine the shape of the surface the equations 2.38 and 2.41 need to be taken into account. The final solution leads to a saddle surface shape. Another technique employs a temperature gradient when plates are cooled in a direction of one main direction whereas heated in the other main direction. More can be read in [15] or [14].

2.3.5   Barrier filters

A typical spectral characteristic of Šolc type BF is a channel spectrum (see figure 2.17). Observing of interesting phenomenons, however, occurs only on one discrete wavelength. From this reason it is necessary to provide a shielding of transmitted neighbor maxima of the desired wavelength by another optical element. It is suitable to use another BF of Šolc type with a different plate thickness. This so called "barrier element" shields out a certain number of neighbor transmitted peaks as showed on figure 2.18, where each filter has a slightly different plate thickness d. The rest of transmitted wavelengths can be easily blocked by wide interference filters or by colored glasses. A detailed method of designing such a barrier filter can be found in [25] or [15].
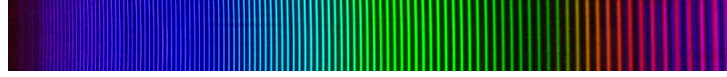
Figure 2.17: A typical channel spectrum of Šolc type BF.
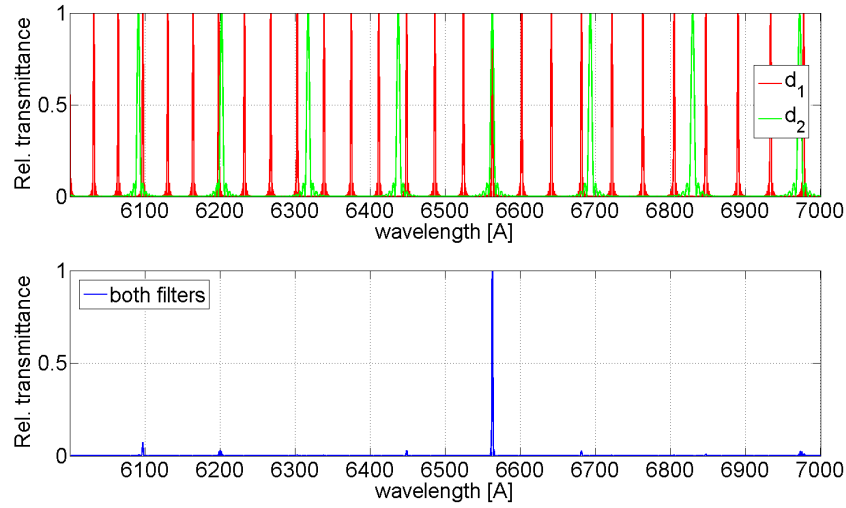
Figure 2.18: A barrier filter of the plate thickness d_2 blocks neighbor peaks of the main filter of the plate thickness d_1. As a result only one designed wavelength in a broad spectral range is transmitted.

Table 6: Table of birefringent materials and their characteristics.

crystal	D@Hα	n_e@Hα	n_o@Hα	diameter [mm]	absolute value of F	length of 1Å filter@Hα [mm]
TiO$_2$ (rutile)	0.282	2.865	2.583	25	3.88E-03	14
YVO$_4$	0.2225	2.2154	1.9929	38	6.32E-03	17
CaCO$_3$ (calcite)	-0.1705	1.4852	1.6557	40		
PbMoO$_4$	-0.124	2.262	2.386	60	2.38E-03	31
α-BBO	-0.1194	1.5555	1.6749	50	6.79E-03	32
TeO$_2$ (paratellurite)	-0.118	2.142	2.26	50	3.11E-03	25
LiNbO$_3$	-0.083	2.203	2.286	100	1.81E-03	46
ADP	-0.04468	1.47727	1.52195		3.21E-03	87
KDP	-0.04052	1.46685	1.50737		3.02E-03	94
MgF$_2$	0.0121	1.3957	1.3836	120	1.12E-03	322
SiO$_2$ (quartz)	0.0091	1.5518	1.5427	100	6.13E-04	419
Al$_2$O$_3$ (sapphire)	-0.00815	1.76355	1.7717		3.66E-04	473

2.3.6   Materials for birefringent filters

On a market there are several birefringent materials that can be used for a BF production. The materials have different physical and economical properties which everybody needs to balance with respect to a specific application. Materials and their properties relevant for BF are stated in the table 6. All values are referred to solar Hα line - 6563 Å. The "diameter" column expresses the maximal available diameter the crystal can be obtained, however, it is important to notice that quality of crystals is needed to be on a highest level for BF application - especially for high birefringence and big diameter crystals - which is not easy to satisfy. These data were obtained by extensive internet and crystal company research. Last column expresses what should be the approximative total length of the filter to reach certain FWHM at Hα line - it is used basic azimuthal distribution (see section 2.3.2).

2.4   Tolerances of Šolc type BF

BF are usually compound of 10 to 30 birefringent plates. Because of production and measurement methods there can be achieved only certain values of precision of different plate's features. Each plate is then actually introducing an error into an ideally designed system. The key features that affects the filter performance with higher or smaller impact are as follows:

- plate thickness

- plate azimuth orientation

- orientation of the plate with respect to a crystal lattice

- temperature

In the following we discuss each feature influence in a closer detail.

2.4.1   Thickness tolerances

The plate thickness plays a most important role in designing BF (see equation 2.23), therefore all thickness deviations from designed values will result in a decrease of BF performance - the transmitted peak can be widen, spectrally shifted, deformed or secondary maxima can arise.
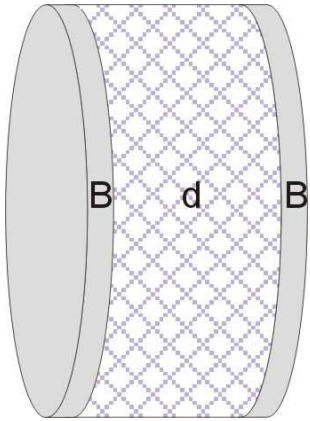
Figure 2.19: Amorphous Beilby layers arise on the crystal during the polishing process.

Especially, during the process of grinding and polishing of crystalline materials a thin layers showing no birefringence arise on both sides of the plate. These layers, called Beilby layers, therefore should be involved in BF design formulae as

$$d = K \cdot M(\lambda, t) + 2B, \qquad (2.53)$$

where B stands for the thickness of Beilby layer. Theory of these layers is very complex and it worths for its own publication. It shows for example that between amorphous surface of and crystalline base there are transition layers where the bottom ones express a residual amount of birefringence. However, we focus here on technologically important values. For a most advantageous birefringent cut of quartz that is perpendicular to the mechanical axis of Y crystal (direction parallel with basic prism plane) it was determined [14] that a thickness of Beilby layer is

$$B = 0.12 \, \mu\text{m} - 0.30 \, \mu\text{m}$$

when polishing technology using optical pitch and FeO_2 is used. For calcite (using the same production technique) the Beilby layer was determined as

$$B = 0.15 \, \mu\text{m} - 1.00 \, \mu\text{m}.$$

These effective values comes from an extended research of many series of samples using optical and X-ray methods [19]. These values are averaged, however, for most application are satisfactory.

An effect of different plate thicknesses can be usually canceled out during a production process when BF plates are made. Because Šolc type filter has all plates of the same thickness they can be processed (and very often are) on one baseplate. This assures that all plates have the same thickness. However, Beilby layer can vary by each of plate. Therefore the precision is within 0.3 μm for quartz and 1 μm for calcite.

2.4.2   Azimuth tolerances

Another important quantity that drives mainly the size of side peaks amplitudes of the transmission characteristic is an azimuth of a plate.

The azimuth of a plate (orientation of the fast and slow axis within the crystal) can be roughly found between crossed polarizers. When the plate rotates about an angle α then the plane of polarized light rotates about 2α, where α is the angle between the first

polarizer and the optical axis of the measured plate. To be able to distinguish between fast and slow axis (main direction) within the crystal we can place this optical system (measured birefringent plate between crossed polarizers) into a spectrometer. Inclining the plate the observed channel spectrum will move to shorter or longer wavelengths depending on whether the inclination is practised along the fast axis or slow one (see figure 2.22; for mathematical expressions see the section 2.3.3). It does not matter which axis we choose for the plate, however, all plates need to be chosen in the same way. Using this rough technique we measure the plate azimuth usually within 5° precision.

High performance filters like BF need more precise azimuth orientation, usually within a magnitude of several arc minutes. This can be achieved by employing half-shade accessories. One of the half-shade techniques is based on Nakamura double plate. It uses a phenomenon of an optical activity of a quartz crystal. The optical activity can rotate a plane of polarization even so when light is traveling along the optical axis. Moreover, the crystalline quartz can be found in a nature in two forms with respect to the optical activity. So-called left handed crystals and right-handed crystals which rotate the polarization plane into contrary directions. The Nakamura bi-plate consists of one half of right-handed and one half of left-handed crystal. Their thickness is the same, but through the optical activity the halves rotate the plane of polarization into opposite angles ($+\delta$ and $-\delta$). When looked at Nakamura bi-plate between crossed polarizers a minimal light intensity is not achieved and a field of view appears grey instead (the plane of polarization is rotated about $\pm\delta$). Inserting the inspected birefringent plate between one polarizer and Nakamura bi-plate the field of view will appears divided into two halves with different intensities when plate is rotated about an angle α with respect to the entrance polarizer (see figure 2.20). Only when birefringent plate is azimuthally parallel with the entrance polarizer the entire field of view appears constantly grey (see figure 2.21). With a human eye as a logarithmic detector one can easily orient the azimuth of plate within 1 arc minute precision.
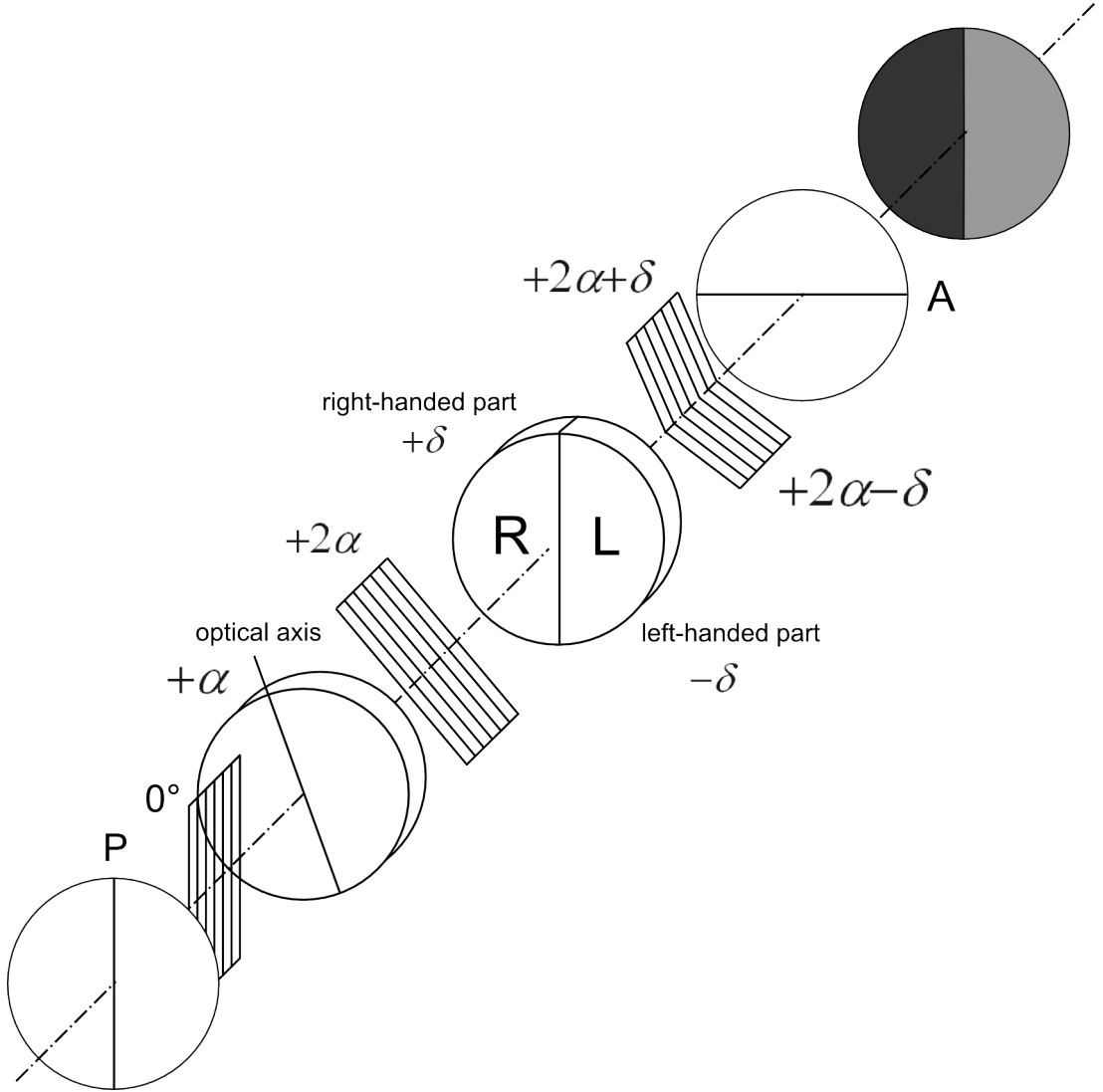
Figure 2.20: Scheme of an optical setup for BF plate azimuth orientation. When a plate is rotated about an angle α then a field of view is divided into two halves with different intensities thanks to Nakamura bi-plate.

2.4.3   Crystal lattice orientation tolerances

A precise orientation of a crystal lattice with respect to a plate surface is another driver of high performance BF. It influences mainly a shape of transmitted peak, and therefore both FWHM and the magnitudes of side maxima.

To control it some optical methods can be used but they result only in order of several degree precision. One of these methods that is widely used employs Armand de Gramond
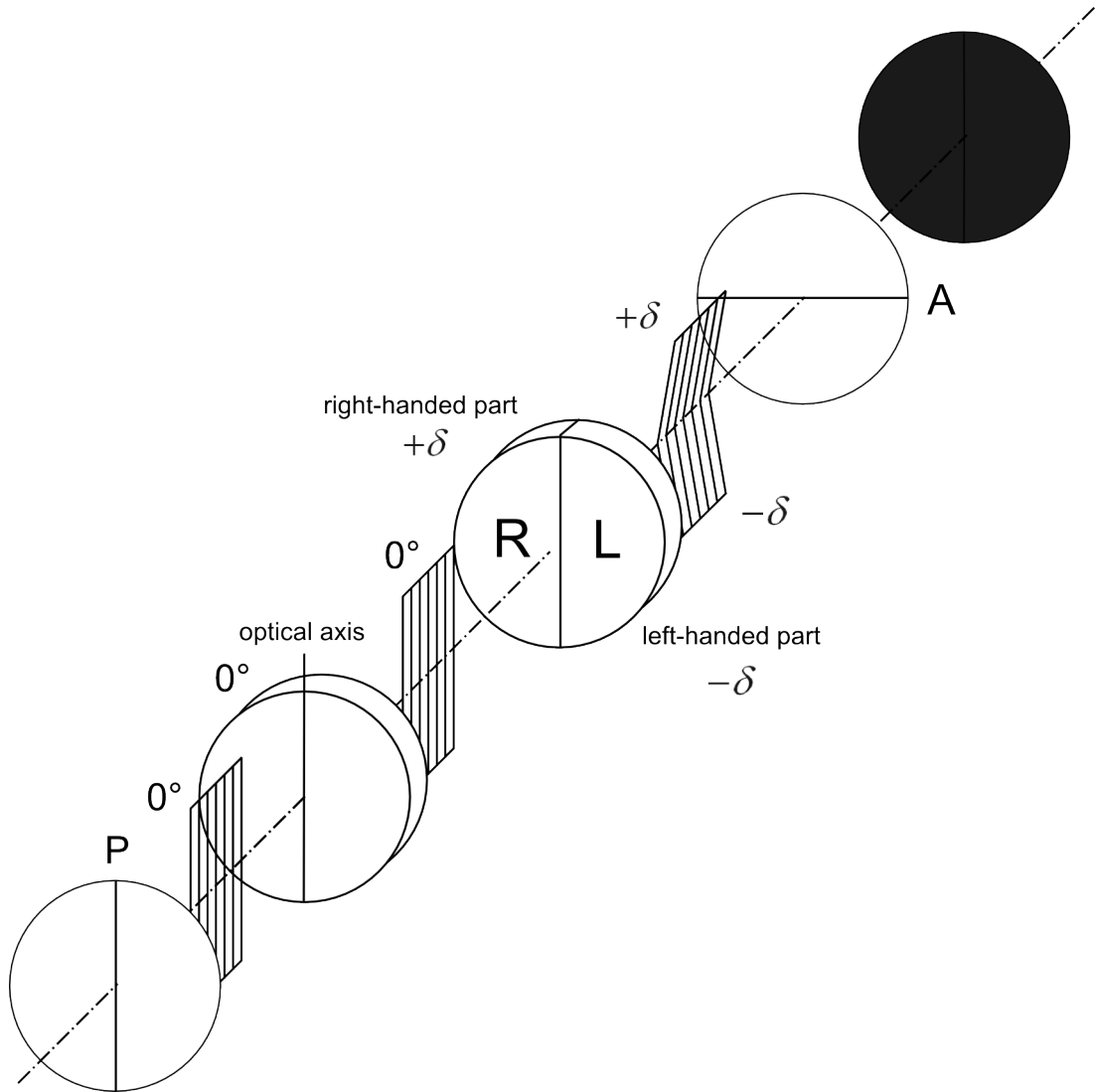
Figure 2.21: Scheme of an optical setup for BF plate azimuth orientation. When a plate is azimuthally parallel with the entrance polarizer then a field of view appears constantly grey thanks to Nakamura bi-plate.

sphere. It is used mainly when plates are cut from raw crystals. It utilizes unique reflection from natural surfaces of the crystal and projects them on the half-sphere. Using this technique crystal lattice vs. birefringent plate surface can be oriented with approximately $2°$ precision. To achieve the orientation within a precision of minutes it is necessary to employ X-ray goniometer [26].
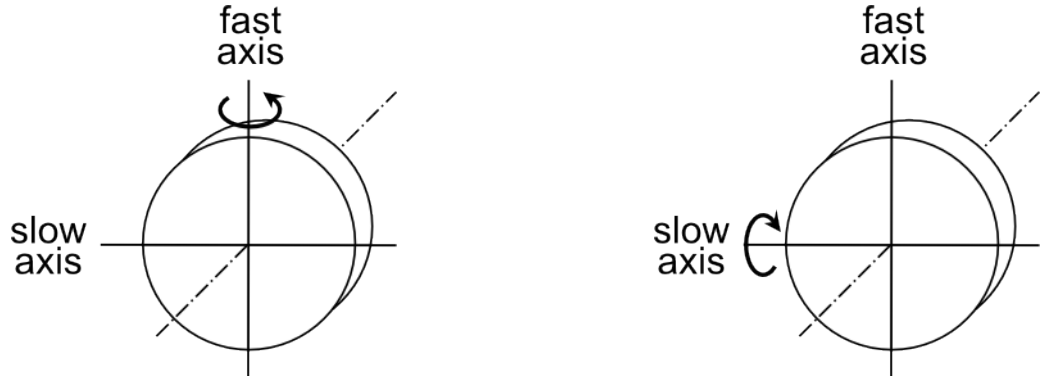
Figure 2.22: Inclination along fast or slow axis of the plate results into a shift to shorter or longer wavelengths when spectrally inspected.

2.4.4   Temperature tolerances

When observing with BF it is important to stabilize a temperature of the filter because it can fluctuate during a solar observation when not controlled. The variation of filter temperature does not change a shape of transmitted peaks or their side maxima, but spectrally shift them. The precision of stabilization depends on the performance of the filter. For instance, frequently used filters for observation at Hα line (6563 Å) have usually 1 Å FWHM. If made of crystalline quartz the transmitted wavelength shift is approximately 0.7 Å per 1 °C. Therefore a thermostated box for BF with precision of 0.1 °C is sufficient in this case.

2.5   Other narrow band filters

In the following section there are described another types of narrow band filter.

2.5.1   Wood filter

Wood birefringent filter consists of two polarizers and a crystalline quartz plate cut parallel with its optical axis (see figure 2.23). It is suitable as a separator of two near spectral lines as for an example the sodium doublet 5890 Å and 5896 Å (see figure 2.24). Rotation of one polarizer from the parallel to crossed position changes the transmitted wavelength. The thickness of the plate depends on wavelengths we want to separate. For already given example of sodium doublet it gives the thickness of approximately 31.8

mm (it depends also on operated temperature). This type of filter is widely used in interferometers that use a sodium discharge lamp as a source. The filter helps to enhance a contrast of interferometric fringes.
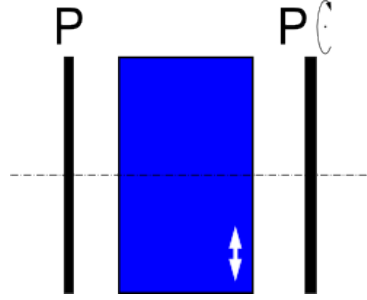
Figure 2.23: Wood birefringent filter - thick birefringent plate sandwiched between pair of polarizers.
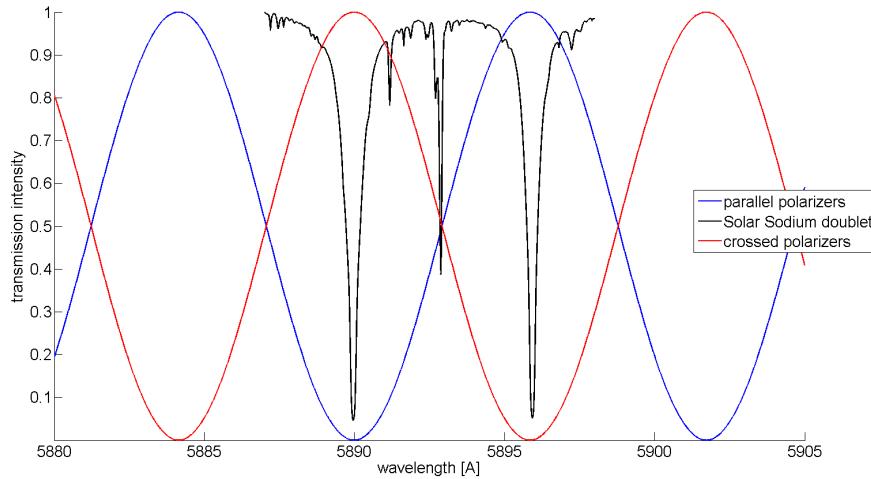
Figure 2.24: Wood birefringent filter can be used for separation of two close spectral line as for instance the sodium doublet is.

2.5.2   Lyot filter

Widely used type of a birefringent filter for solar observations is Lyot filter. This filter is in fact constructed from several Wood filters serially lined up. The thickness d of the first plate is such that transmits the requested wavelength and provides the requested performance of the filter. Each next birefringent plate has a half thickness of the previous

one. That provides two facts, firstly, the requested wavelength is transmitted and secondly, the neighbor transmitted peaks of the previous birefringent plate are filtered out (see figure 2.26).

There is a disadvantage of the Lyot filter in a low intensity transmittance which is caused by numerous polarizers placed inside the filter.
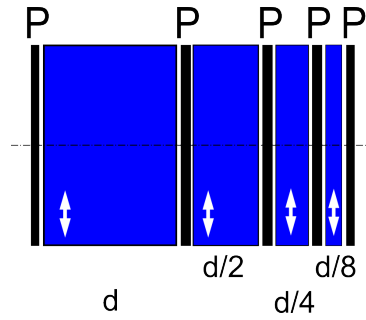
Figure 2.25: Lyot birefringent filter - birefringent plates sandwiched between pairs of polarizers.
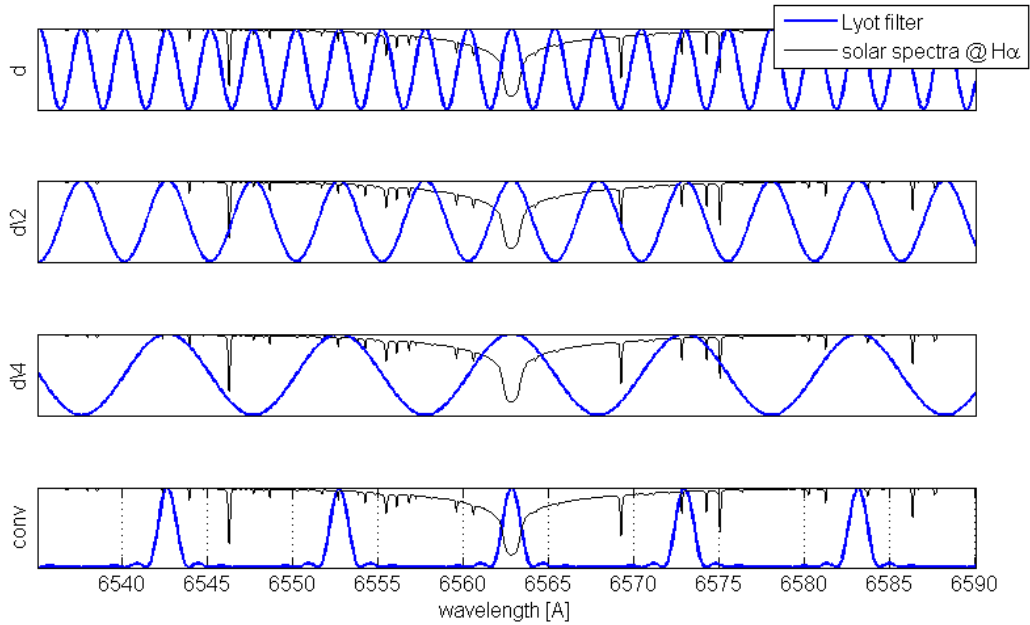
Figure 2.26: First three rows shows transmission profile of individual plates of Lyot birefringent filter. The last row shows the transmission profile of the whole filter.

2.5.3 Lyot element

Lyot has described also wide-angle tunable version of its filter. The design of the Lyot element is at figure 2.27. It consists of two halves of a birefringent plate C1. Between the halves there is placed an $\lambda/2$ waveplate that assures an additive superposition of C1 halves and provides the wide-angle capability. Last $\lambda/4$ waveplate provides the tuning capability of the element. The tuning is then realized by the rotation of the exit polarizer, however can be realized only for such a spectral region where $\lambda/2$ and $\lambda/4$ are designed for - in practise those are usually two chosen spectral lines (double wavelength waveplates). An advantage of such an element is an ability of rapid tuning on spectrally small but interesting region just by a rotation of the exit polarizer.
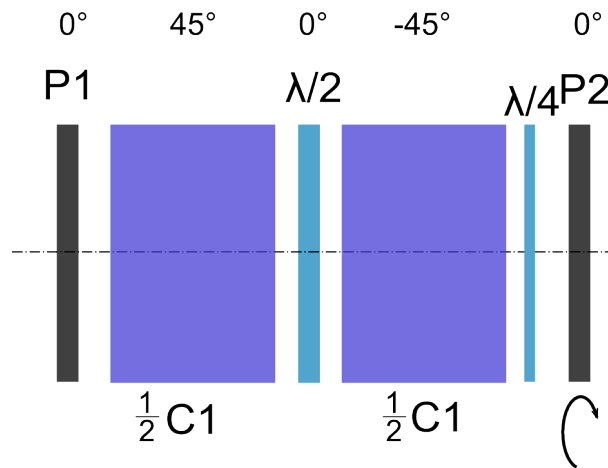
Figure 2.27: Design of wide-angle Lyot element. It consists of two halves of a birefringent plate C1 and $\lambda/2$ and $\lambda/4$, all sandwiched between polarizers.

2.5.4 Evans element

Another easily tunable birefringent element is Evans element (see figure 2.28). It consists of two birefringent plates C1 and C2 divided into halves. C1 is half a thickness of C2 and provides shielding of every second transmittance peak of C2 plate. C2 plate is also divided into two halves separated by a pair of $\lambda/4$ waveplates between which a rotatable $\lambda/2$ waveplate is placed. Birefringent plate C2 is then tunable and wide-angle. The advantage of Evans element in comparison with Lyot element is an reduction of number

of polarizers by one and therefore provides higher transmittance. However, the tuning capability is again limited to the working spectral region of $\lambda/2$ and $\lambda/4$ waveplates.
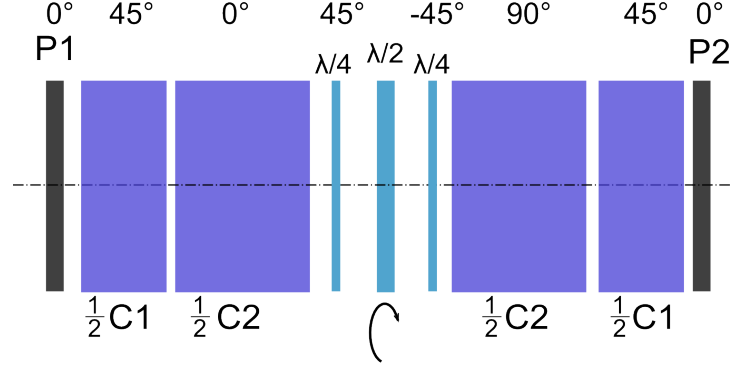
Figure 2.28: Design of wide-angle Evans element. It consist of two pairs of birefringent plates C1 and C2, two $\lambda/4$ waveplates and rotatable $\lambda/2$ waveplate, all sandwiched between polarizers.

2.5.5   Fabry-Peròt filter

These days a widely used type of filter for spectrally narrow band observations is a Fabry-Peròt (FP) filter (figure 2.29) [27]. It is based on an interference principle where a cavity of an optical length $n \cdot l$ transmits only wavelengths λ that fulfill the equation

$$n \cdot l = q \cdot \lambda/2, \tag{2.54}$$

where n is a refractive index of a cavity matter, l is its geometrical length and q is an integer number.

Fabry-Peròt interference filter phase difference can be expressed as

$$\Gamma = \left(\frac{2\pi}{\lambda}\right) 2nl \cos\theta. \tag{2.55}$$

A transmission function T follows the equation

$$T = \frac{(1-R)^2}{1 + R^2 - 2R\cos\Gamma}, \tag{2.56}$$

where R stands for a reflectance of both of FP filter sides. The free spectral range (FSR) of FP filter can be expressed as

$$\text{FSR} = \frac{\lambda_0^2}{2nl \cos\theta + \lambda_0} \approx \frac{\lambda_0^2}{2nl \cos\theta}, \tag{2.57}$$
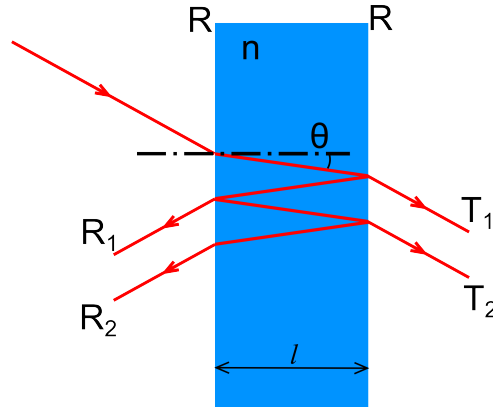
Figure 2.29: Scheme of Fabry-Peròt filter.

where λ_0 is a wavelength of the nearest transmission peak. The full width at a half of maximum (FWHM) of a transmitted peak is calculated with respect to the finesse $\mathcal{F}$

$$\mathcal{F} = \frac{\pi}{2\arcsin(1/\sqrt{F})}, \text{where } F = \frac{4R}{(1-R)^2}, \tag{2.58}$$

$$\text{FWHM} = \frac{\text{FSR}}{\mathcal{F}}. \tag{2.59}$$

A typical spectral transmission of FP filter tuned on Hα line (6562.8 Å) can be seen on figure 2.30. The filter is an air-gapped version with $n = 1, R = 0.95$ and $l = 33$ μm achieving FWHM of 1 Å. Its main advantage compare to BF is a high transmission because it does not employ polarizers as BF where always 50 % of light is lost. Therefore it enables observers to take images with a much faster cadency to beat an atmospheric seeing for instance. On the other hand the field of view is much smaller than within BF (see figures 2.31) and therefore it is suitable for observing of angularly small objects.

2.6   Position of BF within an optical system

2.6.1   Pupil plane vs. image plane

There are two possibilities how to place narrow band filters into optical systems. The first one is to place it to the pupil plane so that an image plane is at infinity (see figure 2.33). By applying this setup each point within an image is created by a parallel beam.
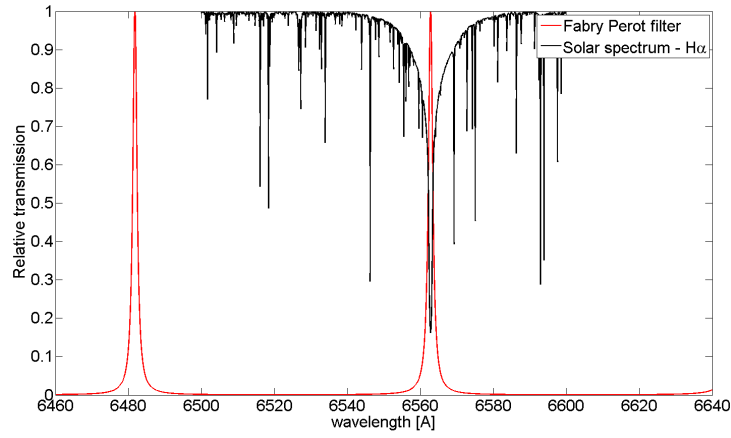
Figure 2.30: A typical spectral transmission profile of Fabry-Peròt filter tuned on Hα line. Imaged air spaced filter has $R = 0.95, l = 33$ μm and FWHM = 1 Å.
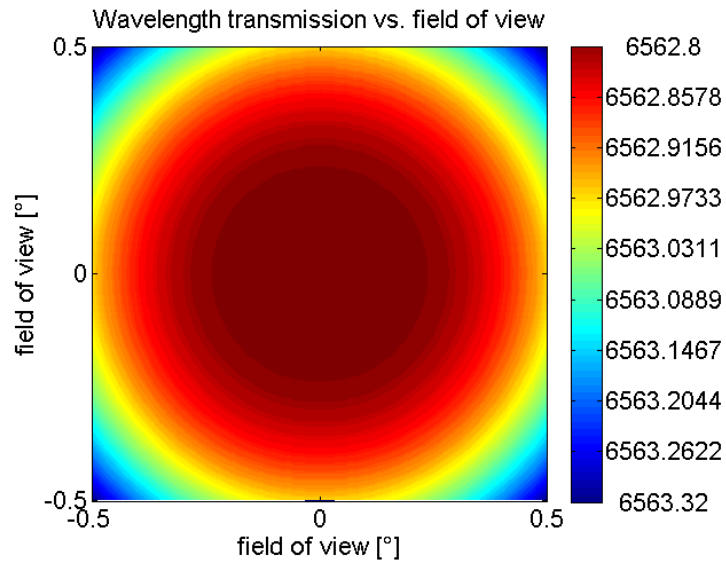
Figure 2.31: Wavelength transmission of air gaped Fabry-Peròt filter ($l = 33\mu$m, $R = 0.95$) as a function of a field of view.

However, each beam travels through the BF under a different angle so that also each image point is imaged at a slightly different wavelength λ in accordance with equations 2.42 and 2.43. The resulting angular field of view vs. the observing wavelength λ can be seen on figure 2.34.

    The second possibility is to place a BF into the focal plane so that the pupil plane is
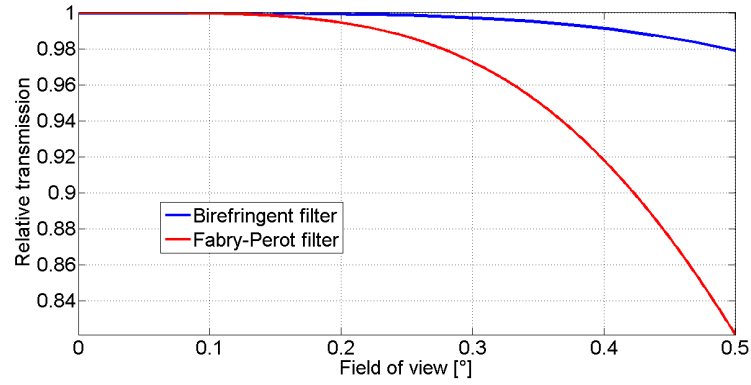
Figure 2.32: Comparison of FP and birefringent filters field of view vs. relative transmission profile.
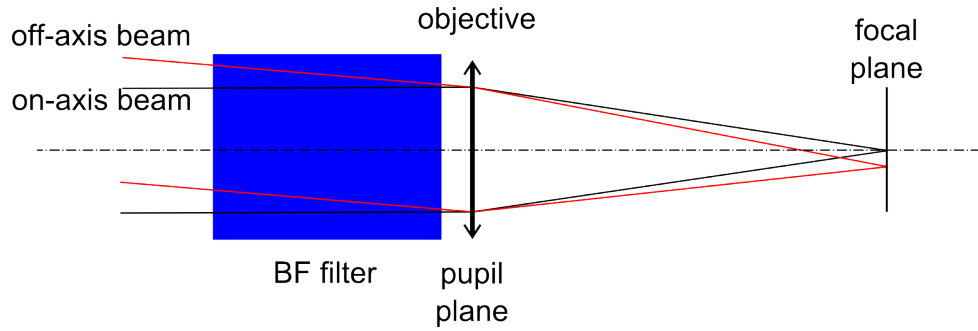
Figure 2.33: BF placed at a pupil plane. All image points are created with parallel beams that travel through the BF at different angles. Each point is then imaged at slightly different wavelengths λ.
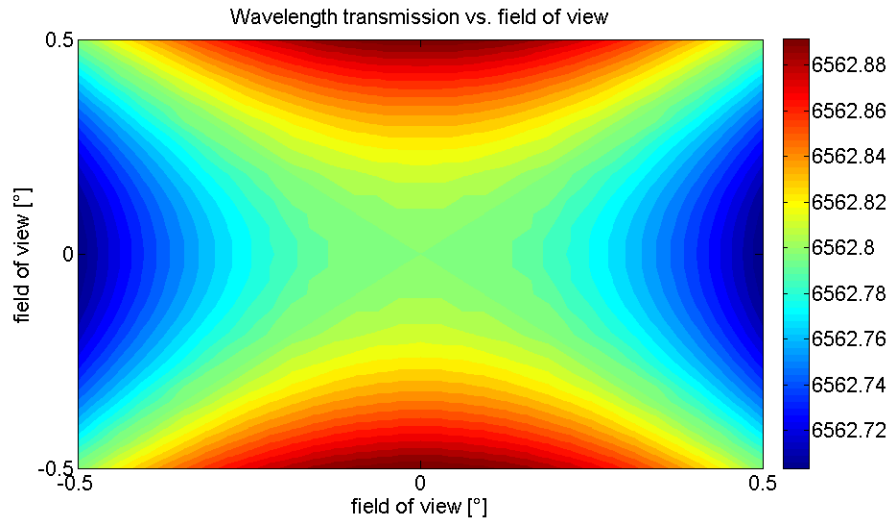
Figure 2.34: Field of view as a function of wavelength of a BF designed for H_α line (6562.8 Å) with 1 Å FWHM that observes 1° object of interest.

at infinity (see figure 2.35). This setup assures that each point within an image is created by a beam of the same convergency that is set by the optical system F-number (F/$\sharp$). As a result each point is imaged by the wavelength λ, however with bigger FWHM than in the previous case. The designed FWHM is broaden because of the angle $\sigma \doteq \frac{1}{2 \cdot F/\sharp}$. The overall spectral resolution is therefore driven also by the optical setup.

To compare both these approaches the spectral resolution of BF placed within the pupil plane is driven mainly by the angular field that is observed. Whereas the spectral resolution of BF placed within the image plane is driven mainly by the optical system and its F/$\sharp$.
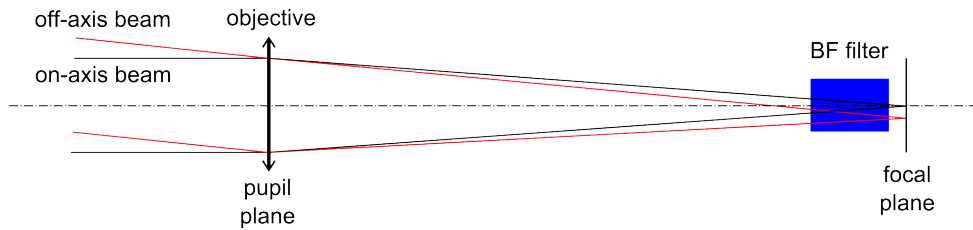
Figure 2.35: BF placed at a focal plane. All image points are created with beams of the same F/$\sharp$ what results in an observation at same wavelength λ but with a broaden FWHM.

3   Methods of thesis solution

3.1   Simulation of Šolc type BF

When studying birefringent filters we deal with an anisotropic layered system. BF are compound of several birefringent plates stacked together when its function is assured through polarization-interference phenomenon. Therefore it is convenient to use a matrix syntax that describes a polarization characteristic of each single element separately (waveplates, polarizers) and put them into a computer algorithm that enable us to get final characteristics of the light that traveled through all optical elements.

3.1.1   Jones calculus

One of the simplest attitudes to describe polarization characteristics of light and optical elements is Jones matrix calculus [28]. Light in a form of a plane monochromatic wave carrying a frequency ν and traveling in a z-axis direction is fully described by complex envelopes $E_x = e_x \exp(\mathrm{i}\varphi_x)$ of x-part and $E_y = e_y \exp(\mathrm{i}\varphi_y)$ y-part of an electric intensity. These complex quantities are put into a 2×1 matrix

$$\mathbf{J} = \left[\begin{array}{c} E_x \\ E_y \end{array} \right], \tag{3.1}$$

that is known as Jones (column) vector. Using this vector we can get intensity of mentioned wave as

$$I = \mathbf{J}^\dagger \, \mathbf{J}, \tag{3.2}$$

where $\mathbf{J}^\dagger$ is a hermitian conjugate vector to $\mathbf{J}$. We also can use ratio of $|E_x|/|E_y|$ and phase difference $\arg(E_y) - \arg(E_x)$ to determine orientation and shape of a polarization ellipse.

A description of optical polarization elements those change a polarization state of the plane wave can be done using 2×2 matrices. Such a device can be for instance a waveplate. A wave with complex envelopes E_{1x} and E_{1y} enters on the first side and on the second side a wave with complex envelopes E_{2x} and E_{2y} exits. A superposition of

waves occurs in the polarizing optical element. This superposition can be expressed using weight of each elements as

$$E_{2x} = T_{11}E_{1x} + T_{12}E_{1y},$$
$$E_{2y} = T_{21}E_{1x} + T_{22}E_{1y}. \tag{3.3}$$

Elements T_{11}, T_{12}, T_{21} and T_{22} fully characterize the mentioned optical element. We can put expression 3.3 into the matrix form so that

$$\begin{bmatrix} E_{2x} \\ E_{2y} \end{bmatrix} = \begin{bmatrix} T_{11} & T_{12} \\ T_{21} & T_{22} \end{bmatrix} \begin{bmatrix} E_{1x} \\ E_{1y} \end{bmatrix}. \tag{3.4}$$

Finally, we can rewrite in a compact way using Jones vectors

$$\mathbf{J}_2 = \mathbf{T}\mathbf{J}_1. \tag{3.5}$$

Matrix $\mathbf{T}$ is so-called Jones matrix and describes the polarization optical element. Jones vectors $\mathbf{J}_1$ and $\mathbf{J}_2$ describe input and output waves. In the table 3.1.1 there are described several Jones matrices for basic polarizing elements.

Considering several polarizing optical elements ($\mathbf{T}_1$, $\mathbf{T}_2$, ..., $\mathbf{T}_N$) stacked in a row in a direction of input wave $\mathbf{J}_1$, for output wave $\mathbf{J}_2$ it is valid that

$$\mathbf{J}_2 = \mathbf{T}_N\mathbf{T}_{N-1}\ldots\mathbf{T}_1\mathbf{J}_1. \tag{3.6}$$

In this way we can easily describe compound optical systems as for example birefringent filters.

3.1.2 Other computational approaches

There are several more matrix methods that are more complex and can be used for birefringent filter calculations too. Among them belongs Stokes - Mueller method and Maxwell - Berreman method. Both of these has some advantages comparing to Jones approach. However, for birefringent filter design it is not necessary to use them.

Table 7: Jones matrices for several polarization optical elements those are used to change a polarization state of light. Another examples can be find in e.g. [16].

optical polarizing element	Jones matrix $\mathbf{J}$
x-direction polarizer	$\begin{bmatrix} 1 & 0 \\ 0 & 0 \end{bmatrix}$
y-direction polarizer	$\begin{bmatrix} 0 & 0 \\ 0 & 1 \end{bmatrix}$
waveplate with fast axis in x-direction	$\begin{bmatrix} 1 & 0 \\ 0 & e^{-i\Gamma} \end{bmatrix}$
ρ-angle rotation matrix	$\begin{bmatrix} \cos\rho & \sin\rho \\ -\sin\rho & \cos\rho \end{bmatrix}$

Stokes method

Stokes method has an advantage of a partially polarized light description. It is widely used in astronomy for polarization description of astronomical objects. It can be used for study of an electro-magnetic field of the Sun or for a polarimetric exo-planets detection.

The monochromatic plane wave is described by Stokes vector [29, 30] as

$$\mathbf{S} = \begin{pmatrix} I \\ Q \\ U \\ V \end{pmatrix} = \begin{pmatrix} <E_x^* E_x + E_y^* E_y> \\ <E_x^* E_x - E_y^* E_y> \\ <E_x^* E_y + E_y^* E_x> \\ <\mathrm{i}(E_y^* E_x + E_y^* E_y)> \end{pmatrix} =$$

$$= \begin{pmatrix} I_{0°} + I_{90°} \text{ or } I_{45°} + I_{-45°} \text{ or } I_{\mathrm{RHC}} + I_{\mathrm{LHC}} \\ I_{0°} - I_{90°} \\ I_{45°} - I_{-45°} \\ I_{\mathrm{RHC}} - I_{\mathrm{LHC}} \end{pmatrix}$$

Stokes formalism is complete in a sense that describes all partially polarization states. However, through the first definition the phase information is lost and therefore Stokes formalism cannot be used to describe an interference phenomena. The modification of Stokes vector by polarizing optical elements is described by 4×4 matrices [31, 16].

Maxwell-Berreman method

Some today application needs to cover also the interference phenomena that can occur for instance on very thin waveplates. Among this applications belongs a precise spectro-polarimetry. For this purposes can be used Maxwell-Berreman calculus that describes the interference phenomena together with polarization states. The electromagnetic field is defined in a form of plane waves

$$\mathbf{E}(\mathbf{r}, t) = E(z) \exp[\mathrm{i}(\omega t - (k_x x + k_y y))], \tag{3.7}$$

$$\mathbf{H}(\mathbf{r}, t) = H(z) \exp[\mathrm{i}(\omega t - (k_x x + k_y y))], \tag{3.8}$$

where $k_x = c_x k_0$, $k_y = c_y k_0$ are tangential components of the wave vector $\mathbf{k} = (k_x, k_y, k_z)$, $k_0 = \omega/c$ is a wave number in vacuum, ω is an angular frequency, c is a speed of light in vacuum and $\mathbf{r} = (x, y, z)$ is a position vector. Coefficients c_x and c_y are given as

$$c_x = n_0 \cos \varphi_0 \sin \theta_0, \ c_y = n_0 \sin \varphi_0 \sin \theta_0, \tag{3.9}$$

where n_0 is a refraction index of a surrounding matter (superstrate) and φ_0, θ_0 are spherical coordinates of the incident wave direction.

Because it is sufficient to consider just tangential field components for the calculation of transfer coefficients, Berreman [32] defines a four-component vector

$$\mathbf{\Psi}(z) = \begin{pmatrix} \sqrt{\varepsilon_0} E_x(z) \\ \sqrt{\mu_0} H_y(z) \\ \sqrt{\varepsilon_0} E_y(z) \\ -\sqrt{\mu_0} H_x(z) \end{pmatrix}. \tag{3.10}$$

Maxwell equations results then in a complex form

$$\frac{\mathrm{d}\mathbf{\Psi}(z)}{\mathrm{d}z} = -\mathrm{i}\frac{\omega}{c}\mathbf{B}\mathbf{\Psi}(z), \tag{3.11}$$

where $\mathbf{B}$ is a 4×4 matrix that enables us to retrieve all interested transfer coefficients. Detailed description of the method for the anisotropic matter can be found for instance in [33].

3.2   MATLAB BF toolbox

To be able to simulate and analyze transmission profiles of birefringent filters and consequently also to design these filters with respect to desired performance it is necessary to develop codes that enable this features. Because these reasons the MATLAB Birefringent Filter toolbox on a basis of Jones polarization matrix method has been developed. The analysis and synthesis are divided into several sections with an accordance to what relevant BF feature wants to be designed or studied. They are summed in the table 8 together with BF toolbox functions in the table 9.

Entire MATLAB codes can be found on the attached CD.

Table 8: BF analysis and synthesis MATLAB sections.

section name	short description
BF transmission	analysis of birefringent filter transmission function
FWHM and FSR	enables to compute FWHM and FSR as a function of plate thickness or wavelength
azimuths	influence analysis of diferent azimuth types on BF perfomance
filter inclination	analysis of influence of BF inclinations
field of view	analysis of BF field of view
barrier (coincidence) filters	analysis and design of barrier (coincidence) BF sub-filters
filter tuning	analysis and design of BF tuning algorithms (temperature and inclination)
tolerances	calculation of BF production tolerances
Lyot filter	compute transmission profile of Lyot filter
achromatic waveplates	analysis and design of low order, zero order, achromatic and superachromatic waveplates; study of non-standard material combinations for achromatic waveplates

Table 9: Contents of BF MATLAB Toolbox.

toolbox main functions	short description
degree − > dms	conversion of degrees on degree, minutes and seconds
azimuths	delivery of different types of azimuth distributions
WM	width of transmission main peak at 3 % of intensity
FWHM	width of transmission main peak at 50 % of intensity
FWHM vedl	width of transmission side peaks at 50 % of their intensity
maxima	selections of main transmission peaks, their wavelength position and order K
side maxima	selections of side transmission peaks, their wavelength position and intensity value
M-files	unit thickness values for several materials
order K to thickness	recalculation of plate order K for specific wavelength to plate thickness
temperature shift	recalculation of wavelength shift with a change of temperature
data print out	print-out fo filter data (material, plate thickness, design wavelength and temperature, plate cut, unit thickness, mechanical and optical diameter, number of plates within the filter, filter mechanical thickness, type of azimuth distribution, p-value, azimuth angles for the individual plates, main peaks wavelength position in a certain wavelength range, its FWHM, its width at 3%, distance between them, size of side peaks)

4   Results of thesis and newly achieved knowledge

4.1   Manufacturing tolerance budget of Šolc BF

Using the MATLAB BF toolbox (see section 3.2) I have prepared a filter performance tolerance simulation of the following plate's features: thickness (d), azimuth orientation (ρ) and crystal lattice orientation (ϕ). These are the main BF plate features that drive the final quality and the performance of BF.

It has been added an error ϵ_x to the each individual plate feature so that:

$$d = d_0 + \epsilon_d,$$
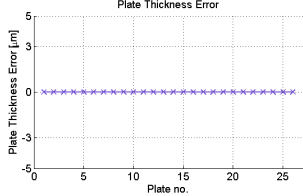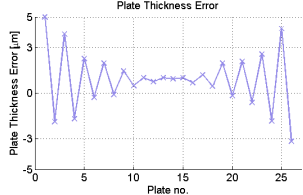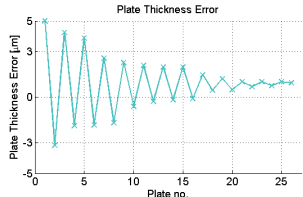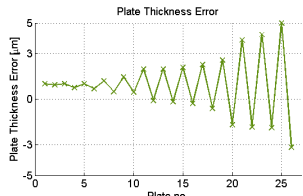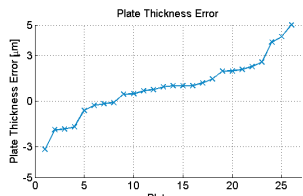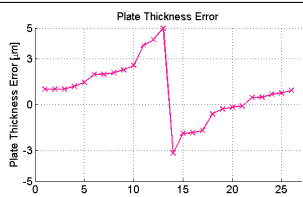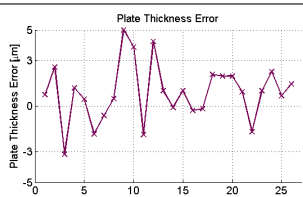
$$\rho = \rho_0 + \epsilon_\rho,$$

$$\phi = \phi_0 + \epsilon_\phi.$$

To generate error values ϵ_x it has been used a standard normal distribution ($\mu = 0$ and $\sigma^2 = 1$) multiplied by estimated values of production errors x_{err} (for the thickness it is $d_{\mathrm{err}} = 5\,\mu$m, for the azimuth orientation ρ_{err} and the crystal lattice orientation ϕ_{err} it is 30 arcminutes). To minimize an impact of these errors it has been tried to re-order plates with its non-optimal features. There are tried 6 different re-ordering distributions in a total. They are summed in table 10. Figure 4.1 shows an example of generated errors for 100 BFs each compound of 26 plates. Only one plate feature was error loaded during the simulation to be easily able to determine the best re-order distribution for each feature.

Results of the simulations (see figure 4.2) shows that certain type of re-ordering applied on BF plate order can significantly help to keep the filter performance close to the designed optimum. As a threshold for the successive re-ordering case was chosen a ratio between an ideal filter transmission FT_0 and transmission of error loaded filter FT_{err} within a certain spectral region to be less than $FT_{\mathrm{err}}/FT_0 \leqq 1.04$. That means that an error loaded filter transmits less than 4 % of parasitic light compare to an ideal filter. This light comes usually from the secondary transmission peaks rising or from the main peaks widening.

Table 10: Tested re-ordering distributions of plate features error values.

	description	graph picture
0	without any errors	
1	absolutely biggest errors at the beginning and the end of BF	
2	from absolutely maximal error to minimal	
3	from absolutely minimal error to maximal	
4	from minimal to maximal	
5	from zero to maximum and from minimum to zero	
6	random	
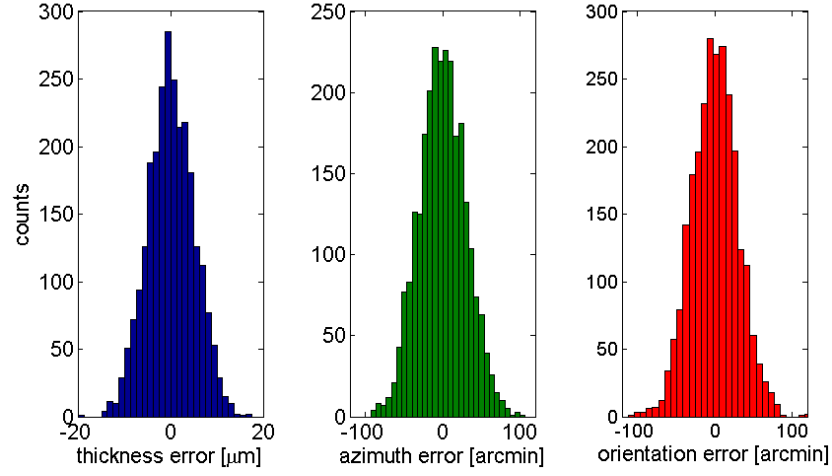
Figure 4.1: Distribution of error values ϵ_x for a simulation of 100 birefringent filters examples. Each filter is compound of 26 plates.
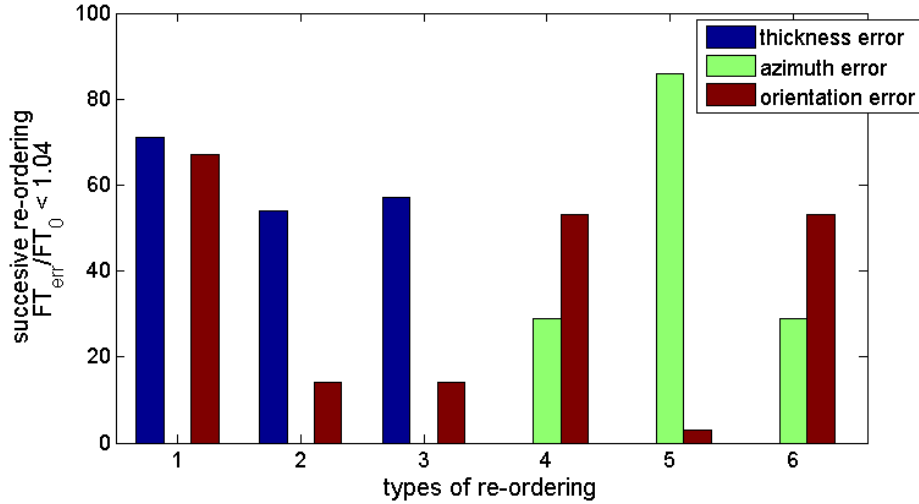
Figure 4.2: Results of tolerance simulations.

For the thickness errors the best re-ordering distributions is number 1 followed by 2 and 3. The azimuth errors can be most effectively suppressed by distribution no. 5. And the orientation errors can be best suppressed by distribution no. 1.

Above it was shown what the re-ordering distribution is suitable for a suppression of a particular plate feature error. However, all three errors are present in plates at the same

time and they combine their influences on the filter performance. Therefore it is necessary to test the plate combination to find out the sensitivity of the BF transmission with respect to error values. It is made one simplification here that comes from the production technique of Šolc type birefringent filters. Because plates for Šolc type filter are produced simultaneously we can assume they all have the same thickness d - except the Beilby layer that has about $0.3\,\mu$m but is expected to be amorphous. As a consequence we have left only two type of errors - azimuth orientation errors ϵ_ρ and crystal lattice orientation ϵ_ϕ errors.

To simulate this with a filter containing for instance 26 plates there is a factorial of 26 possible plate combinations in total. Of course, we want to avoid simulating so many possible plate combinations and therefore only re-ordering distributions that effectively suppressed the negative influence of plate features errors are simulated - that means No. 1, 2 and 3 with respect to the thickness, No. 5 with respect to the azimuth and No. 1 with respect to the crystal lattice orientation. Figure 4.3 shows the result of simulations. Azimuth orientation and crystal lattice orientation error values are generated again by the standard normal distribution ($\mu = 0$ and $\sigma^2 = 1$) multiplied by estimated values of errors ($\rho_{\mathrm{err}} = 20$ arcminutes and $\phi_{\mathrm{err}} = 20$ arcminutes). Plate thickness values are not loaded by any errors because of the production technique as discussed previously. It can be seen that these precisions enable to get about 80 % of successive solutions when the re-ordering distribution No. 5 with respect to the azimuth orientation is applied.

It is interesting to investigate what a precision needs to be achieved to eliminate needs of any plate re-ordering and to be able to sort BF plates in a random order and still achieve good filter characteristics. To be able to do this the error values has been decreased so that every re-ordering type could handle 100 % of successive re-ordering cases. These values were found to be

$$\rho_{\mathrm{err}} = 7 \text{ arcminutes},$$
$$\phi_{\mathrm{err}} = 7 \text{ arcminutes}.$$
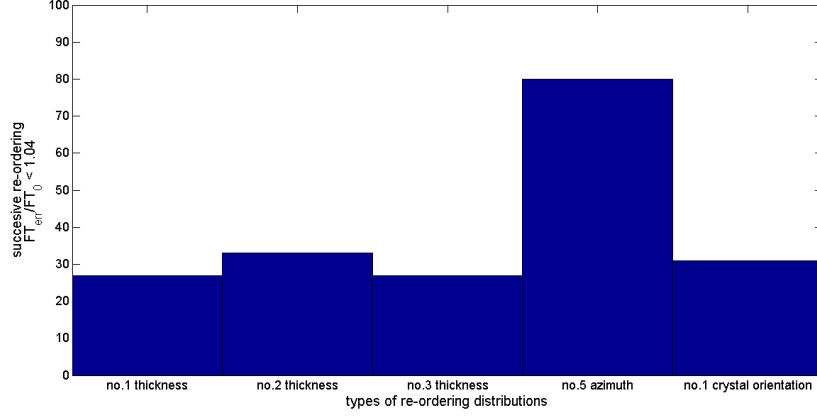
Figure 4.3: Histogram of successive re-ordering distributions.

when $d_{\mathrm{err}} = 0$ as discussed above.

Current precisions that can be achieved are well inside these tolerances. Both the azimuth orientation (thanks to Nakamura bi-plate) and the crystal lattice orientation (thanks to an X-ray goniometer) can be handled to be within 1 arcminute.

4.2   Research on $M(\lambda, T)$

To be able to properly set tuning algorithms for BF filters that are planned to be tuned by temperature - it is necessary to know temperature and dispersion characteristics of used materials. Examined characteristics found in literature [19, 34, 35] turn out to be insufficiently precise [36] when applied on high performance filters as birefringent filters of Šolc type. Therefore we have made a set of measurements in a range of 3900 to 11000 Å and $35 - 55\,°\mathrm{C}$ using 26 plate BF of Šolc type to characterize $M(\lambda, T)$ for a crystalline quartz.

We placed the BF into a collimated solar beam that is spectrally diffracted by a grating into a spectrum. The spectrum is then imaged by an objective to the CCD camera. Because the light is passing the filter, the solar spectrum is modulated by peaks from the filter. Uniquely defined solar lines within the spectrum are used for the precise spectral

determination of filter transmission peaks positions (see the figure 4.4).
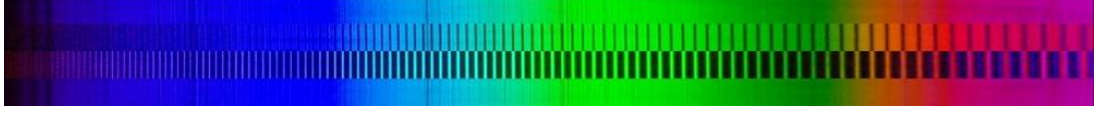
Figure 4.4: Solar spectrum overlayed by a positive and negative channel spectrum of Šolc type BF. Solar lines are used for precise definition of $M(\lambda, T)$.

Figure 4.5 shows the setup of the optical system that has been used for the measurement. "Z1" and "Z2" are heliostat mirrors that feed the objective "obj1" which images the Sun onto the slit "S", collimation objective "obj2" creates a collimated beam that travels through the BF ("p1" and "p2" are input and output polarizers). The beam is then diffracted to the solar spectrum by the diffraction grating "M". Objective "obj3" images the spectral image of the slit onto the CCD camera. To filter out IR spectrum we employed infrared filter - "IRF".
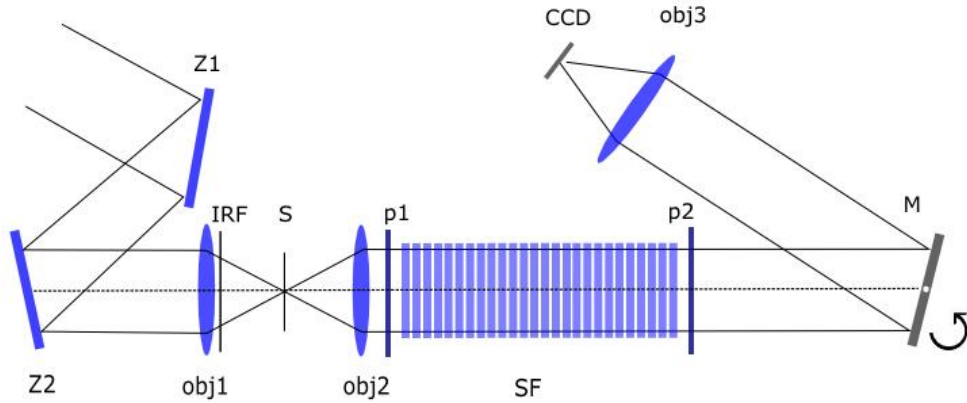
Figure 4.5: Setup for the measurement of BF material characteristics.

To disperse solar light into a spectrum we used a 1200 lines per mm dispersion grating. The dispersion of the grating is a non-linear function [37]

$$\frac{\delta \lambda}{\delta S} = \frac{a}{m \cdot f} \cos \left(\arcsin \frac{m \cdot \lambda}{2 \cdot a \cdot \cos \gamma} - \gamma \right), \tag{4.1}$$

where $\delta \lambda$ is a considered wavelength difference, δS is a geometrical distance corresponding with $\delta \lambda$, a is a grating constant, m is a grating order, f is a focal length of the imaging

objective and γ is a diffraction angle. Figure 4.6 shows measured versus computed data.
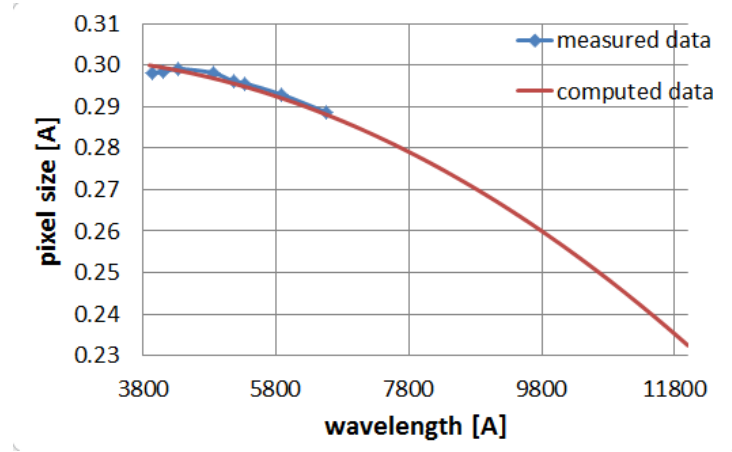
Figure 4.6: Dispersion characteristics of 1200 lines per mm diffraction grating that was used for the measurement.

To save the spectrum we used 768×576 px CCD with spectral response at $3900 - 11000$ Å. Figure 4.7 shows the recorded spectrum in a spectral range of a magnesium triplet. The solar Mg triplet is overlayed by a channel spectrum of the investigated filter. Recorded images were processed by a MATLAB code [38] to localize transmission peaks within CCD.
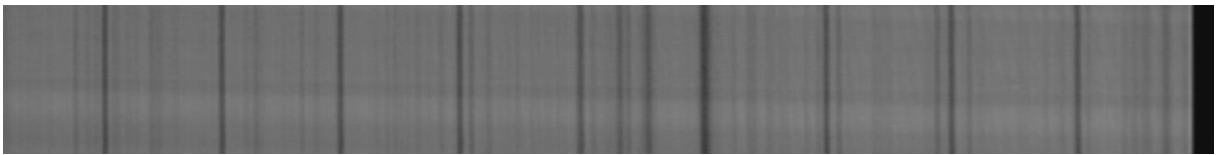
Figure 4.7: Recorded spectrum in a spectral range of a magnesium triplet. The solar Mg triplet is overlayed by a channel spectrum of the investigated filter.

Employing the Solar Survey Archive [39] we localized spectral positions of transmitted peaks within the solar spectrum. To determine a scale factor of the image 4.7 formula 4.1 was used. In such a way we determine the spectral size of one pixel p. To determine the spectral position λ_K of individual transmittance peaks of the filter we use a spectral

position of a known solar line (λ_S) within an image. The following equation

$$\lambda_K = (c_\mathrm{S} - o_K) \cdot p + \lambda_\mathrm{S}, \tag{4.2}$$

where c_S is the solar line position on CCD in pixel units and o_K is the filter transmission peak position also in pixel units.

Next step to obtain the dispersion and temperature characteristics $M(\lambda, T)$ is to determinate the orders K (see equation 2.23) of individual filter transmitted peaks. With an advance we can use a dispersion formula stated by Šolc at [19]

$$M_\mathrm{\check{S}} = 119.27\lambda + 5\log(\lambda - 0.15) + 0.5\lambda^{4.5} + \frac{5.85}{1 + 1.6\lambda^2} - 7.59 \quad [\mu\mathrm{m}]. \tag{4.3}$$

The stated equation is related to 22°C temperature, in which crystalline plates are usually processed. Hence, for the actual temperature T it is necessary to recalculate the wavelength λ using a formula [19]

$$\Delta\lambda_\mathrm{\check{S}} = -\lambda \cdot 10^{-5}[5.5\log(\lambda - 0.12) + 12.3] \cdot (T - 22°\mathrm{C}). \tag{4.4}$$

An equation for the order K_T of the certain transmission peak of a filter tuned at the temperature T can be obtained as

$$K_T = \frac{d}{M_\mathrm{\check{S}}(\lambda + \Delta\lambda_\mathrm{\check{S}})}. \tag{4.5}$$

The computed order K_T is then rounded to the closest value of a half of an integer (0.5, 1.5, 2.5, ...). The rounded order K_T is then put back to the equation 2.21 for unit thickness M_T

$$M_T(\lambda) = \frac{d}{K_T}. \tag{4.6}$$

This way we determined $M_T(\lambda)$ at the measured spectral range for each measured temperatures – $M_{35°\mathrm{C}}$ to $M_{55°\mathrm{C}}$. The characteristics can be described using polynomial equations of a fifth degree

$$M_T(\lambda) = p_1\lambda^5 + p_2\lambda^4 + p_3\lambda^3 + p_4\lambda^2 + p_5\lambda + p_6 \tag{4.7}$$

where coefficients $p_1 - p_6$ are summarized in table 4.2. Equations are graphically expressed at figure 4.8 for the small spectral range near Hα line.

Now let us look at a temperature wavelength correction $\Delta\lambda$. To do that we use measurements of $M_{35°C}$ up to $M_{55°C}$. We begin with $M_{40°C}$ where we determine such a wavelength correction $\Delta\lambda_{40°C}$ so that

$$M_{35°C}(\lambda_{35°C}) - M_{40°C}(\lambda_{40°C} + \Delta\lambda_{40°C}) = 0. \tag{4.8}$$

For $\Delta\lambda_{40°C}$ it is valid that

$$\Delta\lambda_{40°C} = \lambda_{35°C} - \lambda_{40°C}. \tag{4.9}$$

Analogically we look also for the rest of wavelength corrections $\Delta\lambda_T$ at measured temperatures 45°C, 50°C and 55°C. In a next step we divide each $\Delta\lambda_T$ by a difference of temperatures 35°C $- T$ so that we determine a unitary change with respect to 35°C - (how much the wavelength varies when the temperature is changed by 1 °C from 35°C). For instance for $\Delta\lambda_{40°C}$ we got

$$\Delta\lambda_{35°C-40°C} = \frac{\Delta\lambda_{40°C}}{5}. \tag{4.10}$$

Using equations 4.8 - 4.10 we get all characteristics for $\Delta\lambda_{35°C-40°C}$ up to $\Delta\lambda_{35°C-55°C}$ (see figure 4.9). Median of these curves describes how much we need to change the wavelength that we put into equation for unit thickness computation $M_{35°C}(\lambda)$ when a filter will operate at temperature T. The median characteristic $\Delta\lambda$ is described by a fitht-degree polynom

$$\Delta\lambda = \left(p_1\lambda^5 + p_2\lambda^4 + p_3\lambda^3 + p_4\lambda^2 + p_5\lambda + p_6\right) \cdot (35 - T) \tag{4.11}$$

where coefficients p_1 to p_6 are

$$p_1 = -6.22\text{E} - 4;\ p_2 = 1.35\text{E} - 3;\ p_3 = 4.30\text{E} - 4;$$

$$p_4 = -8.41\text{E} - 4;\ p_5 = 8.14\text{E} - 4;\ p_6 = 1.62\text{E} - 4.$$

Because the temperature wavelength correction is compared to 35°C we use the corresponding measurement $M_{35°C}(\lambda)$ as the final unit thickness dispersion characteristics.

Table 11: Coefficients $p_1 - p_6$ of $M_T(\lambda)$ polynomial equations.

	$M_{35°C}(\lambda)$	$M_{40°C}(\lambda)$	$M_{45°C}(\lambda)$	$M_{50°C}(\lambda)$	$M_{55°C}(\lambda)$
p_1	4.09E+01	3.48E+01	4.70E+001	3.65E+001	4.32E+001
p_2	-1.56E+02	-1.35E+02	-1.81E+02	-1.42E+02	1.65E+002
p_3	2.42E+02	2.12E+02	2.79E+02	2.23E+02	2.56E+02
p_4	-1.87E+02	-1.67E+02	-2.15E+002	-1.77E+02	1.98E+002
p_5	1.92E+02	1.86E+02	2.02E+02	1.89E+002	1.96E+002
p_6	-1.68E+01	-1.61E+01	-1.83E+01	-1.66E+01	1.75E+01

Therefore $M(\lambda)$ is expressed as

$$M(\lambda) = \left(p_1\lambda^5 + p_2\lambda^4 + p_3\lambda^3 + p_4\lambda^2 + p_5\lambda + p_6 \right), \tag{4.12}$$

with coefficients

$$p_1 = 4.09\text{E} + 1; \; p_2 = -1.56\text{E} + 2; \; p_3 = 2.42\text{E} + 2;$$

$$p_4 = -1.87\text{E} + 2; \; p_5 = -1.68\text{E} + 1; \; p_6 = 1.68\text{E} + 1.$$

The final temperature and dispersion characteristics of the crystalline quartz are in a form $M(\lambda + \Delta\lambda)$ where the wavelength λ is corrected using the coefficient $\Delta\lambda$ for the filter operating at the temperature T - equations 4.12 and 4.11.

The figure 4.10 shows a minor difference between the original equation used by Šolc (equation 2.24) for a computation of the unit thickness M and our equations 4.12 that comes from recent measurements. Šolc has later slightly upgraded his original equation but did not publish it, however it is used in the optical workshop where he worked for precise design of waveplates. In 2006 we provided similar measurements [36] to the one that is described but only for 45°C temperature and only with 4 quartz plates of 11.4000 mm thickness. All mentioned equations are summarized in table 12 together with proper $\Delta\lambda$ corrections and valid spectral and temperature regions.

To compare these four unit thickness equations it is best to show an impact of their usage on a birefringent filter design. That can be seen at figure 4.11. Using measured

Table 12: Different equations for unit thickness M

author	unit thickness M equation	valid spectral region	$\Delta\lambda$ equation	valid temperature region
Šolc I (1984, [19])	$M = 119.27\lambda + 5\log(\lambda - 0.15) + 0.5\lambda^{4.5} + \frac{5.85}{1+1.6\lambda^2} - 7.59$	$0.18 - 4\ \mu m$	$\Delta\lambda = -\lambda \cdot 10^{-5}[5.5\log(\lambda - 0.12) + 12.3] \cdot (T - 22)$	$25 - 60°C$
Šolc II (1990, private communication)	$M = 119.27\lambda + 5\log(\lambda - 0.15) + 0.5\lambda^{4.5} + \frac{5.85}{1+1.6\lambda^2} + \frac{0.028}{\lambda - 0.1} - 0.06\sin(\frac{\pi\lambda}{0.23})\exp(-\lambda^2) - 7.713$	$0.18 - 4\ \mu m$	$\Delta\lambda = -\lambda \cdot 10^{-5}[5.5\log(\lambda - 0.12) + 12.3] \cdot (T - 22)$	$25 - 60°C$
Melich (2006, [36])	$M = p_1\lambda^5 + p_2\lambda^4 + p_3\lambda^3 + p_4\lambda^2 + p_5\lambda + p_6$ where $p_1 = 310.1637, p_2 = -803.7495, p_3 = 842.8744, p_4 = -454.3735, p_5 = 248.0844, p_6 = -21.1606$	$0.38 - 0.7\ \mu m$	valid for 45°C	valid for 45°C
Becicka (2009, [38])	$M = p_1\lambda^5 + p_2\lambda^4 + p_3\lambda^3 + p_4\lambda^2 + p_5\lambda + p_6$ where $p_1 = 40.8618, p_2 = -156.4452, p_3 = 241.7107, p_4 = -187.1951, p_5 = 192.0057, p_6 = -16.8497$	$0.39 - 1.11\mu m$	$\Delta\lambda = (p_1\lambda^5 + p_2\lambda^4 + p_3\lambda^3 + p_4\lambda^2 + p_5\lambda + p_6) \cdot (35 - T)$, where $p_1 = -6.22\text{E}-4; p_2 = 1.35\text{E}-3; p_3 = 4.30\text{E}-4; p_4 = -8.41\text{E}-4; p_5 = 8.14\text{E}-4; p_6 = 1.62\text{E}-4$	$35 - 55°C$
Šolc for calcite (1984, [19])	$M_{calcite} = (\lambda - 0.1) \cdot \frac{M}{18\lambda - 1.37} + 0.05\sin(300 \cdot \log(4.6\lambda)) - 0.04$	$0.18 - 4\ \mu m$	$\Delta\lambda_{calcite} = -\lambda \cdot 10^{-5}[2.5\log(\lambda - 0.14) + 6] \cdot (T - 22C)$	$25 - 60°C$
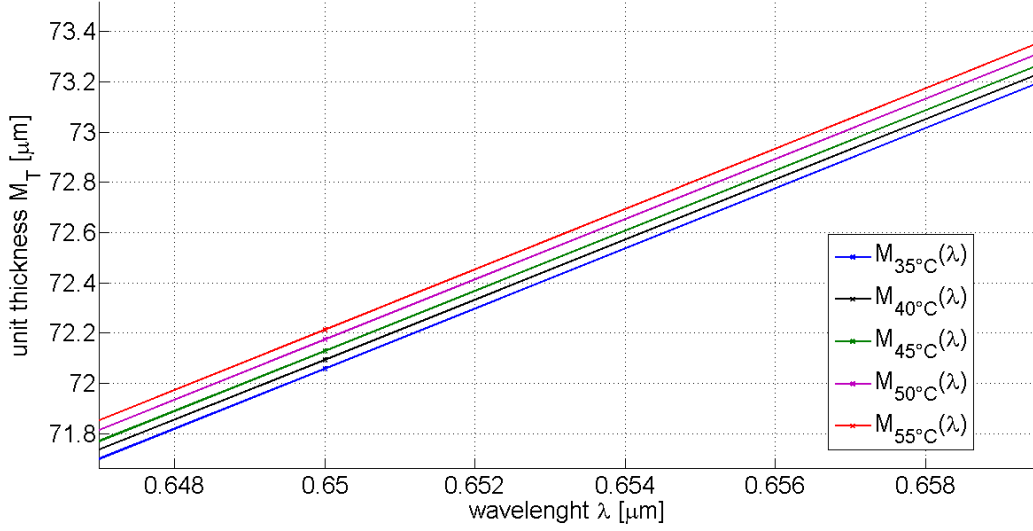
Figure 4.8: Series of measurements of crystalline quartz unit thicknesses $M_T(\lambda)$ at several temperatures.

equations 4.12 and 4.11 we designed BF for Hα line observation at 6562.8 Å for 39.5°C filter operating temperature. We can see that the transmission curves are spectrally shifted with an usage of different equations for the unit thickness M. When it is designed a filter for only one observation wavelength it can be easily corrected by eg. temperature correction. However, when we design filter for multiple wavelength observation this way cannot be used. For the BF design it is therefore necessary to have a precise unit thickness measurements that assure a correct filter design. A paper by Skomorovskij [9] mentions that dispersion characteristics can slightly vary with a place of deposits of a given material. This fact could explain a difference between original Šolc equation, new Šolc equation and equations from Melich and Bečička.

4.3   Achromatic waveplate

A way of including of a fast tuning capability into BF is to use Lyot or Evans element in the filter design. Their usage is, however, restricted to spectral ranges where $\lambda/2$ and $\lambda/4$ waveplates in elements have the proper retardance. To provide an ability of a wide spectral tuning of Lyot and Evans element it is necessary to have an achromatic waveplate in the set. Comparing to simple waveplates, achromatic waveplates provide
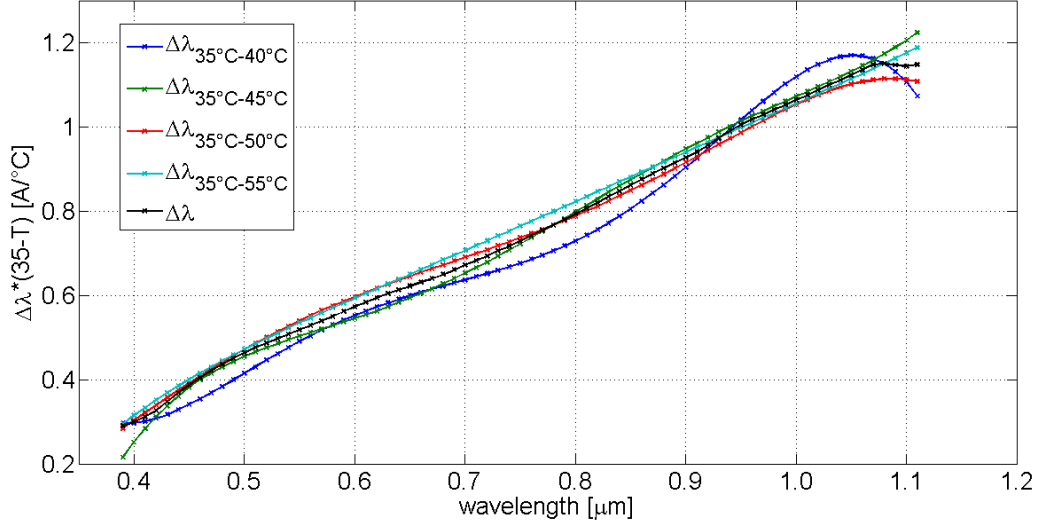
Figure 4.9: Wavelength temperature change $\Delta\lambda$ that is necessary to account for when computing unit thickness M.

more constant path shift that is independent of the transmitted wavelength with a certain precision. This independency is achieved using two different birefringent materials. The chromatic shift of the retardance in the first part of the waveplate is compensated by a suitable material of the second part - these days crystalline SiO_2 a MgF_2 birefringent materials are used almost exclusively.

A crystalline plate thickness of each material for an achromated spectral range $\lambda_1 - \lambda_2$ can be calculated [40] as

$$\mathbf{d} = \frac{\Delta}{2\pi}\text{inv}(\mathbf{D}) \cdot \mathbf{L}, \tag{4.13}$$

where $\mathbf{d}$ stands for a matrix of thicknesses of individual plates

$$\mathbf{d} = \begin{bmatrix} d_{\text{M}} \\ d_{\text{Q}} \end{bmatrix},$$

the index M is for MgF_2 and the index Q is for SiO_2, $\text{inv}(\mathbf{D})$ expresses an inverse birefringent matrix

$$\mathbf{D} = \begin{bmatrix} n_{\text{eM1}} - n_{\text{oM1}} & -(n_{\text{eQ1}} - n_{\text{oQ1}}) \\ n_{\text{eM2}} - n_{\text{oM2}} & -(n_{\text{eQ2}} - n_{\text{oQ2}}) \end{bmatrix}, \tag{4.14}$$
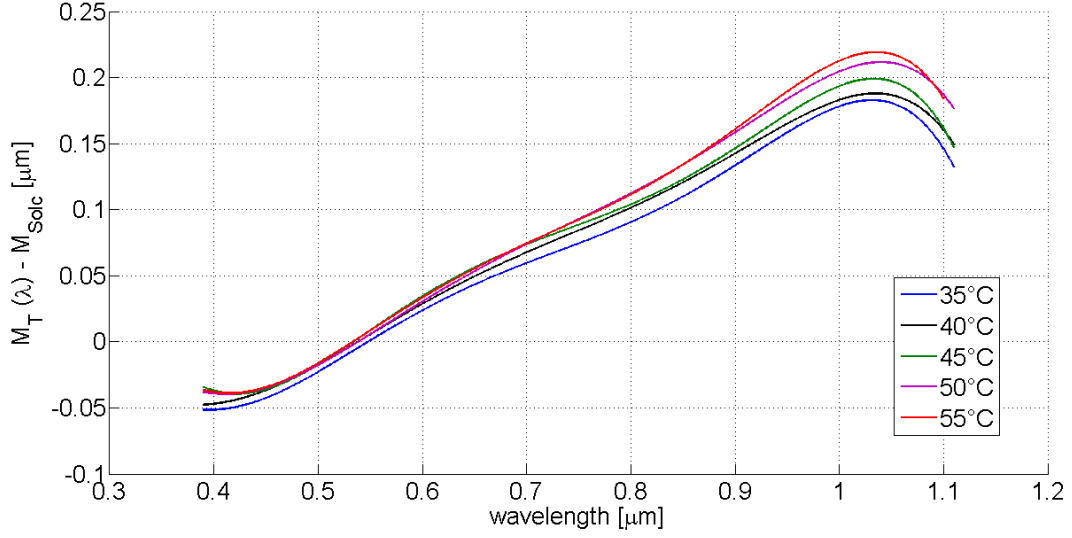
Figure 4.10: Deviations between measured $M_T(\lambda)$ and computed values from Šolc equation.

where the index 1 means a connection with the wavelength λ_1 and the index 2 with λ_2. Finally **L** is a wavelength matrix

$$\mathbf{L} = \left[\begin{array}{c} \lambda_1 \\ \lambda_2 \end{array} \right]$$

For wavelengths $\lambda_1 = 400$ nm and $\lambda_2 = 500$ nm the thickness of MgF_2 is $d_M = 264.15$ μm and SiO_2 $d_Q = 312.14$ μm. The final path retardance can be seen at figure 4.12 where the designed achromatic waveplate achieves the retardance error of approximately $\lambda/100$ at 400 nm - 500 nm spectral range.

Nowadays there is quite a lot of modern birefringent materials widely used in non-linear optics. However, because of their birefringence they can be in principle used to design achromatic waveplates that have a better achromatic performance. Table 13 shows an overview of 12 birefringent materials that have been theoretically studied for this purpose. There can be achieved 66 combinations using them. Not all of the combinations are advantageous but several of them shows the better performance than already mentioned SiO_2/MgF_2 combination, especially for certain spectral regions.

A criterion for a suitable material choice comes from a ratio of path retardance first

Table 13: Birefringent materials that were inspected for an achromatic waveplate combination.

material	spectral region of valid dispersion formula [μm]	n_e @ 500 nm	n_o @ 500 nm	birefringence @ 500 nm	data source
Quartz	0.18 - 3	1.5580	1.5488	0.0093	refractiveindex.info, ZEMAX
MgF$_2$	0.2 - 7.04	1.3917	1.3798	0.0119	refractiveindex.info, ZEMAX
ADP	0.2 - 1.5	1.4832	1.5290	-0.0458	refractiveindex.info, ZEMAX
LiNbO$_3$	0.4 - 5	2.2492	2.3408	-0.0916	refractiveindex.info, ZEMAX
YVO$_4$	0.48 - 1.55	2.2679	2.0297	0.2383	refractiveindex.info, ZEMAX
BBO	0.22 - 1.06	1.5577	1.6781	-0.1203	refractiveindex.info, ZEMAX
KDP	0.2 - 1.5	1.4721	1.5145	-0.0424	refractiveindex.info, ZEMAX
PbMO$_4$	0.44 - 1.08	2.3250	2.4862	-0.1613	refractiveindex.info, ZEMAX
TiO$_2$ (Rutil)	0.4 - 1	2.7746	2.5045	0.2700	refractiveindex.info
CaCO$_3$	0.2 - 2.2	1.4900	1.6665	-0.1764	refractiveindex.info, ZEMAX
TeO$_2$	0.4 - 1.5	2.4849	2.3212	0.1637	refractiveindex.info, ZEMAX
Sapphire	0.2 - 5.5	1.7660	1.7742	-0.0082	refractiveindex.info, ZEMAX
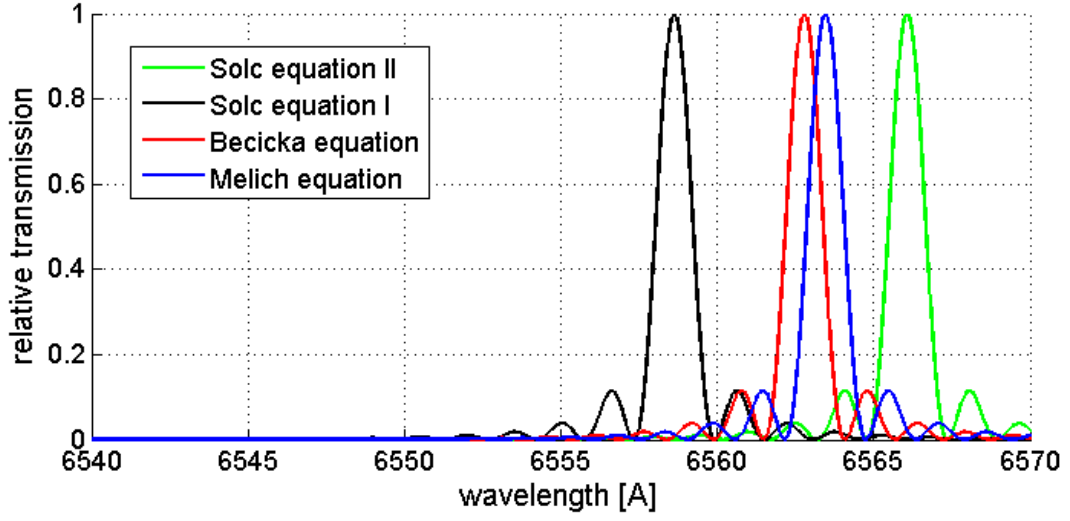
Figure 4.11: An impact of using of 4 different equations for the unit thickness M on a design of a birefringent filter.

derivatives of chosen materials X and Y with respect to a wavelength

$$p = \frac{\left[\frac{1}{n_e - n_o}\frac{d(n_e - n_o)}{d\lambda} - \frac{1}{\lambda}\right]_X}{\left[\frac{1}{n_e - n_o}\frac{d(n_e - n_o)}{d\lambda} - \frac{1}{\lambda}\right]_Y}. \tag{4.15}$$

The more flat is a tendency the ratio p expresses the more suitable choice of materials combination for achromatic waveplates. Figure 4.13 shows the ratio p for several most interested material combinations. From this figure we can see that more convenient combination that already mentioned classical combination SiO_2/MgF_2 is a combination SiO_2/BBO for spectral region $0.4 - 1.0\,\mu m$ and $SiO_2/Sapphire$ for spectral region $0.25 - 0.6\,\mu m$. Figure 4.14 shows the path retardance for the mentioned combinations. The comparison shows that the SiO_2/BBO is about $30\,\%$ better than the classical SiO_2/MgF_2. Great results are achieved for $SiO_2/Sapphire$ in the close UV spectra.

However, as can be seen from the figures the achromatic waveplates retardance is still limited to the certain spectral region and therefore the full spectrum tuning is not able even with the usage of achromatic waveplates in the Lyot or Evans elements.
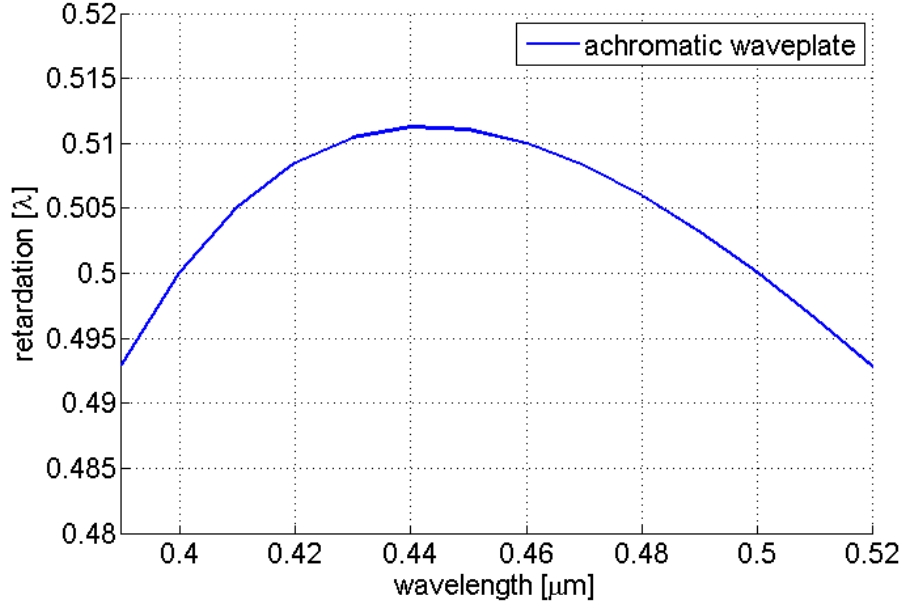
Figure 4.12: Path retardance of an achromatic waveplate compound of SiO_2 and MgF_2.

4.4   Novel tuning method - BF with plates of oblique cut

An important way of tuning for this thesis is an inclination tuning of BF containing oblique cut plates [41]. This is the first time this type of tuning is used for professional birefringent filter tuning.

Instead of the classical cut which is parallel with a crystal optical axis (using the crystalline quartz it is Y-cut) a plate is cut from a crystal under a small angle ϕ with respect to the Y-cut along the optical axis. This leads to the possibility to tune the filter in the entire spectrum employing an inclination in only one plane instead of two as described in the subsection 2.3.3.

Using a unit thickness M_Y of Y-cut we can express the a unit thickness M_ϕ of the cut ϕ as

$$M_\phi = M_Y \; \frac{1}{\cos^2 \phi}. \tag{4.16}$$

If we incline the filter from its mechanical axis about an angle β the light beam is traveling via the filter according to Snell's law $\beta' = \beta/n'$ (where where n' stands for $\frac{n_e + n_o}{2}$ for small
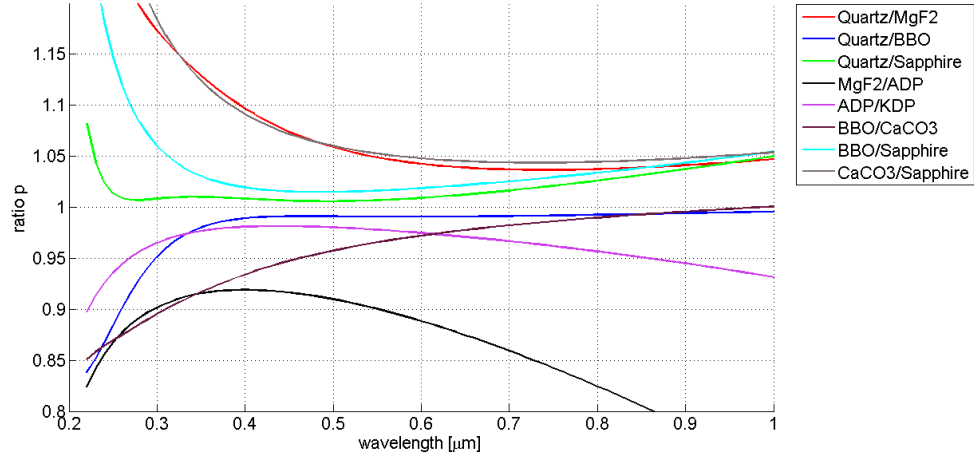
Figure 4.13: Ratio of path retardance first derivatives of chosen materials X and Y. The more flat is the ratio p the more suitable choice of materials combination for achromatic waveplates.
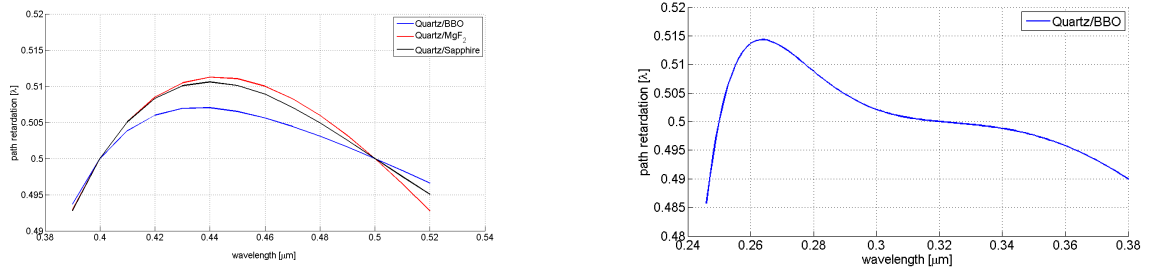
Figure 4.14: Path retardances for optimally chosen material combinations.

angles of inclination). The unit thickness $M_{\phi,\beta}$ is

$$M_{\phi,\beta} = M_Y \; \frac{1}{\cos^2(\phi + \beta/n')}. \tag{4.17}$$

This value can then be used for a calculation of a filter transmission and a corresponding filter plate thickness

$$d_\phi = K \cdot M_{\phi,\beta}(\lambda, t) = K \cdot M_Y \; \frac{1}{\cos^2(\phi + \beta/n')}. \tag{4.18}$$

This expression shows what should be the plate thickness when we want to transmit the wavelength λ if applying the inclination β on BF made of plates with the oblique cut ϕ.

Because of a usage of the oblique cut with respect to the optical axis, an extraordinary ray deviates with respect to an ordinary ray (see figure 4.15). Considering a maximal

extraordinary ray deviation ψ_{max} of cuts close to 45° with respect to optical axis then we can write for oblique cut φ (measured from Y-cut, where $\varphi = 0°$, to Z-cut, where $\varphi = 90°$) with good approximation

$$\psi_\varphi = \psi_{\mathrm{max}} \cdot \sin^2(2\varphi) \tag{4.19}$$

Approximative values for a crystalline $\mathrm{SiO_2}$ are $\psi_{\mathrm{max}} = 20'$. From the equation 4.19 it results for 6° oblique cut in $\psi_{6°} = 52''$. Using for instance 5 mm thick plates we obtain about 1 μm displacement which in a comparison with a camera pixel size is a negligible value. Our observation with 26 quartz plates Šolc filter compound of oblique cut plates of 6° and 3.5015 mm thickness using 20 μm pixel size CCD camera confirm that.
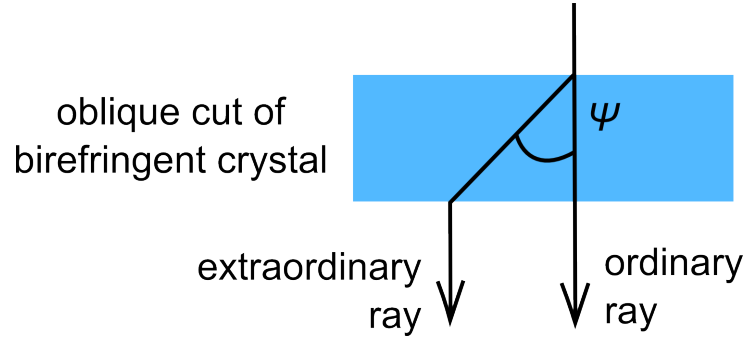
Figure 4.15: Ray paths in an oblique cut of a birefringent plate.

4.5   Realization of universal birefringent filter

Observing the Sun chromosphere with polarization interference birefringent filters has an advantage of their long lasting and high stability [42, 22]. Such filters are mainly constructed for just one spectral line (e.g. Hα, Ca II K, etc.). Construction of a filter for more spectral lines [8, 43] or tunable via a wider spectral range is more sophisticated, however, such a solution is theoretically possible. In [8] we can find a description of Lyot type filter recently used for observing in Hα and He I lines. A fully tunable filter working in a wide spectral range was realized by Title [24].

Together with astronomers from Solar Department of Astronomical Institute AS CR, v.v.i. a production of several pieces of birefringent filters for professional solar observation

has been consulted. The set of filters has been considered to observe at several astronom-
ically interesting spectral lines - Hα, D1, D2, D3, Hβ, BaII, Hγ and CaIIK. Physical
calculations showed that it is possible to apply BF of Šolc type with a properly chosen
construction of BF plates. The filter will be capable to transmit all chosen wavelengths,
however, during the observation only one line will be considered. The rest of transmitted
lines will be blocked by barrier filters.

4.5.1   Design of the universal tunable filter

After a theoretical analysis it has been concluded that the filter cannot be accom-
plished as a simple optical element. However, it can be built up using a combination of
several interdependent optical elements (called sub-filters) in the way shown at figure 4.16.

The first barrier element of the filter is considered as a dielectric filter set together
with color glass (DF1 and DF2) that are placed in two carousel wheels. Spectrally, those
are the widest elements. The second barrier element (SF1) of the filter is realized as a
Šolc type filter built up of quartz obliquely cut plates (the cut of the plates that is not
parallel to optical axis of a crystal - see section 4.4) [41]. Such a sub-filter is tunable in
a wide spectrum range with a simple inclination in one axis only (see figure 4.20). After
barrier sub-filters a main sub-filter (SF2) is placed in the optical path. SF2 is designed as
Šolc type filter built of 26 quartz plates. The thickness of its plates is designed in such a
way it is able to be tuned on numerous astronomically interesting lines by a temperature
variation. Finally, there is a most narrow part SF3 that is also designed as a Šolc filter.
It is compound from 6 plates of $CaCO_3$ that has about a 17$\times$ higher birefringence than
quartz and provides most narrow lines from all sub-filters.

4.5.2   Barrier interference sub-filters and colored glasses

In front of birefringent sub-filters SF1, SF2 and SF3 there is a double carousel with 2$\times$6
positions for wide interference and color glass filters DF1 and DF2 (see figure 4.17). They
are going to be chosen with respect to the observed spectral line. Their usual FWHM
is in a range of 10 nm. These kind of filters and color glasses are easily commercially
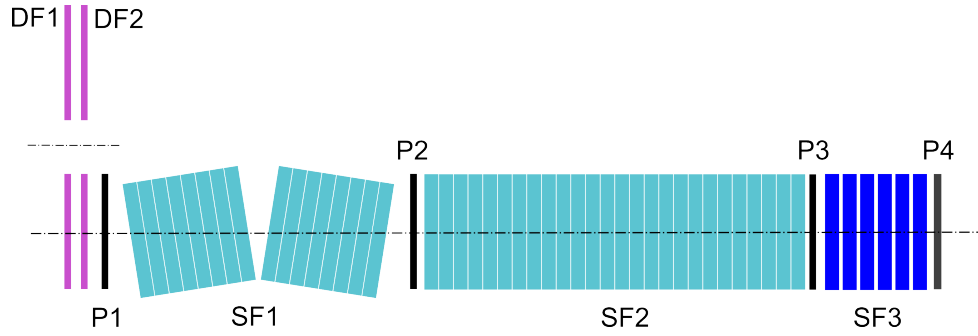
Figure 4.16: An optical scheme of the multi-wavelength Šolc birefringent filter. The filter consists of three birefringent sub-filters of Šolc type - SF1, SF2 and SF3 and sets of interference filters and color glasses - DF1 and DF2. Each birefringent element is separated by polarizers P1, ..., P4.

available.
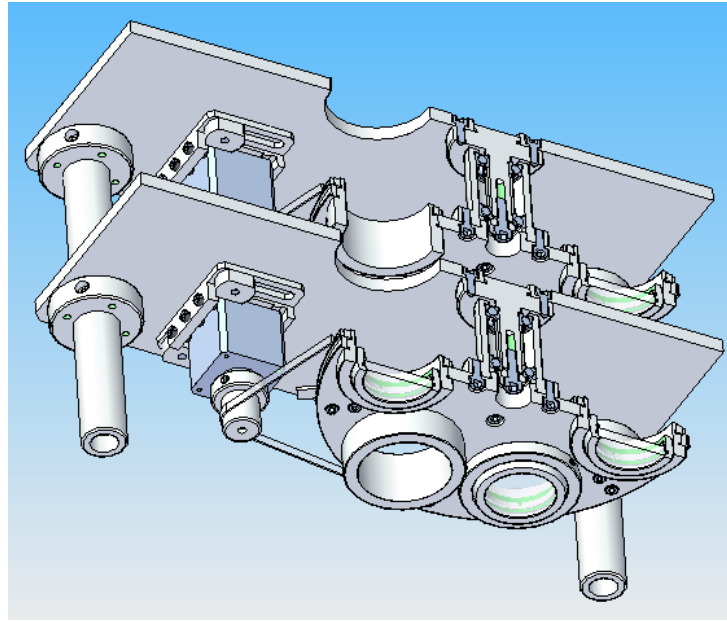
Figure 4.17: Double carousel with 2×6 positions for wide interference and color glass filters DF1 and DF2.

4.5.3   Barrier inclination sub-filter

The sub-filter SF1 acts as a barrier filter for SF2. The design of barrier inclination sun-filter SF1 comes from the study provided in section 4.4. To be able to tune the filter over entire visible spectrum it has been concluded to built up the filter from plates with $6°$ oblique cut from the Y crystal plane. The SF1 compounds of 26 quartz plates

of 3.5015 mm thickness. The overall thickness of the SF1 sub-filter is 91.0390 mm. Its mechanical diameter is 32 mm, the optical diameter is 30 mm. The azimuth distribution function is chosen as a triangular function with a factor $p = 0.644$ resulting in 2.93 % high of side maxima (see table 14 of SF1 azimuths and transmission profile figure 4.18).
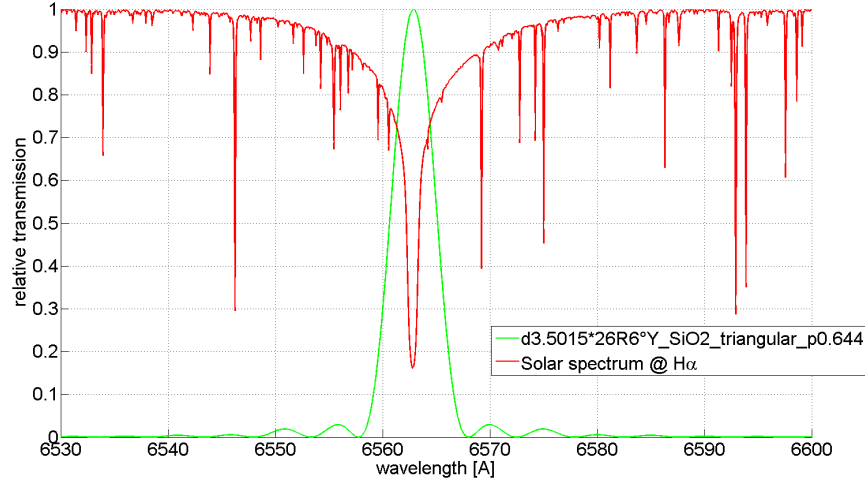
Figure 4.18: Relative transmission profile of SF1 sub-filter tuned at Hα line.

Its tuning is provided by an inclination in one axis only which is possible thanks to the chosen 6° oblique cut [41, 44]. Application of this cut provide full spectral tunability within the inclination range of $\langle -3°; +3° \rangle$ for the Mg2 line range (see figure 4.20) and $\langle -4°; +4° \rangle$ for Hα line.

FWHM and FSR for visible spectrum of SF1 sub-filter is showed at figure 4.19.

Inclination values for desired wavelengths are calculated using MATLAB simulations toolbox (see the section 3.2) and are summed in table 15.

From a point of view of keeping a position and a direction of the sub-filter optical axis identical with the mechanical axis of the entire filter it is necessary to split the SF1 into two parts of the same thickness. From this reason the SF1 sub-filter has to be build up

Table 14: Triangular azimuth distribution of SF1 sub-filter plates with a factor $p = 0.644$.

plate	azimuth		plate	azimuth	
number	degree	minutes	number	degree	minutes
1	1	6.92	14	-2	-20.77
2	-1	-13.08	15	2	14.62
3	1	19.23	16	-2	-8.46
4	-1	-25.38	17	2	2.31
5	1	31.54	18	-1	-56.15
6	-1	-37.69	19	1	50.00
7	1	43.85	20	-1	-43.85
8	-1	-50.00	21	1	37.69
9	1	56.15	22	-1	-31.54
10	-2	-2.31	23	1	25.38
11	2	8.46	24	-1	-19.23
12	-2	-14.62	25	1	13.08
13	2	20.77	26	-1	-6.92

Table 15: Inclination values of SF1 sub-filter that assures the filter to be tuned on desired wavelengths.

spectral line	wavelength [Å]	line FWHM [Å]	inclination [°]
CaIIK	3933.682	13	-0.43
Hγ	4340.475	1.4	-2.02
BaII	4554.03	0.2	-2.28
Hβ	4861.342	1.2	-2.64
Na$-$D1	5895.940	0.4	-0.91
Na$-$D2	5889.973	0.4	-0.43
He$-$D3	5875.625	0.3	0.82
Hα	6562.808	1.5	0.17
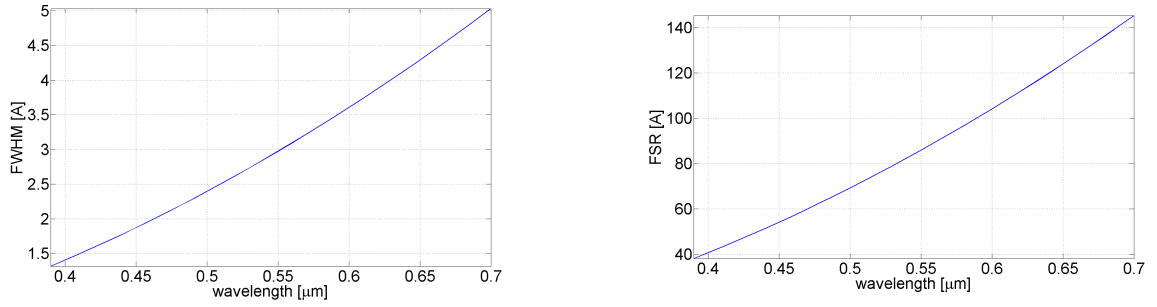
Figure 4.19: Full width at half maximum and free spectral range of SF1 sub-filter as a function of wavelength.
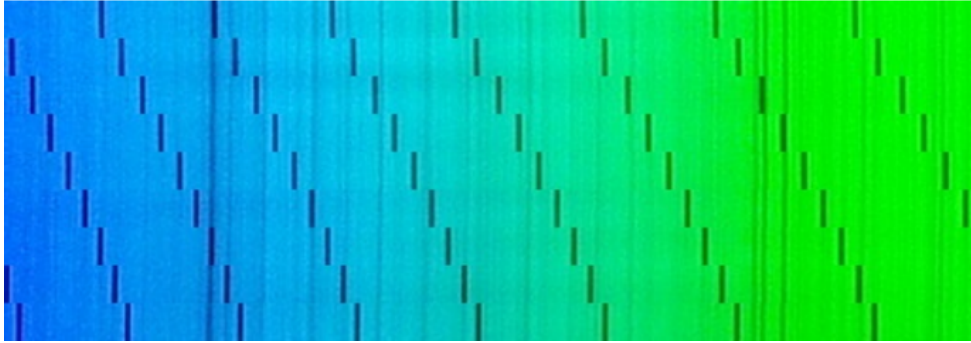
Figure 4.20: Channel spectrum of Šolc barrier sub-filter and tuning by its inclination. Each horizontal line represents the inclination of 1°. As a result we can see tuning of the filter maxima. The transmittance of the sub-filter is negative in this figure so that you can see the solar spectrum.

from an even number of plates. Each half is then inclined in a sense of figure 4.21 so that a spectral shift of transmission peaks can occur. The second half of SF1 has to be rotated with respect to its mechanical axis about 180° so that the inclination of two halves is done in a same direction with a respect to the optical axis within the sub-filter plates.
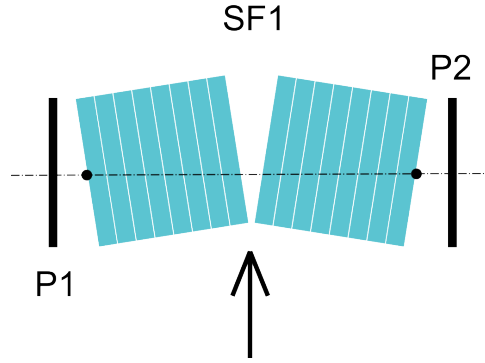
Figure 4.21: A special way of an inclination of the barrier sub-filter SF1. The sub-filter is divided into two halves of the same thickness. The second half is rotated about 180° with respect to the optical axis. The center of the inclination for the two halves is the black point. In such a way of inclining the spectral shift is provided and the position and direction of the optical axis remains unchanged.

4.5.4   Main sub-filter

The main sub-filter SF2 is constructed as Šolc type birefringent filter compound of 26 crystalline quartz plates of 11.4000 mm thickness that are cut parallel with optical axis. The overall length of the filter is 296.4000 mm. Its mechanical diameter is 32 mm, the optical diameter is 30 mm. The azimuth distribution function is chosen as a triangular function with a factor $p = 0.644$ resulting in side maxima amplitudes of 2.93% peak value (see table 16 of SF2 azimuths and transmission profile figure 4.22).

Figure 4.22: Relative transmission profile of SF2 sub-filter tuned at Hα line.

Table 16: Triangular azimuth distribution of SF2 sub-filter plates with a factor $p = 0.644$.

plate number	azimuth degree	azimuth minutes	plate number	azimuth degree	azimuth minutes
1	1	6.92	14	-2	-20.77
2	-1	-13.08	15	2	14.62
3	1	19.23	16	-2	-8.46
4	-1	-25.38	17	2	2.31
5	1	31.54	18	-1	-56.15
6	-1	-37.69	19	1	50.00
7	1	43.85	20	-1	-43.85
8	-1	-50.00	21	1	37.69
9	1	56.15	22	-1	-31.54
10	-2	-2.31	23	1	25.38
11	2	8.46	24	-1	-19.23
12	-2	-14.62	25	1	13.08
13	2	20.77	26	-1	-6.92

The thickness of plates within this filter is carefully chosen to be able to tune the filter on the most astronomically interesting lines within a temperature range of $35 - 55\,°C$. Nevertheless, the filter can be tuned over an entire spectrum within a temperature range of $10 - 70\,°C$. Out of this range a dew-point can be achieved or a degradation of polarizers due too high temperature can occur. Table 17 shows spectral lines tuning temperatures the filter was originally designed for. However, it is possible to observe also on other spectrally interesting wavelengths. Those between 3900 Å and 6650 Å are stated in table 18 together with SF2 working temperature. An efficient liquid super-thermostat is used as a temperature controller. It enables both cooling and heating of crystalline quartz plates that are placed within a specially designed housing enabling free float of a coolant.

FWHM and FSR for SF2 sub-filter within a visible spectral region is showed at figure 4.23.
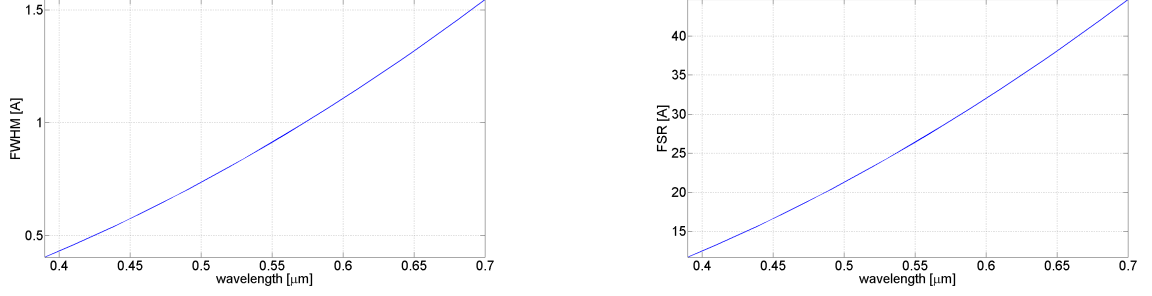
Figure 4.23: Full width at half maximum and free spectral range of SF2 sub-filter as a function of wavelength.

Table 17: Temperature values for SF2 sub-filter that assure the filter to be tuned on desired wavelengths.

spectral line	wavelength [Å]	line FWHM [Å]	temperature [°]
CaIIK	3933.682	13	50.30
Hγ	4340.475	1.4	34.06
BaII	4554.03	0.2	23.93
Hβ	4861.342	1.2	43.52
Na$-$D1	5895.940	0.4	49.63
Na$-$D2	5889.973	0.4	59.38
He$-$D3	5875.625	0.3	35.59
Hα	6562.808	1.5	39.49

4.5.5   Narrowing sub-filter

The sub-filter SF3 acts in the whole filter as a spectrally narrowing element. It is made of 5 plates of crystalline $CaCO_3$, each of 8.9303 mm. That makes the sub-filter as long as 44.6515 mm. However, $CaCO_3$ has about 17× higher birefringence than a crystalline quartz and therefore this sub-filter provides most narrow transmission peaks even thought the filter is shorter than the quartz one. The mechanical diameter is 32 mm, the optical diameter is 30 mm. The azimuth distribution function is chosen as a triangular function with a factor p = 0.644 resulting in 0.3 % high of side maxima (see table 20 of SF3 azimuths and transmission profile at figure 4.24). Figure 4.25 shows the FSR and FWHM of SF3 as a function of wavelength.

Table 18: Table of spectral lines observable with the main Šolc sub-filter SF2. T is 'working temperature' used for the main Šolc sub-filter to be tuned on a proper line.

Line	λ [Å]	T [°C]	Line	λ [Å]	T [°C]	Line	λ [Å]	T [°C]
Al	3961.535	61.54	Fe	4404.761	29.61	Fe	5269.550	53.45
Ca-H	3968.492	43.29	Fe	4415.135	42.50	Cr	5298.283	43.97
Fe	4005.254	44.85	Mn	4762.375	42.17	Fe	5302.307	36.32
Mn	4030.763	43.66	Mn	4783.424	38.22	Fe2	5316.620	56.27
Fe	4045.825	39.00	Ni	4786.542	31.00	Fe	5328.051	33.72
Fe	4071.749	37.86	Ti2	4805.099	32.68	Fe	5364.880	58.76
H-d	4101.748	28.30	Mn	4823.514	34.68	Fe	5367.476	53.82
Fe	4118.555	52.81	Fe	4918.998	45.05	Fe	5369.974	49.17
Fe	4132.067	53.16	Fe	4920.514	41.22	Fe-Ni	5371.501	45.98
Fe	4134.438	47.44	Fe	4938.820	45.68	Fe	5429.706	31.59
Fe	4152.176	37.19	Fe-Dy2	4957.613	69.75	Fe	5442.080	42.21
Fe	4153.906	31.89	Fe	5074.753	29.27	Fe	5816.380	32.14
Mg	4167.277	32.68	Fe	5110.435	47.69	Ca	5857.459	67.01
Fe	4187.047	53.02	Fe	5137.393	38.55	Fe	5914.213	20.30
Fe	4191.437	42.12	Fe	5139.473	34.60	Fe	5987.070	58.74
Fe	4233.612	43.24	Fe	5142.936	27.32	Fe	6003.022	30.40
Fe	4235.949	37.28	Mg-3	5167.327	23.77	Fe	6494.994	24.46
Mo2-Fe	4250.797	36.56	Mg-2	5172.698	59.39	Fe-Ba2	6496.908	21.65
Fe	4260.486	48.42	Mg-1	5183.619	37.08	Ca	6499.654	16.98
Ca-Cr	4289.729	49.11	Cr-Fe	5208.432	34.11	Fe	6592.926	52.88
Fe	4325.775	34.11	Fe	5227.192	43.39	Fe	6633.758	51.21
Mg	4351.921	43.58	Fe	5232.952	31.46	Ni	6643.638	35.62
Fe	4383.551	42.85						

Table 19: Temperature values for SF3 sub-filter that assure the filter to be tuned on desired wavelengths. For some interesting lines it is not necessary to use the SF3 sub-filter. Observation is provided only by DF1, DF2, SF1 and SF2.

spectral line	wavelength [Å]	line FWHM [Å]	temperature [°C]
CaIIK	3933.682	13	not necessary
Hγ	4340.475	1.4	not necessary
BaII	4554.03	0.2	55.0
Hβ	4861.342	1.2	not necessary
Na$-$D1	5895.940	0.4	35.0
Na$-$D2	5889.973	0.4	55.0
He$-$D3	5875.625	0.3	51.0
Hα	6562.808	1.5	not necessary

Table 20: Triangular azimuth distribution of SF3 sub-filter plates with a factor $p = 0.644$.

plate number	azimuth degree	minutes
1	5	48.00
2	-9	-48.00
3	13	48.00
4	-9	-48.00
5	5	48.00

The SF3 tuning capability is provided by a temperature change. Filter is placed within a thermally controlled case enabling to heat up the sub-filter. For some interesting spectral lines it is not necessary to employ the SF3 narrowing capability because lines have wider FWHM. An observation employing only DF1, DF2, SF1 and SF2 is sufficient. To keep an optical length of the filter constant a glass substitution is placed into the optical path instead of SF3.
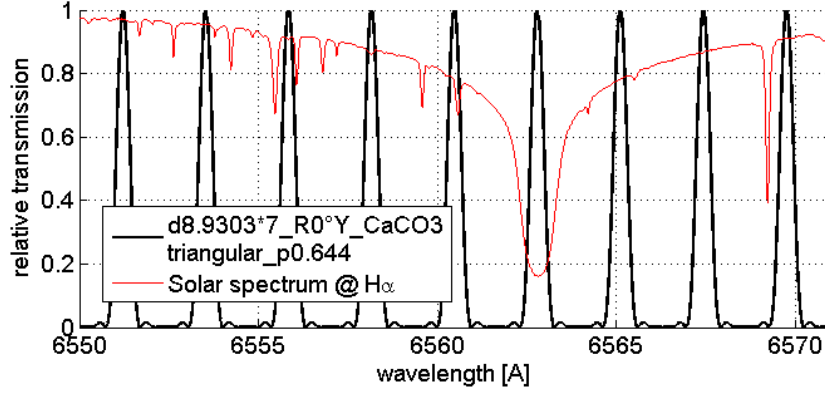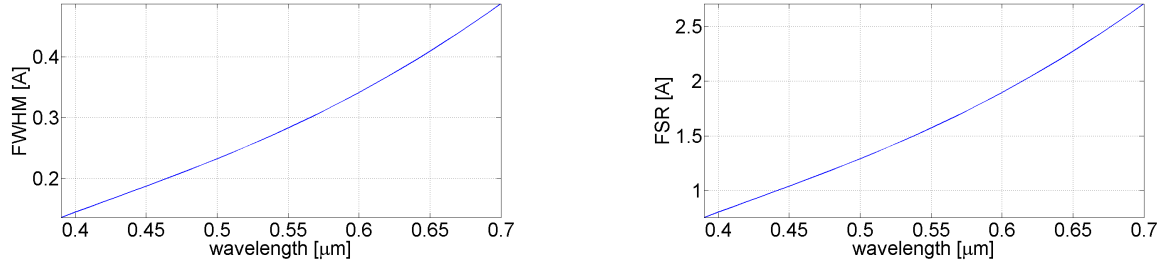
Figure 4.24: Relative transmission profile of SF3 sub-filter tuned at Hα line.

Figure 4.25: Full width at half maximum and free spectral range of SF3 sub-filter as a function of wavelength.

4.5.6   Tuning algorithms

The described universal birefringent filter can be used to observe at a desired wavelength just when all its sub-filters (interference dichroic filters, SF1, SF2 and SF3) are tuned at the wavelength.

Tuning algorithms of particular sub-filters are based on their individual ways of tuning. Interference dichroic filters in a two carousel wheels are designed to transmit corresponding wavelength, so that it is necessary to have placed the correct filter in the optical path. The barrier crystalline quartz sub-filter SF1 compound from oblique cut plates is based on the inclination tuning type described in the section 4.4 and employs the equation 4.17. Its tuning is fast and accurate. The main crystalline quartz sub-filter SF2 is based on the temperature tuning described at the section 2.3.3 when the unit thickness is changed by $\Delta\lambda$ characterized in the equation 4.11. Tuning speed is slower, usually tens of minutes.

The narrowing sub-filter SF3 is also designed to be temperature tuned. Because it is made of crystalline calcite it is necessary to consider equations valid for this material (see table 12). It can be also placed out from the optical path if the observation does not require its usage. Table 21 summarizes tuning types of individual sub-filters of the universal filter.

I have used equations stated in the table 21 to numerically scan the "tuning space" to determine a table of values that needs to be used for a correct wavelength selection. The results of scanning for SF1, SF2 and SF3 are shown at figures 4.26, 4.27 and 4.28 accordingly for the spectral region of Hα line.

Figure 4.26: Transmitted wavelength vs. SF1 filter inclination. The horizontal lines shows values that represent astronomically interesting lines. The intersection determines the value the filter should be adjusted to transmit the desired wavelength. Eg. for Hα (6563 Å) the SF1 should be inclined at $+0.445°$.

Results of the tuning space scanning for the individual sub-filters and for the spectral lines of interests can be seen at table 22.

Table 21: Equation for tuning algorithms of individual sub-filters.

sub-filter	type of tuning	employed equation	speed of tuning	notes
Interference dichroic filters	change in carrousel	no equation	immediate	10 filters in 2 carousels
SF1	inclination	$M_{\phi,\beta} = M \, \frac{1}{\cos^2(\phi+\beta/n')}$ a	immediate	$\beta = <\, -4°; +4°\, >$ inclination range assuring continuous tuning
SF2	temperature change	$M = p_1\lambda^5 + p_2\lambda^4 + p_3\lambda^3 + p_4\lambda^2 + p_5\lambda + p_6$, where $p_1 = 40.8618$, $p_2 = -156.4452$, $p_3 = 241.7107$, $p_4 = -187.1951$, $p_5 = 192.0057$, $p_6 = -16.8497$; $\Delta\lambda(T) = (p_1\lambda^5 + p_2\lambda^4 + p_3\lambda^3 + p_4\lambda^2 + p_5\lambda + p_6) \cdot (35-T)$, where $p_1 = -6.22\mathrm{E}-4$; $p_2 = 1.35\mathrm{E}-3$; $p_3 = 4.30\mathrm{E}-4$; $p_4 = -8.41\mathrm{E}-4$; $p_5 = 8.14\mathrm{E}-4$; $p_6 = 1.62\mathrm{E}-4$	tens of minutes	valid for $0.39 - 1.11\ \mu m$
SF3	temperature change	$M_{\text{calcite}} = (\lambda - 0.1) \cdot \frac{M}{18\lambda-1.37} + 0.05\sin(300 \cdot \log(4.6\lambda)) - 0.04$; $\Delta\lambda_{\text{calcite}} = -\lambda \cdot 10^{-5}[2.5\log(\lambda - 0.14) + 6] \cdot (T - 22C)$	tens of minutes	valid for $0.18 - 4\ \mu m$

$^a \phi$ is an inclination of the oblique cut - 6° for SF1; β in a value of inclination; $n' = \frac{n_e+n_o}{2}$ for small angles of inclination; for M see equation 4.12
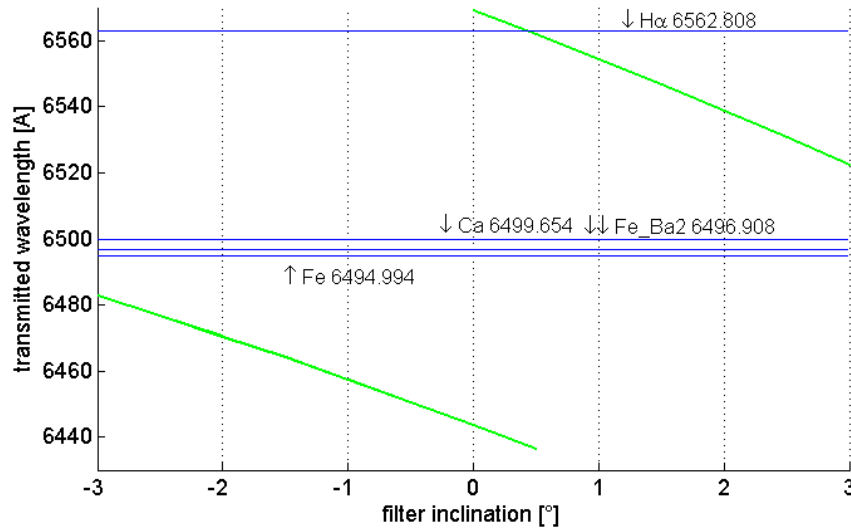
Figure 4.27: Transmitted wavelength vs. SF2 filter temperature. The horizontal lines shows values that represent astronomically interesting lines. The intersection determines the value the filter should be set to transmit the desired wavelength. Eg. for Hα (6563 Å) the SF2 should have temperature of 39.5 °C.
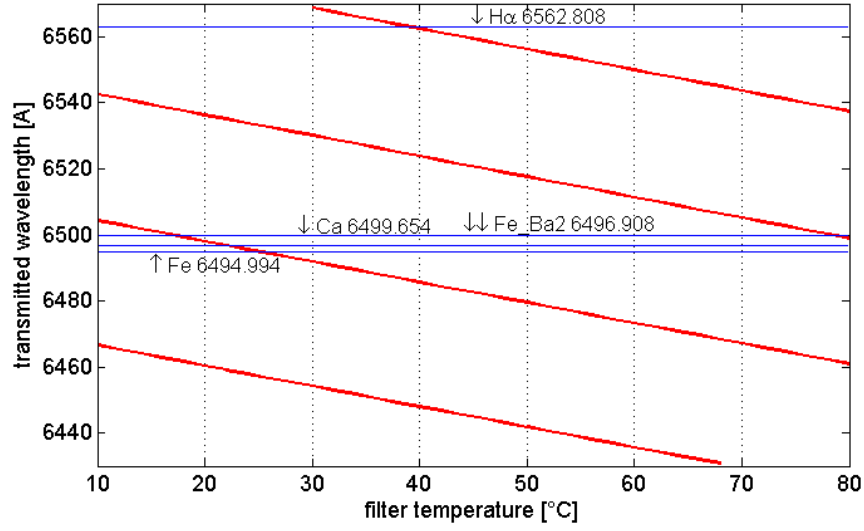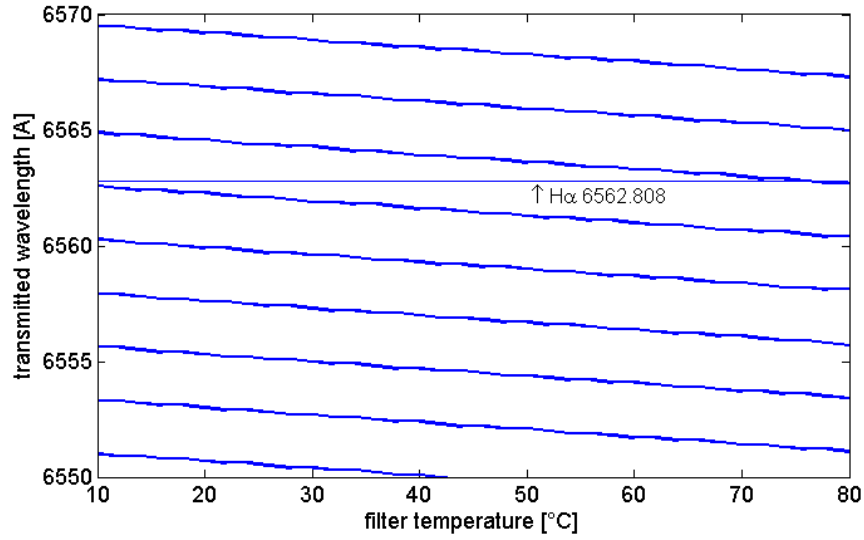

Figure 4.28: Transmitted wavelength vs. SF3 filter temperature. The horizontal lines shows values that represent astronomically interesting lines. The intersection determines the value the filter should be set to transmit the desired wavelength. Eg. for Hα (6563 Å) the SF3 should have temperature of 76.0 °C.

Table 22: Tuning values for individual sub-filters that assure the entire filter to be tuned on desired wavelengths.

spectral line	wavelength [Å]	line FWHM [Å]	SF1 inclination values [°]	SF2 temperature values [°C]	SF3 temperature values [°C]
CaIIK	3933.682	13	-0.43	50.30	not necessary
Hγ	4340.475	1.4	-2.02	34.06	not necessary
BaII	4554.03	0.2	-2.28	23.93	55.0
Hβ	4861.342	1.2	-2.64	43.52	not necessary
Na-D1	5895.940	0.4	-0.91	49.63	35.0
Na-D2	5889.973	0.4	-0.43	59.38	55.0
He-D3	5875.625	0.3	0.82	35.59	51.0
Hα	6562.808	1.5	0.17	39.49	not necessary

4.5.7   Filter set

Individual birefringent sub-filters SF1, SF2 and SF3 and their convolution for Hα spectral region can be seen at figure 4.29, however, in practise only SF1 and SF2 are sufficient to use for Hα observation.

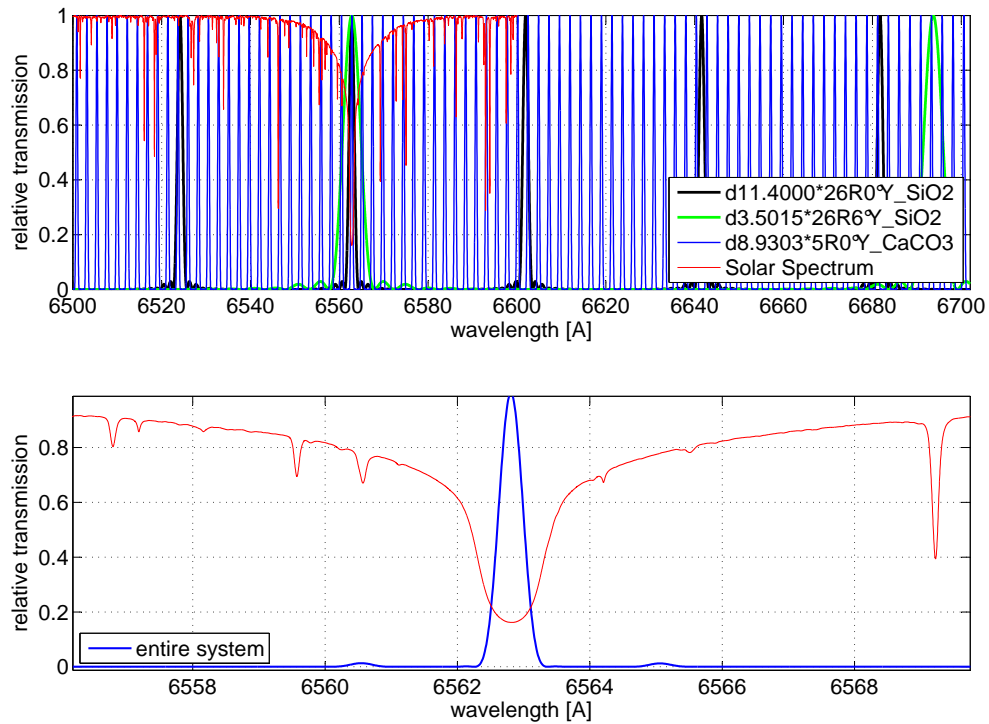

Figure 4.29: The top figure shows individual BF sub-filters SF1, SF2 and SF3 coincidentally tuned on Hα solar line. The bottom figure shows their convolution. In practise only SF1 and SF2 are sufficient to use.

4.6   Optical system design for universal birefringent filter

Professional solar astronomers use high-quality objectives providing a sufficient resolution of observed details of interest. In the Czech Republic the seeing reaches a value in order of seconds, rarely and only at good observation posts it decreases under one second. Considering an observation of the entire solar disc and using our experience with similar

telescopes design, the objective of optical diameter $\varnothing = 140$ mm and image focal length $f' = 2000$ mm has been chosen. Hence, the primary image of the Sun has a diameter about 19 mm. A theoretical resolution of objective is 0.7 second of arc.

A criterion for the objective design is a low value of a longitudinal chromatic aberration. Best results regarding a correction of a spherical aberration, a coma and a modulation transfer function are obtained using an off-axis version of Maksutov system (see figure 4.30) where there is no shading of the primary mirror. The spherochromatic aberration of our objective reaches only $ds' = 0.03$ mm for a spectral range $380 - 760$ nm. Geometrical images in a view field of a solar disc size are smaller than diffraction patterns of 20 μm diameter [45] (see figure 4.31).
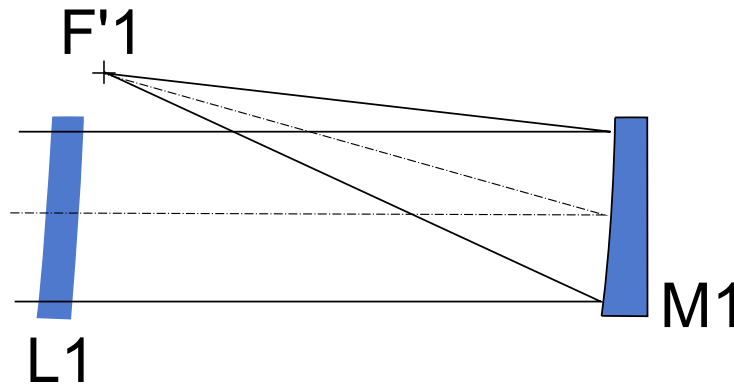

Figure 4.30: Scheme of Maksutov off-axis system. It uses an eccentric meniscus and a spherical mirror. The focal length of 2000 mm and the optical diameter of 140 mm has been chosen.

The entire system, including the imaging system and the filter (see figure 4.32), is optimized as a unit. As a sensor we use a CCD camera SoftHard Technology with a 2/3" chip SONY ICX285AL (10.2×8.3 mm with matrix of 1376×1038 pixels, one pixel has 6.5×6.5 μm). As can be seen from the figure 4.32 the filter is placed in the pupil plane (see the section 2.6.1) which results in a drift of imagined wavelength with the angular space of observation. However, in the case of 0.5° object, for instance the Sun, the drift is about 20 mÅ in Hα region which is acceptable for the 0.5 Å filter.
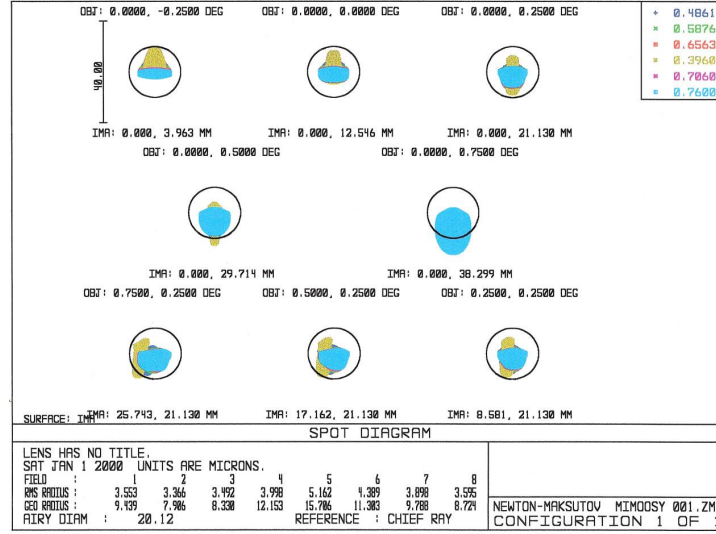
Figure 4.31: A spot diagram of the off-axis Maksutov optical system. In a field of view of the Sun spot diagrams are smaller than a diffraction limit expressed as a diffraction ring of 20 μm diameter.
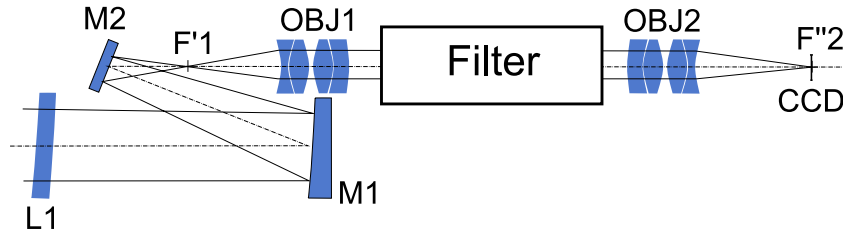

Figure 4.32: An optical scheme of the chromospheric telescope. Elements L1, M1 and M2 form the entrance objective, OBJ1 is the collimating objective that feeds the filter and OBJ2 is the objective focusing light onto the CCD element.

4.7 Mechanical design of the universal birefringent filter

A detailed mechanical design of the universal birefringent filter has been prepared for hundreds hours by mechanical experts working in TOPTEC research centre (former Optical Developmental Workshop) with my close cooperation. Its detailed description is out of a scope of this thesis. Nevertheless, precise mechanics play one of the key role in the high performance optical systems. It has to house the optics within a certain precision with respect to decentering and tilting, in the same time provide precise inclination for SF1 inclination tuning feature and carry the heating systems for SF2 and SF3 sub-filters. From these reasons I show on the following figures at least the outline of the filter individual section mechanics. Detailed design can be found on the enclosed CD in Solid Edge

data format (ASM and PAR files).

Figure 4.33 shows the entire filter whose individual segments are carried by four guide rods. At the beginning and at the end system there are two objectives. The first one is a collimation objective that provides collimated beam, the second objectives is an imaging one. Between objectives the collimated beam is traveling through the individual filter segments.

First two carousel wheels carry the barrier dichroic filters DF1 and DF2. In each wheel there is 6 positions but one of carousel positions is kept filterless (see figure 4.34).

Figures 4.35 and 4.36 show the housing of the barrier inclination sub-filter SF1 and its inclination mechanism.

The figure 4.37 shows the cross-section of the main sub-filter SF2. In the filter case there is a circuit enabling free float of coolant for precise temperature control to enable tuning of the filter.

The figure 4.38 shows the mechanical housing of the narrowing sub-filter SF3.

There is also a set of pictures in the appendix 6 showing the mechanics of the filter in a current state.
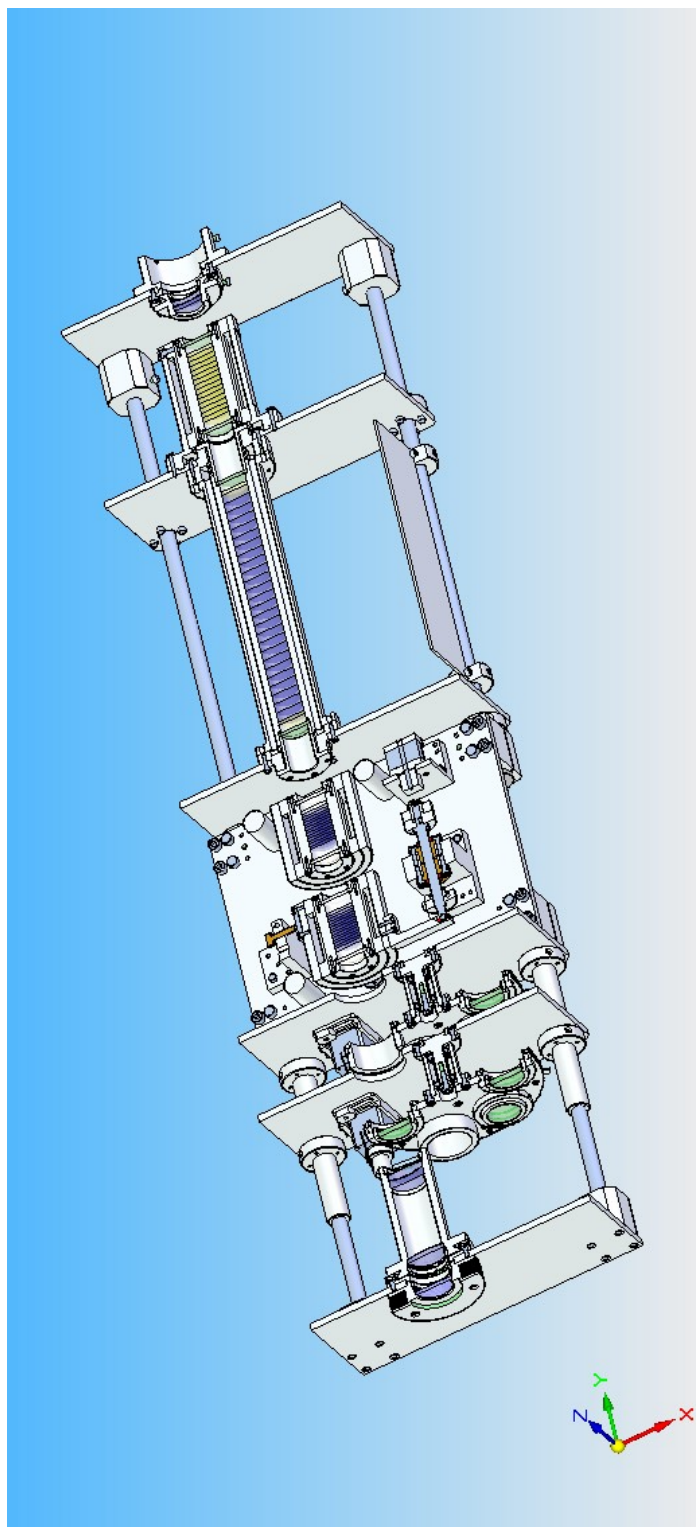
Figure 4.33: A half-cut through the entire filter mechanics.
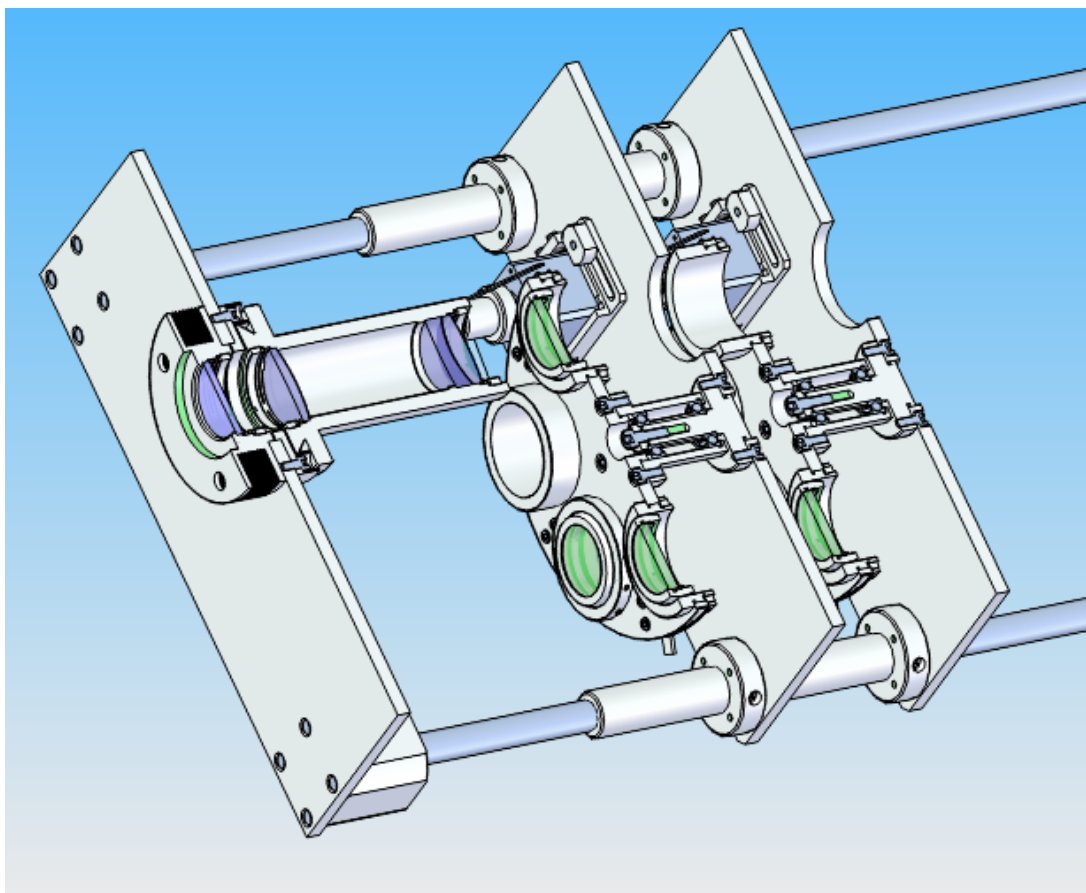
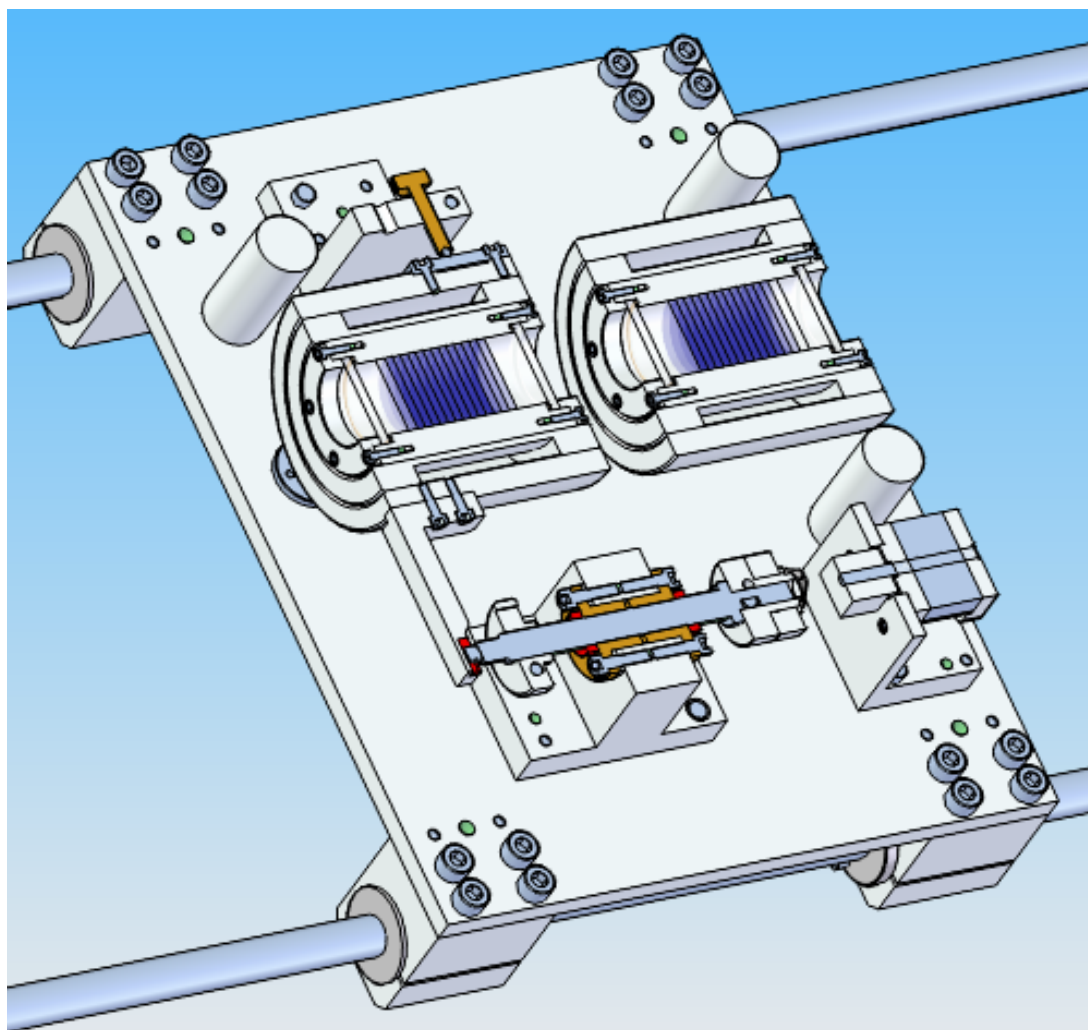Figure 4.34: A half-cut through two carousel segments holding barrier interference filters.

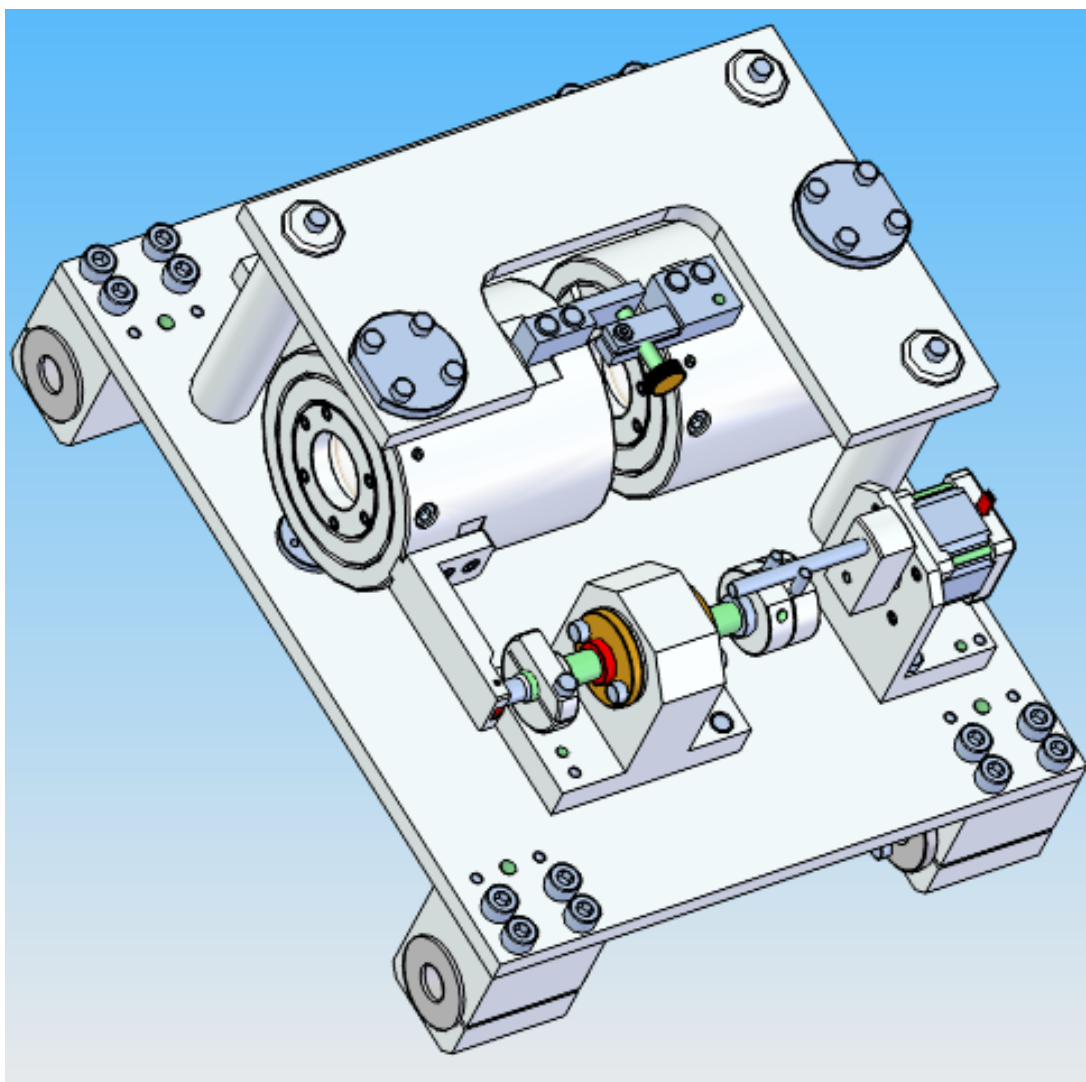Figure 4.35: A half-cut through mechanics of the barrier inclination sub-filter.

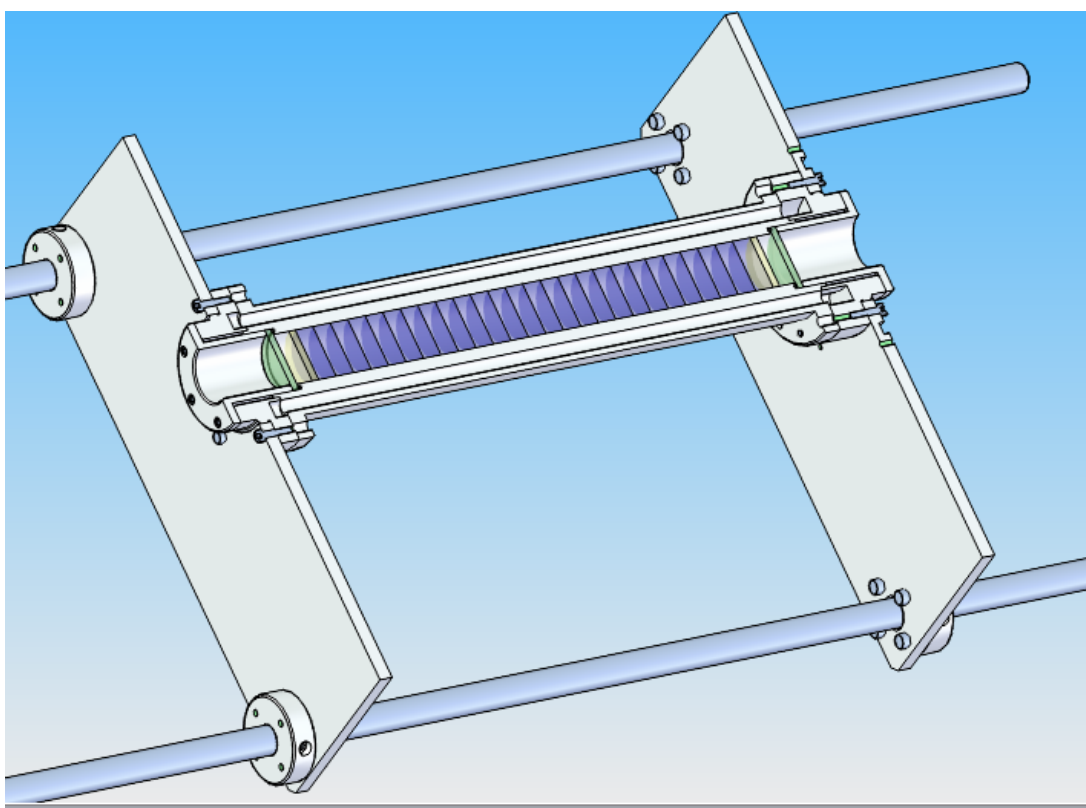Figure 4.36: Mechanics of the barrier inclination sub-filter.

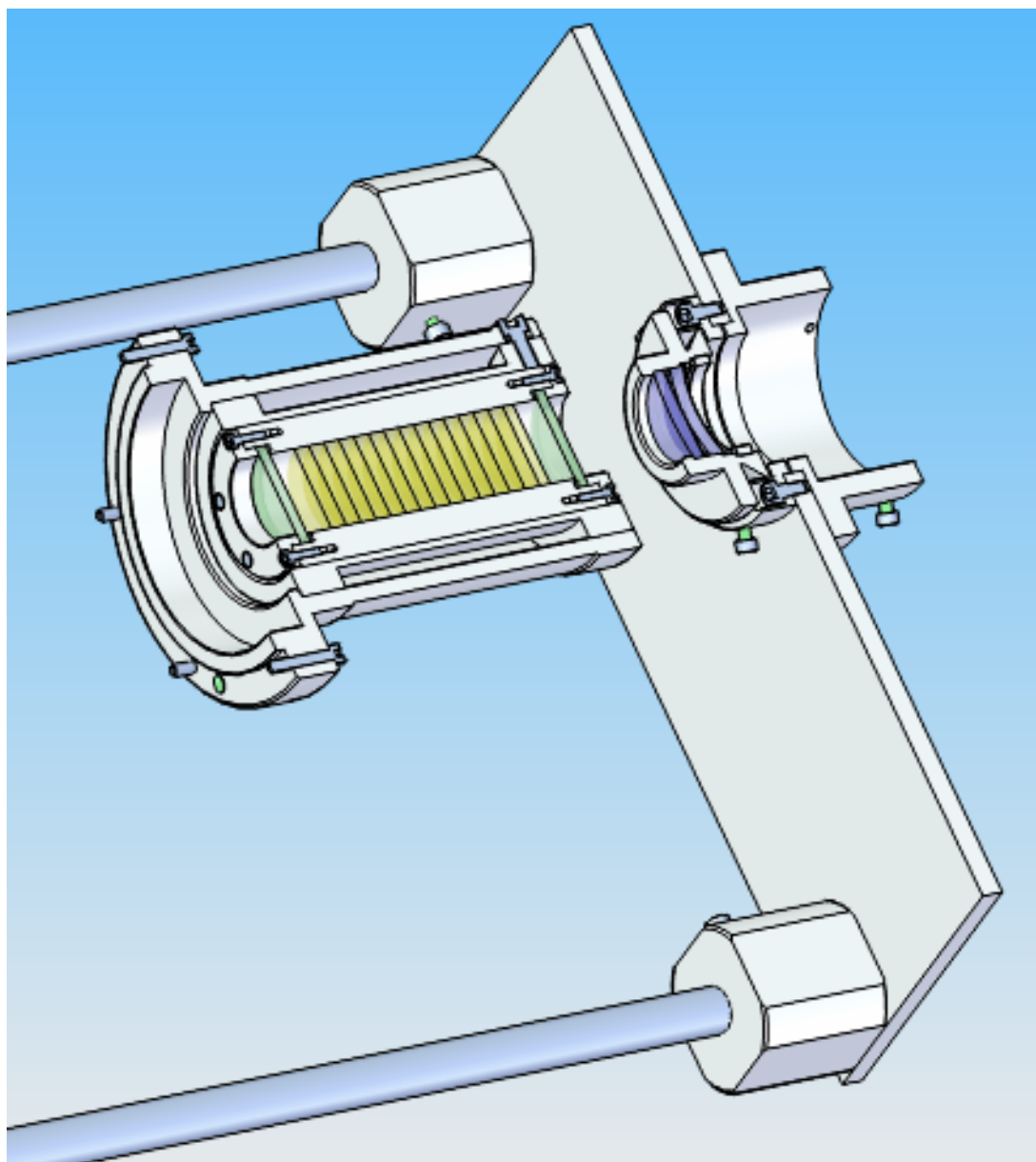Figure 4.37: Cross-section of the main sub-filter mechanics.

Figure 4.38: Mechanical housing cross-section of the narrowing sub-filter SF3.

5 Specific conclusions and the usage of thesis results in practice

Among theoretical contributions of the thesis I consider the manufacturing tolerance budget of Šolc BF individual parts calculated in section 4. Results of analysis determine tolerances that are necessary to be satisfied in order to keep a designed performance of narrow-band birefringent filters. Other conclusion of the analysis suggests a special way of individual parts sorting that enable a usage of parts with loosen tolerances.

Another theoretical contribution of the thesis is the analysis of nowadays available birefringent materials and their usage for a production of achromatic waveplates (section 4.3). Compare to commonly used pair of SiO_2 and MgF_2 materials it is possible from the achromatic point of view to use combinations of BBO and SiO_2 for visible spectral region or SiO_2 and Sapphire for close UV region and achieve a higher achromatism.

The next theoretical contribution, important especially for designers, are precise measurements of crystalline quartz dispersion and its temperature dependency. These data are highly essential especially for the double wavelengths design where the thickness of used plates needs to satisfy the condition 2.20 for both wavelengths simultaneously. Very important is this knowledge also for precise BF tuning.

As a practical contribution of the thesis I consider the analysis and consequent realization of the rapid tunable BF of Šolc type made from birefringent plates of an oblique cut. This type of plates assures the possibility of inclination tuning in one axis only. Within a range of $-4°$ - $+4°$ the full visible spectral tunability is achieved.

Already known and in this work newly achieved knowledge has been utilized in a design and realization of the universal birefringent filter. An advantage is taken especially from the novel design of BF compound of oblique cut plates that enable a rapid tuning - this design is used for the first time in a professional solar filter solution. The other

important entry is a knowledge of quartz dispersion characteristics and their temperature dependency that enable precise tuning based on filter temperature change.

Together with the filter it was designed a dedicated optical system where both the filter and the optical system are optimized as a unit. Entire optical system is housed into customized mechanics which fulfil manufacturing tolerances of the filter and provides tuning capability for individual sub-filters.

6   Conclusion

The Ph.D. thesis gives a comprehensive review on the issue of narrow-band birefringent filters. It results from several year effort and training in a field of optical sciences with a focus on birefringent systems and close cooperation between TOPTEC research centre of Institute of Plasma Physics ASCR, v.v.i. (former Optical Developmental Workshop), Úpice Observatory, Astronomical Institute ASCR, v.v.i. in Ondřejov and Joint Laboratory of Optics of Palacký University and Institute of Physics of AS CR, v.v.i.

To reach the objectives of the thesis I choose program environment MATLAB in order to create a birefringent filter toolbox - dedicated set of codes analyzing physical properties of birefringent filters. Analytical possibilities were employed to study a manufacturing tolerance budget, material dispersion characteristics, an usage of unusual birefringent materials combinations for achromatic waveplate design and a design of a novel tuning method of birefringent filters. Results of analyzes were used afterwards for the synthesis, design and control techniques of tunable birefringent filter of Šolc type.

References

[1] E. W. Max Born, *Principles of Optics*. Cambridge University Press, 2006.

[2] B. Lyot, "Le Filtre Monochromatique Polarisant et ses Applications en Physique Solaire," *Ann. dAstrophys.*, vol. 7, pp. 31–79, 1944.

[3] Y. Öhman, "A new monochromator," *Nature*, vol. 141, pp. 157–158, 1938.

[4] I. Šolc, "Nový typ dvojlomného filtru," *Čs. čas. fyz.*, vol. 3, pp. 366–376, 1953.

[5] I. Šolc, "Další studie k dvojlomnému filtru," *Čs. čas. fyz.*, vol. 4, pp. 669–674, 1954.

[6] J. W. Evans, "Solc Birefringent Filter," *Journal of the Optical Society of America*, vol. 48, pp. 142–145, 1958.

[7] K. Fredga and J. Högbom, "A Versatile Birefringent Filter," *Solar Physics*, vol. 20, p. 204, 1971.

[8] G. Kustal and V. Skomorovski, "Dvochpolosnij i regulirujemyj interferencionno-polarizacionyj filtr na linii HeI i Hα," *Journal of Optics*, vol. 6, pp. 99–105, 2000.

[9] V. Skomorovskij, "Advance of design and technology of birefrigent filters," *Proc. SPIE*, vol. 2265, pp. 413 – 421, 1994.

[10] R. H. Hammerschlag, V. I. Skomorovsky, F. C. M. Bettonvil, G. I. Kushtal, V. L. Olshevsky, R. J. Rutten, A. P. Jgers, G. Sliepen, and F. Snik, "The Irkutsk Barium filter for narrow-band wide-field high-resolution solar images at the Dutch Open Telescope," in *SPIE Astronomical Instrumentation*, 2010.

[11] J. Wang, H. Wang, P. R. Goode, T. J. Spirock, C.-Y. Lee, N. M. Ravindra, J. Ma, and C. Denker, "Optical design of near-infrared birefringent filter system and measurement of birefringent index of calcite at 1.56 um," *Optical Engineering*, vol. 40, pp. 1016–1023, 2001.

[12] P. R. Goode, V. Yurchyshyn, W. Cao, V. Abramenko, A. Andic, K. Ahn, and J. Chae, "Highest Resolution Observations of the Quietest Sun," *The Astrophysical Journal Letters*, vol. 714, pp. L31–L35, 2010.

[13] T. Sakurai, ed., *The Hinode Mission.* Springer, 2008.

[14] I. Šolc, "Laboratorní zpráva," tech. rep., VÚM Turnov, 1959.

[15] R. Melich, "Šíření rovinné elektromagnetické vlny anizotropním prostředím," Master's thesis, Palacký University in Olomouc, 2005.

[16] W. Shurcliff, *Polarized Light, Production and Use.* Harvard University Press, Cambridge, Massachusetts, 1962.

[17] I. Šolc, "Řetězové dvojlomné filtry," *Čs. čas. fyz.*, vol. 10, pp. 16–34, 1960.

[18] I. Šolc, "Grafické řešení dvojlomných filtrů," *Čs. čas. fyz.*, vol. 16, pp. 128–136, 1966.

[19] I. Šolc, "Dispersion relation of quartz and calcite birefringence," *Fine Mechanics and Optics*, vol. 2, pp. 43–48, 1984.

[20] R. Melich, Z. Melich, I. Šolc, V. Mikule, and H. Oupická, "Materiál MgF_2 pro výrobu dvojlomných filtrů.," in *Zborník referátov z 19. celoštátného slnečného seminára* (I. Dorotovič, ed.), pp. 161–164, Sloveská ústredná hvezdareň, Hurbanovo, 2008. ISBN 978-80-85221-60-2.

[21] I. Šolc, "Birefringent Chain Filter," *J.O.S.A.*, vol. 55, pp. 621–625, 1965.

[22] A. Yariv and P. Yeh, *Optical Waves in Crystals.* John Wiley & Sons, Inc., Hoboken, New Jersey, 2003.

[23] I. Šolc, "Chain Bi-refringent Filters," *Czechoslovak Journal of Physics*, vol. 9, pp. 237–249, 1959.

[24] A. Title and W. Rosenberg, "Research on Spectroscopic Imaging, Lunar and Planetary Programs," tech. rep., NASA Headquarters, 1979.

[25] I. Šolc, "Coincidence chain birefringent filters (in Czech)," *Fine Mechanics and Optics*, pp. 159–161, 1971.

[26] Šolc. I. and Šrytr. V., "Rentgenový spektrometr pro přesnou orientaci krystalových výbrusů," *Jemná mechanika a optika*, vol. 2, pp. 43–45, 1960.

[27] G. B. Scharmer, "Comments on the optimization of high resolution Fabry-Pérot filtergraphs," *A&A*, vol. 447, pp. 1111–1120, 2006.

[28] B. Saleh and M. Teich, *Fundamentals of Photonics*. Wiley-Interscience, 1991.

[29] S. Chandrasekhar *Astrophys. J.*, vol. 104, p. 110, 1946.

[30] G. Stokes, "On the composition and resolution of streams of polarized light from different sources," *Trans. Cambridge Philos. Soc.*, vol. 9, pp. 399 – 416, 1852.

[31] H. Mueller, "The foundation of optics," *J. Opt. Soc. Am.*, vol. 38, p. 661, 1948.

[32] D. Berreman *J. Opt. Soc. Am.*, vol. 62, pp. 502 – 510, 1967.

[33] J. Křepelka, *Tenké vrstvy*. Univerzita Palackého v Olomouci, 1993.

[34] A. I. of Physics, *American Institute of Physics Handbook*. McGraw-Hill Book Company, 1972.

[35] D. G. P. I. Voronkova E.M., Grechushnikov B.I., *Optical materials for infrared techniques*. Nauka, Moscow, 1965.

[36] R. Melich, "Measurement of basic material characteristics of birefringent filter transmittance," in *Proceedings of conference "Man in his terrestrial and cosmis neigbourhood"*, 2006.

[37] F. J. M. J. Maessen and J. A. Tielrooij, "Dispersion of grating monochromators," *Fresenius' Journal of Analytical Chemistry*, vol. 323, p. 490.

[38] O. Bečicka, "Temperature characteristics of crystalline quartz birefringence," Master's thesis, UP Olomouc, Department of Optics, 2009.

[39] "Solar Survey Archive BASS2000." http://bass2000.obspm.fr/solar_spect.php.

[40] K. Serkowski, *Methods of experimental physics: Astrophysics.* Academic press: New York and London, 1974.

[41] R. Melich, Z. Melich, I. Šolc, J. K. sr., and J. K. jr., "New type of a birefringent barrier element for narrow-band chain filter," in *Proceedings of conference "Man in his terrestrial and cosmic neigbourhood"*, 2006.

[42] I. Šolc, "Birefringent crystal monochromators are still actual," in *Proceedings of Úpice Observatory Conference "The man in his terrestrial and cosmic neighbourhood"*, 1997.

[43] I. Šolc, "Birefringent filter for two optional wavelengths," *Fine Mechanics and Optics*, vol. 21, pp. 279 – 281, 1976.

[44] Z. Melich, J. Klimeš, and I. Šolc, "Chain filters built of oblique cut birefringent plates," in *Proceedings of Úpice Observatory Conference "The man in his terrestrial and cosmic neighbourhood"*, pp. 30–36, Upice Observatory, 2005.

[45] Z. Rail, D. Jareš, and V. Lédl, "Imaging system for spectrographe with multichannel Solc filter," in *Proceedings of Úpice Observatory Conference "The man in his terrestrial and cosmic neighbourhood"*, 2006.

[46] "ASEP." http://www.library.sk/i2/i2.entry.cls?ictx=cav&logout=1&language=2&skin=1&show.

Pictures from realization of thesis objectives

Figure 6.1: Radek Melich, the author of the Ph.D. thesis, and Ivan Šolc, the inventor of Šolc birefringent filter.

Figure 6.2: Radek Melich, the author of the Ph.D. thesis, and Jaromír Křepelka, his supervisor.

Figure 6.3: Ivan Šolc, Jan Klimeš,sr. and Zbyněk Melich at Úpice Observatory. Jan Klimeš is a professional astronomer who is running the solar patrol telescope at Úpice Observatory. The telescope was used for a measurement of a unit thisckness dispersion characteristics. Zbyněk Melich is a head of a scientific program at TOPTEC research centre where the universal birefringent filter is developed.

Figure 6.4: Staff of former Optical Developmental Workshop (recent TOPTEC research centre) who contribute to production of the universal birefringent filter.

Figure 6.5: Ondřej Bečicka helped to investigate the crystalline quartz dispersion characteristics which is necessary for a precise design of narrow-band birefringent filters and their precise tuning.

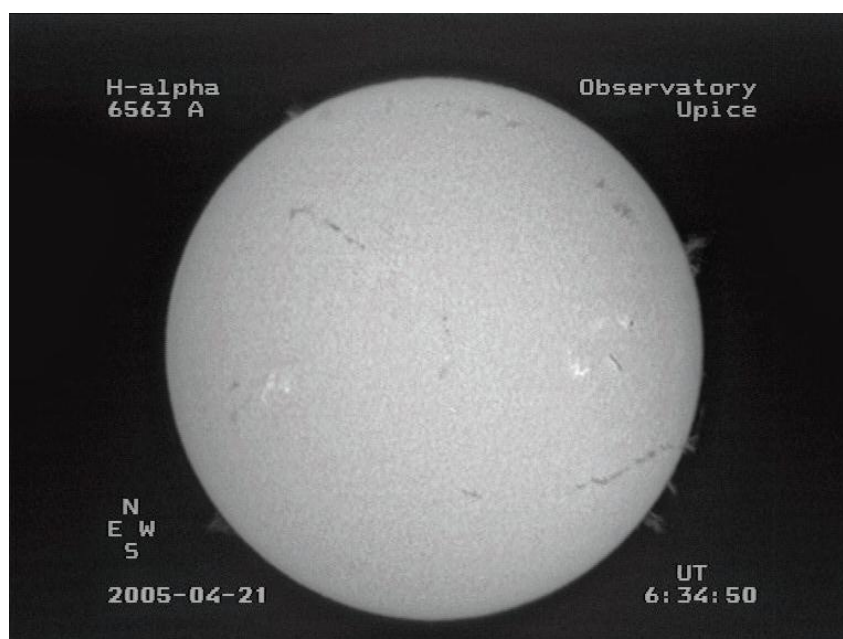Figure 6.6: Birefringent filter of Šolc type currently used at Úpice observatory for solar observations at Hα line.

Figure 6.7: An image of solar chromosphere at Hα line taken by the chromospheric telescope at Úpice observatory.
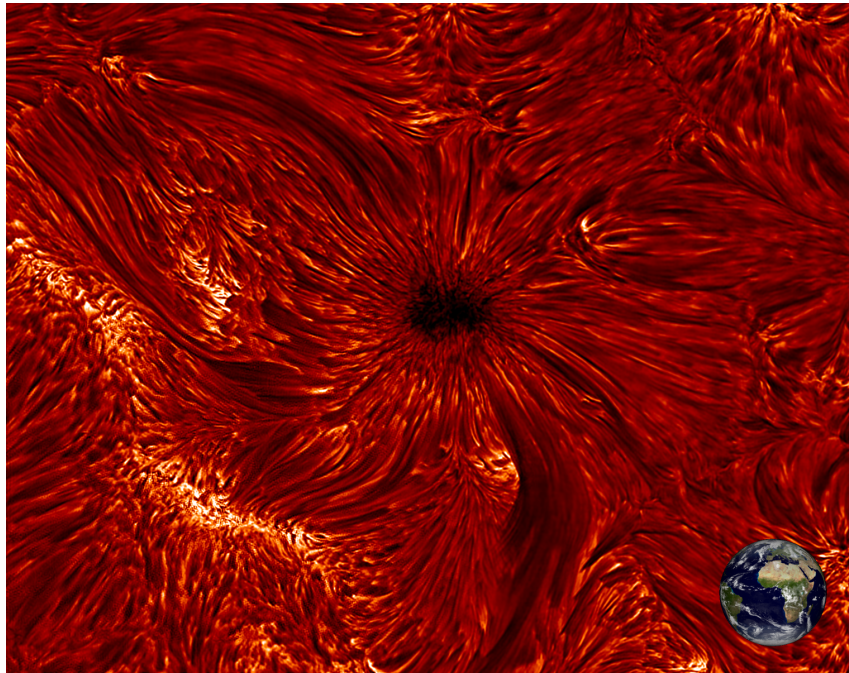
Figure 6.8: Detail of solar chromosphere at Hα line taken by DOT telescope at La Palma.

Figure 6.9: DOT telescope at La Palma with its designer Dr. Robert Hammerschlag. At the background the SST telescope can be seen.

Figure 6.10: Jan Klimeš, sr. taking an image of solar spectra in Hα region. The solar spectrum is overlayed by a channel spectrum of Šolc type BF.
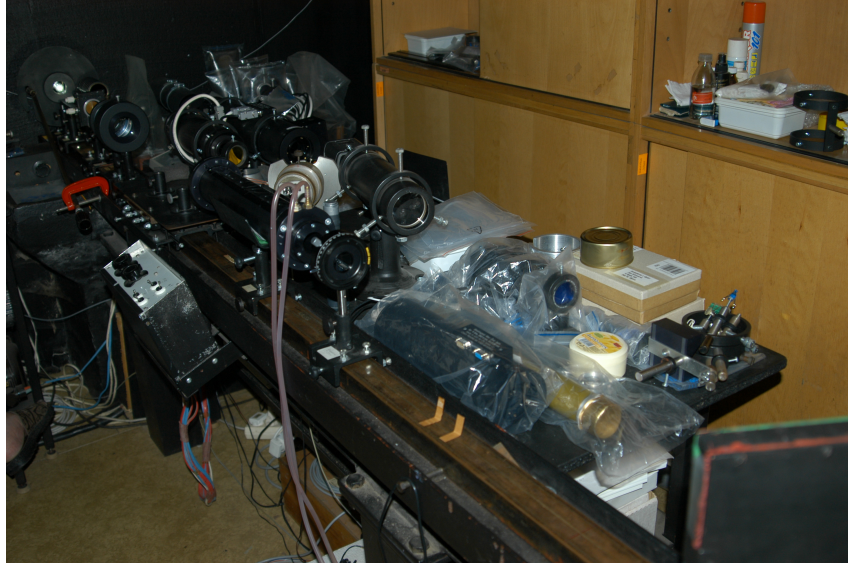
Figure 6.11: Setup for measurement of crystalline quartz dispersion characteristics. It corresponds with the figure 4.5.

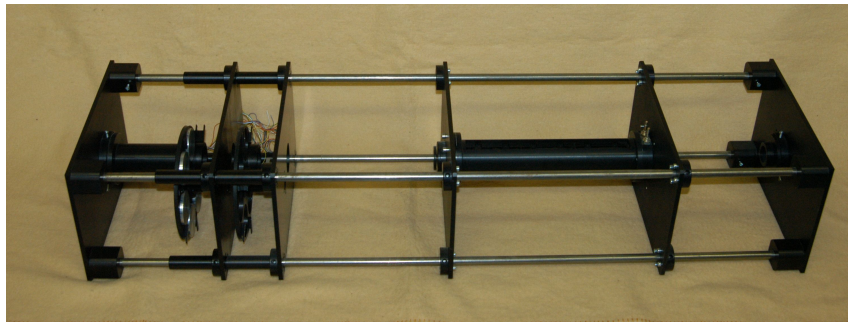Figure 6.12: DF1, DF2, SF2 parts of the universal birefringent filter on the four guiding rots. At the beginning of the system and at the end there are collimating and imagining objectives.

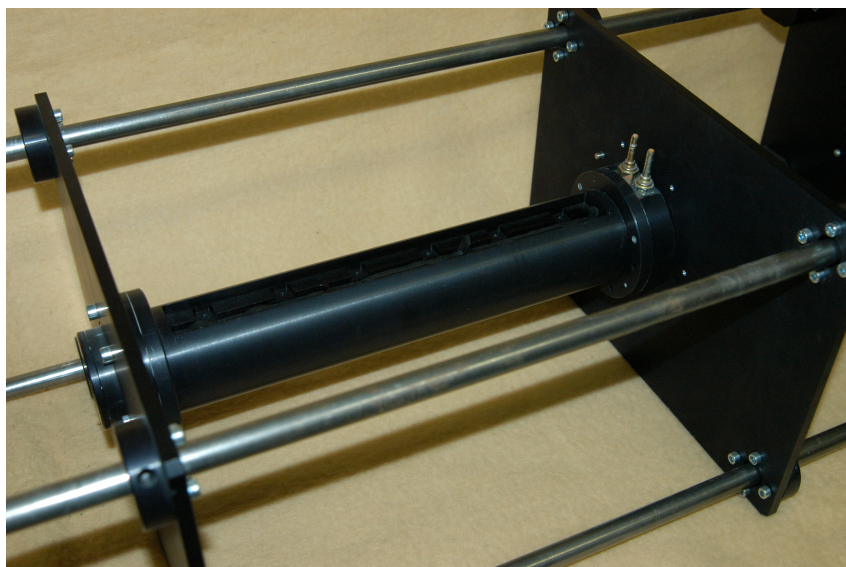Figure 6.13: Housing of the SF2 filter containing special inside cavities for coolant liquid that enables precise temperature control.
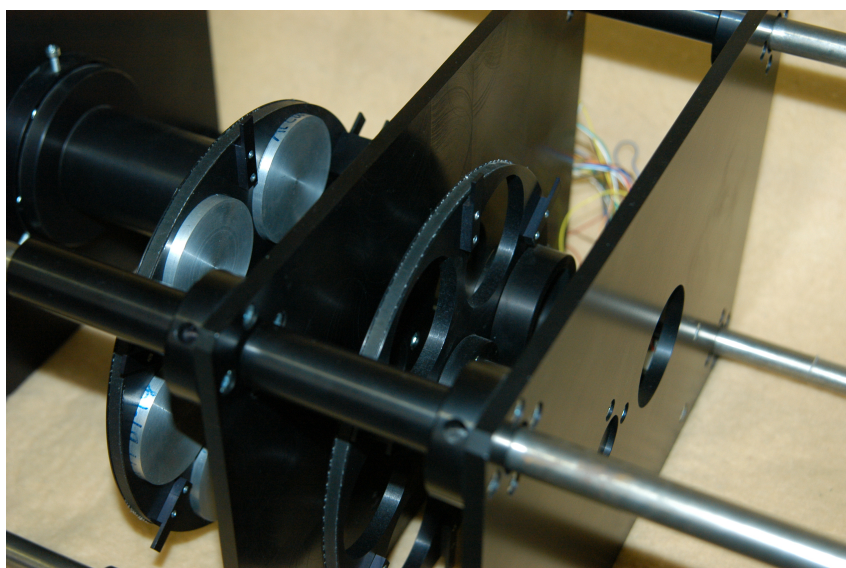
Figure 6.14: Two rotating carousels house dichroic filters and color glasses - DF1 and DF2.

Figure 6.15: Housing of SF3 filter.

Figure 6.16: Two optical and mechanical parts of SF1 filter ready for an assemble.

Figure 6.17: Housing for the SF1 inclination sub-filter.

Contents of enclosed CD

- Ph.D. thesis in original latex files and final pdf version

- MATLAB BF toolbox

- Universal birefringent filter mechanics in Solid Edge data format (ASM and PAR files)

- Optical design of solar telescope utilizing universal birefringent filter in ZEMAX data format

Author's publications

All detailed information about author's publications can be found on ASEP system (Register of publication of Academy of Sciences of the Czech Republic) [46].

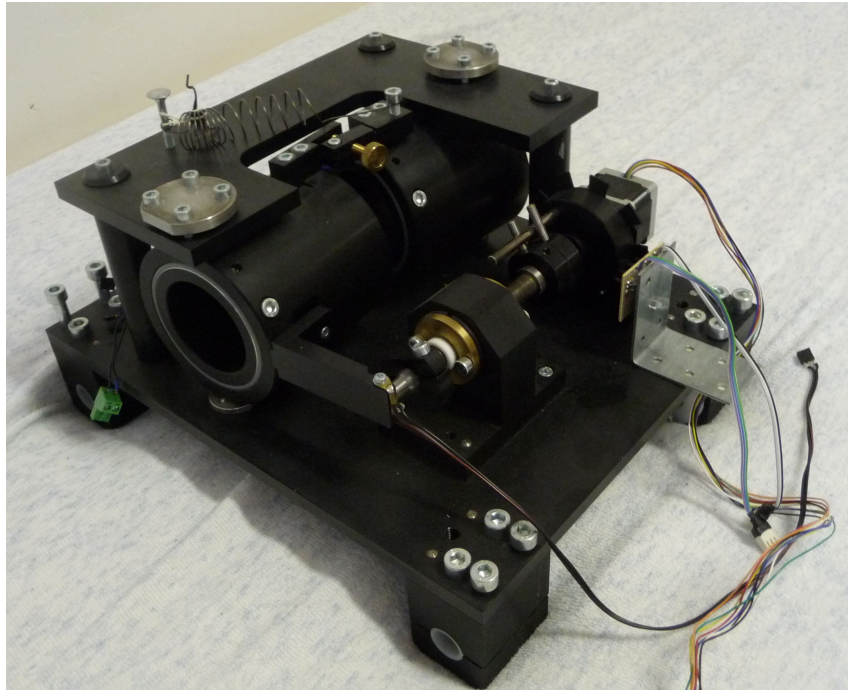[1] Melich, Radek; Rail, Zdeněk; Melich, Zbyněk. Zvýšení rozlišovací schopnosti malých chromosférických dalekohledů. In Člověk ve svém pozemském a kosmickém prostředí. Bulletin referátů z konference. Úpice: Hvězdárna v Úpici, 2011. pages: 37-40. ISBN 978-80-86303-26-0. [Člověk ve svém pozemském a kosmickém prostředí/31./, Úpice, 18.05.2010-20.05.2010, CZ]. Available at: http://www.cbks.cz/upice2010/037.pdf

[2] Weinzettl, Vladimír; Pánek, Radomír; Hron, Martin; St¨ckel, Jan; Žáček, František; Havlíček, Josef; Bílková, Petra; Naydenkova, Diana; Háček, Pavel; Zajac, Jaromír; Dejarnac, Renaud; Horáček, Jan; Adámek, Jiří; Mlynář, Jan; Janky, Filip; Aftanas, Milan; Böhm, Petr; Brotánková, Jana; Šesták, David; Ďuran, Ivan; Melich, Radek; Jareš, Daniel; Ghosh, Joydeep; Anda, B.; Veres, G.; Szappanos, A.; Zoletnik, S.; Berta, M.; Shevchenko, V. F.; Scannell, R.; Walsh, D.; Müller, H. W.; Igochine, V.; Silva, A.; Manso, M.; Gomes, R.; Popov, Tsv.; Sarychev, D.; Kiselov, V.K.; Nanobashvili, S. Overview of the COMPASS diagnostics. Fusion Engineering and Design, 2011, Vol. 86, 6-8, pages: 1227-1231. ISSN 0920-3796. Available at:
http://www.sciencedirect.com/science/article/pii/S0920379610005594

[3] Bílková, Petra; Aftanas, Milan; Böhm, Petr; Weinzettl, Vladimír; Šesták, David; Melich, Radek; Stöckel, Jan; Scannell, R.; Walsh, M. Design of new Thomson scattering diagnostic system on COMPASS tokamak. Nuclear Instruments & Methods in Physics Research Section A, 2010, Vol. 623, No. 2, pages: 656-659. ISSN 0168-9002. Available at: www.elsevier.com/locate/nima

[4] Bílková, Petra; Melich, Radek; Aftanas, Milan; Böhm, Petr; Šesták, David; Jareš, Daniel; Weinzettl, Vladimír; Stöckel, Jan; Hron, Martin; Pánek, Radomír; Scannell, R.;

Walsh, M. Progress of development of Thomson scattering diagnostic system on COM-PASS. Review of Scientific Instruments, 2010, Vol. 81, No. 10, 10D531-10D531. ISSN 0034-6748. Available at: http://link.aip.org/link/?RSI/81/10D531

[5] Rail, Zdeněk; Jareš, Daniel; Lédl, Vít; Melich, Radek; Melich, Zbyněk; Václavík, Jan; Oupický, Pavel. Optický návrh zobrazovací soustavy spektrografu s vícekanálovým filtrem. In Člověk ve svém pozemském a kosmickém prostředí Bulletin referátů ze semináře. Úpice: Hvězdárna Úpice, 2010. pages: 45-52. ISBN 978-80-86303-23-9. [Člověk ve svém pozemském a kosmickém prostředí, Úpice, 19.05.2009-21.05.2009, CZ].

[6] Weinzettl, Vladimír; Naydenkova, D.I.; Šesták, David; Vlček, Jiří; Mlynář, Jan; Melich, Radek; Jareš, Daniel; Malot, J.; Sarychev, D.; Igochine, V. Design of multi-range tomographic system for transport studies in tokamak plasmas. Nuclear Instruments & Methods in Physics Research Section A, 2010, Vol. 623, No. 2, pages: 806-808. ISSN 0168-9002. Available at:
http://www.sciencedirect.com/science?_ob=ArticleURL&_udi=B6TJM-4YTFBF2-C
&_user=6542793&_coverDate=11%2F11%2F2010&_rdoc=1&_fmt=high
&_orig=search&_origin=search&_sort=d&_docanchor=&view=c
&_searchStrId=1546173561&_rerunOrigin=google&_acct=C000070123
&_version=1&_urlVersion=0&_userid=6542793
&md5=1642ebdad07f4009a3a7b81bb4d11c8f&searchtype=a

[7] Bílková, Petra; Aftanas, Milan; Böhm, Petr; Weinzettl, Vladimír; Šesták, David; Melich, Radek; Stöckel, Jan; Scannell, R.; Walsh, M. Conceptual design of High resolution Thomson scattering system on COMPASS tokamak. In 14th International Symposium on Laser Aided Plasma Diagnostics - Book of Abstracts. Castelbrando, Treviso: Consorzio RFX, 2009. P03-P03.

[8] Bílková, Petra; Böhm, Petr; Aftanas, Milan; Šesták, David; Melich, Radek; Weinzettl, Vladimír; Stöckel, Jan; Scannell, R.; Walsh, M. Design of Thomson scattering diagnostic

system on COMPASS tokamak. In 1st International Conference on Frontiers in Diagnostic Technologies - Book of Abstracts. Frascati: ENEA-FPN Department, 2009. pages: 1-1. Available at: http://cfdt.frascati.enea.it/

[9] Klvaňa, Miroslav; Sobotka, Michal; Melich, Radek; Melich, Zbyněk; Rail, Zdeněk. Celodiskový dalekohled pro teleskop EST. In Zborník referátov z 19. celoštátného slnečného seminára Popradno 2008. Sloveská Ústredná hvezdareň, Hurbanovo: Slovak Academy of Sciences, 2008. pages: 1-4. ISBN 978-80-85221-60-2. [Celoštátny slnečný seminár Popradno 2008 /19./, Popradno (Považská Bystrica), 12.05.2008-16.05.2008, SK].

[10] Melich, Radek; Melich, Zbyněk; Šolc, Ivan; Mikule, Václav; Oupická, Hana. Materiál MgF2 pro výrobu dvojlomných filtrů. In Zborník referátov z 19. celoštátného slnečného seminára Popradno 2008. Sloveská Ústredná hvezdareň, Hurbanovo: Slovak Academy of Sciences, 2008. pages: 161-164. ISBN 978-80-85221-60-2. [Celoštátny slnečný seminár Popradno 2008 /19./, Popradno (Považská Bystrica), 12.05.2008-16.05.2008, SK]. Available at: http://www.suh.sk/obs/slnsem/melich.pdf

[11] Melich, Radek; Melich, Zbyněk; Šolc, Ivan. Multi-wavelength Šolc birefringent filter. In Proceedings of the Advanced Optical and Mechanical Technologies in Telescopes and Instrumentation 7018.. Bellingham, Washington: Society of Photo-Optical Instrumentation Engineers, 2008. pages: 1-7. ISBN 9780819472281. [The Physics of Chromospheric Plasma, Marseille, 23.06.2008-27.06.2008, FR].

[12] Melich, Radek; Melich, Zbyněk; Šolc, Ivan; Klimeš st., J.; Klimeš ml., J. Návrh dvojlomného filtru pro čáry HeI a CaII v infračerveném oboru. In Člověk ve svém pozemském a kosmickém prostředí .Bulletin referátů z konference. Úpice: Hvězdárna Úpice, 2008. pages: 4-7. ISBN 978-80-86303-14-7. [Člověk ve svém pozemském a kosmickém prostředí, Úpice, 20.05.2008-22.05.2008, CZ].

[13] Melich, Radek; Melich, Zbyněk; Šolc, Ivan; Klimeš st., J.; Klimeš ml., J. Nový

typ dvojlomné předsádky Úzkopásmového filtru. In Člověk ve svém pozemském a kosmickém prostředí. Bulletin referátů z konference. Úpice: Hvězdárna v Úpici, 2008. pages: 156-161. ISBN 978-80-86303-11-6. [Člověk ve svém pozemském a kosmickém prostředí, Úpice, 22.05.2007-24.05.2007, CZ].

[14] Rail, Zdeněk; Šrajer, Bohdan; Lédl, Vít; Jareš, Daniel; Oupický, Pavel; Melich, Radek; Melich, Zbyněk. Objektiv Merz 160/1790 refraktoru Hvězdárny v Úpici. In Člověk ve svém pozemském a kosmickém prostředí .Bulletin referátů z konference. Úpice: Hvězdárna Úpice, 2008. pages: 70-75. ISBN 978-80-86303-14-7. [Člověk ve svém pozemském a kosmickém prostředí, Úpice, 20.05.2008-22.05.2008, CZ].

[15] Melich, Radek; Melich, Zbyněk. Influence of image doubling on modulation transfer function of optical systems. In Proceedings of SPIE 6609., 2007. 66091F-1-66091F-8. ISBN 978-0-8194-6748-5. ISSN 0277-786X. [Czech-Polish-Slovak Conference on Wave and Quantum Aspects of Contemporary Optics/15th./, Liberec, 11.10.2006-15.10.2006, CZ].

[16] Melich, Radek. Měření základních materiálových charakteristik propustnosti řetězového filtru. In Člověk ve svém pozemském a kosmickém prostředí; Bulletin referátů z konference. Úpice: Hvězdárna v Úpici, 2007. pages: 38-50. ISBN 80-86303-10-1. [Člověk ve svém pozemském a kosmickém prostředí, Úpice, 16.05.2006-18.05.2006, CZ].

[17] Melich, Radek; Melich, Zbyněk; Šolc, Ivan. Šolc birefringent filter for several interesting spectral lines. In Proceedings of the Physics of Chromospheric Plasma 368, 2007. pages: 621-625. ISBN 978-1-58381-236-5. [The Physics of Chromospheric Plasma, Coimbra, 11.10.2006-15.10.2006, PT].

[18] Melich, Zbyněk; Melich, Radek. Influence of small deformation of optical element surfaces on optical system imaging quality. In Proceedings of SPIE 6609, 2007. 66091E-1. ISBN 978-0-8194-6748-5. ISSN 0277-786X. [Czech-Polish-Slovak Conference on Wave and Quantum Aspects of Contemporary Optics/15th./, Liberec, 11.10.2006-15.10.2006, CZ].

[19] Melich, Radek; Melich, Zbyněk; Šolc, Ivan; Klimeš st., Jan; Klimeš, J. Řetězový filtr pro více astronomicky zajímavých spektrálních čar. In Zbornik referatov z 18. celostatneho slnecneho seminara. Hurbanovo: Slovenska ustredna hvezdaren, 2006. pages: 1-5. [Celoštátny slnečný seminár/18./, Modrá, 22.05.2006-26.05.2006, SK]. Available at: http://www.suh.sk/obs/slnsem/melich.pdf

[20] Melich, Radek; Melich, Zbyněk. Vliv zdvojení obrazu na funkci přenosu kontrastu optické soustavy. Jemná mechanika a optika, 2006, Vol. 51, 11-12, pages: 308-312. ISSN 0447-6441.

[21] Melich, Zbyněk; Melich, Radek; Oupický, Pavel; Šolc, Ivan; Klimeš st., J.; Klimeš ml., J. Řetězový filtr pro více astronomicky zajímavých spektrálních čar. In Člověk ve svém pozemském a kosmickém prostředí. Úpice: Hvězdárna v Úpici, 2006. pages: 21-28. ISBN 80-86303-10-1. [Člověk ve svém pozemském a kosmickém prostředí, Úpice, 16.05.2006-18.05.2006, CZ].

[22] Tidemand-Lichtenberg, P.; Janousek, J.; Mortensen, J.; Jesper, L.; Buchhave, P.; Melich, Radek. Synchronization of 1064 and 1342 nm pulses using passive saturable absorbers. Optics Communications, 2004, Vol. 241, 4-6, pages: 487-492. ISSN 0030-4018.

Research Reports

[1] Melich, Radek. Illumination study under 3SU1 project - E-Stop Button. Technical Report for Siemens AG Amberg, Germany. TOPTEC, Institute of Plasma Physics AS CR, v.v.i. Turnov 2011

[2] Melich, Radek. Illumination study under 3SU1 project - Push Button. Technical Report for Siemens Electrical Apparatus Ltd.,Suzhou, China. TOPTEC, Institute of Plasma Physics AS CR, v.v.i. Turnov 2011

[3] Melich Radek. Optical design optimization of yarn quality sensor. Technical report for Rieter CZ s.r.o., Optical Diagnostics, Institute of Plasma Physics AS CR, v.v.i., Turnov 2009

[4] Melich Radek. Solar collector solved as Cassegrain type objective. Technical Report for Ditech SK, s.r.o., Optical Diagnostics, Institute of Plasma Physics AS CR, v.v.i., Turnov 2009

[5] Melich Radek. Off-axis version of solar collector. Technical Report for Ditech SK, s.r.o., Optical Diagnostics, Institute of Plasma Physics AS CR, v.v.i., Turnov 2009

[6] Melich, Radek. Illumination study under 3SU1 project - Pilot Light. Technical Report for SIEMENS s.r.o., o.z. Nízkonapěťová spínací technika, Trutnov. Optical Diagnostics, Institute of Plasma Physics AS CR, v.v.i., Turnov 2009

[7] Melich, Radek. Illumination study under 3SU1 project - E-Stop Button. Technical Report for Siemens AG Amberg, Germany. TOPTEC, Institute of Plasma Physics AS CR, v.v.i. Turnov 2011

[8] Melich, Radek. Illumination study under 3SU1 project - Push Button. Technical Report for Siemens SIEMENS Electrical Apparatus Ltd.,Suzhou, China. TOPTEC, Institute of Plasma Physics AS CR, v.v.i. Turnov 2011

Industrial models

[1] Jareš, Daniel; Melich, Radek; Rail, Zdeněk. Držák svazků optických vláken. Praha: Úřad průmyslového vlastnictví ČR, 2011. 182 00 Praha 8, Za Slovankou 1782/3: Ústav fyziky plazmatu AV ČR, v.v.i, 10.10.2011. 22770. Available at: http://spisy.upv.cz/UtilityModels/FullDocuments/FDUM0022/uv022770.pdf

[2] Jareš, Daniel; Melich, Zbyněk; Melich, Radek; Lédl, Vít. Objímka Šolcova dvojlomn/ve polariza/vcn/'iho filtru. Praha: Úřad průmyslového vlastnictví ČR, 2008. Praha 8, Za Slovankou 1782/3: Ústav fyziky plazmatu AV ČR, v.v.i, 22.09.2010. 2009-159. Available at:

http://isdv.upv.cz/portal/pls/portal/portlets.pts.det?xprim=1254319&lan=cs

[3] Jareš, Daniel; Lédl, Vít; Melich, Radek. Zařízení na přesné celoplošné leštění sférických těles. Praha: Úřad průmyslového vlastnictví ČR, 2008. Praha 8, Za Slovankou 1782/3: Ústav fyziky plazmatu AV ČR, v.v.i, 02.06.2008. 18622. Available at:

http://spisy.upv.cz/UtilityModels/FullDocuments/FDUM0018/uv018622.pdf

Patents

[1] Co-author of patent "Illumination optical system for Pilot Light system"; in cooperation with SIEMENS s.r.o., o.z. Nízkonapěťová spínací technika, Trutnov; patent pending 2011

[2] Co-author of patent NP2011/46 "Integrated sensor with bi-cylindric asphere lens"; in cooperation with Rieter CZ s.r.o., Ústí nad Orlicí; patent pending 2011